Cape Peninsula
University of Technology

The effect of temperature on the kinetics of microbial ferrous-iron oxidation in a packed column bioreactor

by

Faysol Chowdhury

Thesis submitted in fulfilment of requirements for the degree
MTech: Chemical Engineering

in the FACULTY OF ENGINEERING

at the Cape Peninsula University of Technology

Supervisor: Dr T.V. Ojumu

Cape Town Campus
January 2012

DECLARATION

I, Faysol Chowdhury, declare that the contents of this thesis represent my own unaided work, and that the thesis has not previously been submitted for academic examination towards any qualification. Furthermore, it represents my own opinions and not necessarily those of the Cape Peninsula University of Technology.

....

Signed Date

ABSTRACT

The microbial ferrous-iron oxidation process plays a significant role in bioleaching, providing ferric-iron (Fe^{3+}) − a strong oxidising agent for the dissolution of most sulphide minerals. An extensive literature review has shown that several studies have been carried out on microbial ferrous-iron oxidation, mostly in stirred tank reactors and in conditions close to optimum. However, limited studies have been carried out on this subject in the context of heap bioleach situation. Despite the fact a packed column system may be used to represent heap bioleaching, most of the studies on microbial ferrous-iron oxidation in such systems were carried out under flooded/fluidised conditions which do not adequately represent solution flow dynamics in a heap system.

The microbial ferrous-iron oxidation kinetics of *Leptospirillum ferriphilum* were studied at substrate loading rates of 0.17 – 0.5 $g.L^{-1}h^{-1}$ (dilution rates 0.033 – 0.1 h^{-1}). The study was conducted in a packed column with a view to investigating the kinetics in a system which simulates the solution flow dynamics of a typical heap bioleach operation. Glass marbles, 15 mm in diameter, were used as reactor packing. The microbial oxidation kinetics were investigated in a continuous mode at the desired loading rates. The pH of the bioreactor was maintained at pH 1.45 ± 0.05 and the aeration at 15 $mL.s^{-1}$. Both Monod and Hansford models were used to describe the biooxidation kinetics.

The effect of temperature on the kinetic parameters was investigated at 25, 30 and 35 °C respectively. The results showed that the maximum rate of microbial ferrous-iron oxidation, $r_{Fe^{2+}}^{max}$, and the kinetic constant, $K_{Fe^{2+}}$, increased linearly with an increase in temperature within the range studied. The maximum oxidation rate, $r_{Fe^{2+}}^{max}$ = 15.10 $mmol.L^{-1}h^{-1}$, obtained at 35 °C was greater than the rate obtained in a similar study conducted in a continuous, stirred tank bioreactor. The result also showed that the Arrhenius equation may be used to describe the relationship between the maximum overall microbial oxidation rate and temperature. An activation energy, (E_a= 20.97 $kJ.mol^{-1}$), was obtained which is, in turn, indicative of a system that is limited by both diffusion and biochemical factors.

The contribution of ferric-iron precipitate to the kinetic parameters was investigated at 30 °C. The results showed that it is possible to obtain approximately 4% jarosite from the bioreactor effluent at every dilution rate investigated and that most of the precipitate accumulated within the bioreactors. This precipitate served as support for the microbial attachment, thereby retaining more microbial cells in the column bioreactor for enhanced performance. However,

the ferrous-iron conversion did not show a consistent trend with dilution rate as a result of the jarosite accumulation. A ferrous-iron conversion of >95% was obtained at the highest dilution rate (0.10 h^{-1}) investigated. The analysis of the results using both a simplified ferric-inhibition model (a modified Hansford model) and a Monod equation revealed that the maximum overall rates of microbial ferrous-iron oxidation, $r'^{max}_{Fe^{2+}}$, obtained from both equations were the same. However, the average value increased by 38.80% as a result of an accumulation of jarosite, while both the substrate affinity constant, $K_{Fe^{2+}}$, and the apparent affinity constant, $K'_{Fe^{2+}}$, decreased significantly with the jarosite accumulation. This decrease is indicative of enhanced microbial activity.

This study showed that the microbial oxidation kinetics of ferrous-iron by *L. ferriphilum* is more likely to be enhanced in a simulated heap bioleach system as compared to an agitated vessel. It also showed that jarosite, although known to be undesirable in bioleach heaps, may be of advantage to heap bioleach operators if managed carefully.

DEDICATION

This thesis is dedicated to my parents, for their endless love, support and encouragement. I have also been extremely fortunate to receive tremendous moral support from several members of my extended family, especially my eldest sister and brother-in-law, whose financial support and encouragement were so instrumental in helping me overcome numerous hurdles in my life. This work is also dedicated to my younger brother, whose moral support I cannot afford to ignore.

ACKNOWLEDGEMENTS

I would like to thank:

- The almighty ALLAH, for giving me the strength and courage to pursue a higher degree.
- Dr T.V. Ojumu, whose excellent supervisory role, wise advice, insightful criticisms and patient encouragement helped in the writing of this thesis in innumerable ways.
- Dr M.S. Sheldon for unselfishly loaning the equipment essential for this study and her willingness to always be of assistance.
- H.N. Ongendangenda and D. de Jager for their wise advice and assistance in editing this thesis.
- A. Bester and H. Small for their technical assistance throughout this project.
- All my postgraduate colleagues and the Chemical Engineering staff for their support and assistance.
- The financial assistance of the Cape Peninsula University of Technology towards the research is acknowledged. The opinions expressed in this thesis and the conclusions arrived at are those of the author and are not necessarily attributable to the Cape Peninsula University of Technology

LIST OF PUBLICATIONS AND PRESENTATIONS

Oral presentation

1. **Chowdhury, F**. and Ojumu, T.V. 2011. The effect of temperature on the kinetics of ferrous-iron biooxidation by *Leptospirillum ferriphilum* in a packed column bioreactor. *19th International Biohydrometallurgy Symposium*, Changsha Hunan, China, 18–22 September 2011.

2. **Chowdhury, F**. and Ojumu, T.V. 2011. Contribution of ferric-iron precipitate to the kinetics of microbial ferrous-iron oxidation by *Leptospirillum ferriphilum* in a packed column. *19th International Biohydrometallurgy Symposium*, Changsha Hunan, China, 18–22 September 2011.

Poster presentation

1. **Chowdhury, F**. and Ojumu, T.V. 2010. The kinetics of microbial ferrous-iron oxidation by *Leptospirillum ferriphilum* in the packed column: The effects of jarosite. *Mineral Processing Confercence*, Cape Town, South Africa, 05–06 August 2010**.**

Journal publication

1. **Chowdhury, F**. and Ojumu, T.V. 2012. Investigation of ferrous-iron biooxidation kinetics by *Leptospirillum ferriphilum* in a packed column: effects of temperature and jarosite accumulation (submitted to Hydrometallurgy).

TERMS AND CONCEPTS CITED

Bioleaching: Bioleaching refers to the dissolution of metals from their ores in solution, which is facilitated/catalysed by certain microorganisms, e.g. bacteria and archea.

Heap bioleaching: Heap bioleaching is a minerals processing technology whereby large piles of low grade, crushed ores or rock are leached with various chemical solutions that extract valuable minerals facilitated by microorganisms.

Jarosite: Jarosite is a basic hydrous sulfate of iron with a chemical formula of $XFe_3(SO_4)_2(OH)_6$, where $X = K^+$ (potassium jarosite), Na^+ (natrojarosite), NH_4^+ (ammoniojarosite), or H_3O^+ (hydronium Jarosite). This mineral is formed in ore deposits by the oxidation of iron sulphides.

Mesophilic bacteria: These are most common iron-oxidising and sulphur-oxidising microorganisms found in commercial bioleaching processed at optimum temperatures below 40 °C.

Packed column reactor: A packed column is a hollow tube, tank, pipe, or other vessel that is filled with a packing material. The packing may be randomly filled with small objects such as Raschig rings or else with a specifically designed structured packing.

TABLE OF CONTENTS

DECLARATION ii

ABSTRACT ii

DEDICATION iv

ACKNOWLEDGEMENTS v

LIST OF PUBLICATIONS AND PRESENTATIONS vi

TERMS AND CONCEPTS CITED vii

TABLE OF CONTENTS viii

LIST OF FIGURES xii

LIST OF TABLES xiv

NOMENCLATURE xv

LIST OF ABBREVIATIONS xvii

Chapter 1: Introduction 1

1.1 Background 1

1.2 Objectives of the study 3

1.3 Research design and methodology 3

1.4 Delineation of the study 3

1.5 Significance of the study 4

1.6 Thesis outline 4

Chapter 2: Literature review 5

2.1 Historical background: Heap bioleaching 5

2.2 Microbial bioleaching 8

2.3 The category of microorganisms involved in bioleaching 10

2.4 The application of bioleaching techniques 16

2.5 General characteristics of bioleaching microorganisms 20

2.6 Microbial ferrous-iron oxidation 20

2.7 The kinetics of microbial ferrous-iron oxidation 23

2.8 Development of the fundamental rate equation for microbial ferrous-iron oxidation 31

2.9 A theoretical development of the kinetic model of microbial ferrous-iron oxidation 33

2.10 Effects of relevant parameters on microbial ferrous-iron oxidation 37

2.10.1 Effect of operating temperature 37

2.10.2 Effect of solution pH 40

2.10.3 Accumulation of jarosite 41

2.10.4 Effect of packing height on ferrous-iron biooxidation 42

2.10.5 Effect of packing size 43

2.11 Gas-liquid mass transfer in packed column 43

2.12 Oxygen and carbon dioxide uptake rate in cells 45

2.13 Summary 45

Chapter 3: Materials and Methods 47

3.1 Materials 47

3.1.1 Experimental rig 47

3.1.2 Growth medium 49

3.1.3 Bacterial culture 49

3.2 Methods 49

3.2.1 Microbial ferrous-iron oxidation under continuous operation 49

3.2.2 Experimental study on the effects of operating temperature 50

3.2.3 Experimental study on the effects of ferric-iron precipitate 50

3.3 Analytical procedure 51

3.3.1 Iron determination 51

3.3.2 Redox probe calibration 51

3.4 Analysis of kinetic data 52

3.4.1 Kinetic equation of microbial ferrous-iron oxidation 52

3.4.2 The effect of temperature 52

3.5 Conclusion 53

Chapter 4: The effect of temperature on the kinetics of ferrous-iron biooxidation by *Leptospirillum ferriphilum* in a packed column bioreactor 54

4.1 Introduction 54

4.2 Methodology 55

4.3 Results and discussion 55

4.3.1 Variation of iron species concentrations, ferrous-iron biooxidationconversion rate, and solution redox potential with dilution rate 55

4.3.2 The rate of microbial ferrous-iron oxidation 57

4.3.3 The activation energy determination 60

4.4 Conclusion 62

Chapter 5: Contribution of ferric-iron precipitate to the kinetics of microbial ferrous-iron oxidation by *Leptospirillum ferriphilum* in a packed column 63

5.1 Introduction 63

5.2 Methodology 63

5.3 Results and discussion 64

5.3.1 The effect of jarosite on microbial ferrous-iron oxidation and conversion 64

5.4 Conclusion 68

Chapter 6: Conclusions and Recommendations 70

6.1 Conclusions 70

6.2 Recommendations for future studies 72

Chapter 7: References 74

Appendix A 91

A1.1 A theoretical development for the kinetics of microbial ferrous-iron oxidation 91

Appendix B 95

B1.1 Calculation of dilution rate by weight decrease of feed vessels 95

B1.2 The theoretical aspect of the calibration using the Nernst equation 95

Appendix C **97**

Statistical analysis: Relationship between sum of squares and correlation coefficient **97**

C1.1 Sum of squares 97

C1.2 Error analysis between modelled and measured data 98

Appendix D: Determination of concentration of iron species **100**

D1.1 Reagent preparation 100

D1.1.1 Spekker acid 100

D1.1.2 Ferric acid 100

D1.1.3 Stannous chloride solution ($SnCl_2$) 100

D1.1.4 Mercuric Chloride solution ($HgCl_2$) 101

D1.1.5 Potassium Dichromate solution (0.0149 M $K_2Cr_2O_7$) 101

D1.1.5 Barium Diphenyllamine Sulphonate (BDS) solution ($C_{24}H_{20}BaN_2O_6S_2$) 101

D1.2 Determination of ferrous-iron concentration by titration with potassium dichromate solution[3] 101

D1.3 Determination of total iron concentration by titration with potassium dichromate solution[4] 102

D1.4 Vishniac Trace Metal Solution 103

Appendix E: Experimental data at different temperatures **104**

LIST OF FIGURES

Figure 2.1: A schematic representation of the bioleaching mechanism (Hansford and Vargas, 2001; Breed and Hansford, 1999) 9
Figure 2.2: Classification of the microorganisms involved in bioleaching 11
Figure 2.3: Distribution of microorganisms as a function of temperature and the development of an idealised bioleaching heap, distinguishing bacteria and archaea, autotrophs and heterotrophs and the different pathways of CO_2 fixation used by the autotrophs (Valdés *et al.*, 2010) 12
Figure 2.4: Schematic diagram of a) tank (modified from Rawlings (2002)), b) heap, and c) in-situ bioleaching processes 18
Figure 2.5: Schematic representation of the proton circuit and ferrous-iron oxidation by *At. ferrooxidans* (modified from Ingledew (1982) and Crundwell (1997)) 22
Figure 2.6: Schematic representation of the iron oxidation electron transport pathway of *At. ferrooxidans* showing the electron transfer generating proton gradient and reverse electron transport for nicotinamide adenine dinucleotide (NADH) formation (Rawlings, 2005) 22
Figure 2.7: Linearised Monod equation using (a) the Lineweaver-Burk method, (b) the Eadie-Hofstee method, and (c) the Langmuir method 30
Figure 2.8: Schematic diagram of ideal pack bioreactor 34
Figure 2.9: Predicted cell concentration as a function of the dilution rate based on both the Hansford model (▲) and the Monod model (■) 37
Figure 2.10: Ratkowsky plots showing the relationship of temperature to the oxidation of iron for a range of common bioleaching organisms *L. ferrooxidans* (●), *L. ferriphilum* (∆), *Acidimicrobium ferrooidans* (X), *Sulfobacillus thermosulfidooxidans* (O), *Acidianus brierleyi* (■) (Franzmann *et al.*, 2005) 38
Figure 2.11: Oxygen and carbon dioxide transfer from a gas bubble to the liquid phase 44

Figure 3.1: (a) Schematic representation of experimental rig; and (b) Photographic representation of the experimental set-up 48

Figure 4.1: Dilution rate vs (a): residual ferrous-iron; (b): ferric-iron; (c): solution redox potential (Ag/AgCl); (d): ferrous-iron oxidation rate and conversion 56
Figure 4.2: The effect of temperature on (a) the ferrous iron oxidation rate versus residual ferrous-iron concentration compared with the trend of the Monod model (Equation 2.42); (b) the fit of the rate data to the Boon and Hansford model, Equation 2.53 58
Figure 4.3: (a) Arrhenius plot to show the effect of temperature on the maximum overall ferrous-iron oxidation rate; (b) The effect of temperature on the kinetic constants $K_{Fe^{2+}}$ and $K'_{Fe^{2+}}$ 61

Figure 5.1: Steady-state ferrous iron conversion and oxidation rate as a function of dilution rate at 30 °C 65

Figure 5.2: Photograph indicating (a) Packed bioreactor without jarosite accumulation; and (b) Packed bioreactor with jarosite accumulation on the packing material 66
Figure 5.3: The effect of ferric-iron precipitate on (a) the ferrous iron oxidation rate versus residual ferrous-iron concentration compared with the trend of the Monod model (Equation 2.42); (b) the fit of the rate data to the Boon and Hansford model, Equation 2.53 67

LIST OF TABLES

Table 2.1: Commercial copper heap bioleaching plants (historical and current)..... 7
Table 2.2: The characteristics of the most popular microorganisms used in bioleaching and microbial process activation energies derived from Arrhenius plots for temperatures below optimum microbial growth temperature..... 13
Table 2.3: Selected published kinetic models for ferrous-iron oxidation with *At. ferrooxidations*..... 32
Table 2.4: Measured reaction rates for sulphur oxidation and iron oxidation by common bioleaching organisms and the temperature at which those rates were measured (Franzmann *et al*., 2005) 39

Table 4.1: Precipitation ferric-iron at different dilution rates and different temperatures..... 57
Table 4.2: Maximum overall ferrous-iron oxidation and kinetic constant, determined from the fit of rate data to the Hansford and Monod models..... 59

Table 5.1: Jarosite accumulation data..... 65
Table 5.2: Percentage (%) of jarosite in the effluent stream at different dilution for jarosite accumulation experiment..... 66
Table 5.3: Maximum ferrous-iron oxidation and kinetic constants at 30 °C, determined from the fit of rate data to the Hansford and Monod models..... 68

Table B1.1: Parameters determined from the standard calibration curve for redox probes used in this study..... 96

Table C1.1: Error analysis of experimental data..... 99

Table E1.1: Experimental data..... 104

NOMENCLATURE

Symbol	Description	Unit
a	Gas-liquid interfacial area per unit volume of fluid	$m^2.L^{-1}$
$a_{Fe^{2+}}$	Activities of species ferrous-iron	$mmol.L^{-1}$
$a_{Fe^{3+}}$	Activities of species ferric-iron	$mmol.L^{-1}$
A_h	The gas-liquid interfacial area at a height h	m^2
a_h	Specific interfacial area at height h	m^2
a_i	activity of species i	$mmol.L^{-1}$
C_{AL}	Oxygen concentration in the broth	$mmol.L^{-1}$
C_{AL}^*	Solubility of oxygen in the broth	$mmol.L^{-1}$
C_X	Cell concentration	$mmol\ C.L^{-1}$
C_{X_0}	Initial bacteria concentration	$mmol\ C.L^{-1}$
D	Dilution rate	h^{-1}
d_{ih}	Diameter of bubble	M
[E]	Concentration of the enzyme	$mmol.L^{-1}$
E_a	Activation energy	$kJ.mol^{-1}$
E_h	Standard redox potential	mV
E'_h	Solution potential	mV
[ES]	Concentration of the enzyme-substrate complex	$mmol.L^{-1}$
E_h^0	Standard electrode potential	mV
$[E_T]$	Total concentration of the enzyme	$mmol.L^{-1}$
F	Flow rate in Equation 2.45	$L.h^{-1}$
F	Faraday's constant in Equation 3.3	$Coulomb.mol^{-1}$
$[Fe^T]$	Total iron	$mmol\ Fe.L^{-1}$
$[Fe^T]_{In}$	Total iron influent	$mmol\ Fe.L^{-1}$
$[Fe^T]_{Out}$	Total iron effluent	$mmol\ Fe.L^{-1}$
$[Fe^{2+}]$	Ferrous-iron concentration	$mmol\ Fe^{2+}.L^{-1}$
$[Fe^{3+}]$	Ferric-iron concentration	$mmol\ Fe^{3+}.L^{-1}$
f_{ih}	Bubble number fraction	Dimensionless
$[Fe^{2+}]_{In}$	Influent ferrous-iron concentration	$mmol\ Fe^{2+}.L^{-1}$
$[Fe^{2+}]_{Out}$	Effluent ferrous-iron concentration	$mmol\ Fe^{2+}.L^{-1}$
$[Fe^{2+}]_t$	Threshold ferrous-iron concentration	$mmol\ Fe^{2+}.L^{-1}$
K_0	Frequency factor of activation energy	$mmol\ Fe^{2+}.h^{-1}$
K_d	Specific death rate constant	h^{-1}
$K_{1,ES}$	Rate constant for enzyme-substrate complex formation	$L.mmol^{-1}h^{-1}$
$K_{2,ES}$	Rate constant for reverse enzyme-substrate complex formation	$L.mmol^{-1}h^{-1}$
$K_{3,ES}$	Rate constant for product formation	$L.mmol^{-1}h^{-1}$
$K'_{Fe^{2+}}$	Affinity constant in Equation 2.43	Dimensionless
$K_{Fe^{2+}}$	Ferrous-iron based affinity constant	$mmol\ Fe^{2+}.L^{-1}$

$K_{Fe^{3+}}$	Ferric-iron based affinity constant	mmol $Fe^{3+}.L^{-1}$
K_L	Liquid-phase mass transfer coefficient	$m.s^{-1}$
K_m	Michaelis-Menten constant	mmol $Fe^{2+}.L^{-1}$
$m_{Fe^{2+}}$	Maintenance coefficients based on ferrous-iron	mmol $Fe^{2+}.(mol\ C)^{-1}h^{-1}$
n	Numbers of moles of electrons transferred in the half reaction	Dimensionless
N_A	The rate of O_2 and CO_2 transfer from gas to liquid	$mmol.s^{-1}$
n_{Th}	Total number of bubbles at height h	Dimensionless
$q_{Fe^{2+}}$	Microbial specific ferrous-iron utilisation rate	mmol $Fe^{2+}.(mol\ C)^{-1}h^{-1}$
$q_{Fe^{2+}}^{max}$	Maximum microbial ferrous-iron utilisation rate	mmol $Fe^{2+}.(mol\ C)^{-1}h^{-1}$
q_{O_2}	Microbial specific oxygen utilisation rate	mmol $Fe^{2+}.(mol\ O_2)^{-1}h^{-1}$
$q_{O_2}^{max}$	Maximum microbial specific oxygen utilisation rate	mmol $Fe^{2+}.(mol\ O_2)^{-1}h^{-1}$
R	Universal gas constant	$J.mol^{-1}K^{-1}$
R^2	Regression coefficient	Dimensionless
r_{CO_2}	Oxygen utilisation rate	mmol $CO_2.L^{-1}h^{-1}$
$r_{(ES)}$	Net rate of formation of the enzyme-substrate complex	$L.mmol^{-1}h^{-1}$
$-r_{Fe^{2+}}$	Ferrous-iron utilisation rate	mmol $Fe^{2+}.L^{-1}h^{-1}$
$r_{Fe^{2+}}^{max}$	Maximum ferrous-iron utilisation rate	mmol $Fe^{2+}.L^{-1}h^{-1}$
$-r_{O_2}$	Oxygen utilisation rate	mmol $O_2.L^{-1}h^{-1}$
r_X	Cell production rate	mmol $C.L^{-1}h^{-1}$
[S]	Substrate concentration	$mmol.L^{-1}$
S_h	Average surface area of bubbles at height h	m^2
T	Absolute temperature	K
V_{AR}	Reactor active volume	m^3
V_{Gh}	Average volume of gas bubbles at a height h	m^3
V_{max}	Maximum rate of reaction in Equation 2.20	$mmol.h^{-1}$
v_0	Volumetric flow rate	$m^3.s^{-1}$
Y	Microbial yield coefficient	mmol $C.(mmol\ Fe^{2+})^{-1}$
$Y_{Fe^{2+}X}$	Microbial yield on ferrous-iron	mmol $C.(mmol\ Fe^{2+})^{-1}$
$Y_{Fe^{2+}X}^{max}$	Maximum microbial yield on ferrous-iron	mmol $C.(mmol\ Fe^{2+})^{-1}$
Y_{O_2X}	Microbial yield on oxygen	mmol $C.(mmol\ O_2)^{-1}$
Y_{sx}	Microbial yield on substrate, S	mmol $C.(mmol\ S)^{-1}$

Greek Symbols

τ	Residence time	H
μ	Specific growth rate	h^{-1}
μ_{max}	Maximum specific growth rate	h^{-1}
γ_i	Activity coefficient	Dimensionless

LIST OF ABBREVIATIONS

Abbreviation	Description
ADP	Adenosine diphosphate
AMD	Acid mine drainage
ARD	Acid rock drainage
At.	*Acidothiobacillus*
ATP	Adenosine triphosphate
BDS	Barium Diphenyllamine Sulphonate
CSTR	Continuous stirred tank reactor
CycA1	Cytochrome-cA1
Cyc1	Cytochrome-c1
Cyc2	Cytochrome-c2
E	Enzyme
EDTA	Ethylenediaminetetraaacetic acid
EPS	Exoplysaccharide layer
ES	Enzyme-substrate
L.	*Leptospirillum*
NADH	Nicotinamide adenine dinucleotide
P	Product
PLS	Pregnant leach solution
PSSH	Pseudo-Steady-State Hypothesis
S	Substrate
SHE	Standard hydrogen electrode
SSE	Sum of squares error
TDS	Total dissolved solids
UCT	University of Cape Town
USA	United States of America

Chapter 1

Introduction

1.1 Background

Bioleaching is a simple technology which involves the use of microorganisms in the extraction of metals from low-grade ore and mineral concentrates (Bosecker, 1997). The process involves the solubilisation of one or more components of a complex solid into a liquid phase. It has been used as a pretreatment method for refractory gold ores prior to cyanidation and in the extraction of copper from copper sulphide ores. It has also been reported that the application of bioleaching is currently being extended to the extraction of minerals, such as cobalt, zinc and uranium, from their ore deposits (Ojumu, 2008). Industrially, various bioleaching techniques have been used for mineral extraction, depending on the ore grade. These techniques include stirred tank and heap or dump bioleaching. Tank bioleaching offers good control of the operating variables and, therefore, it is operated mostly under optimum conditions. However, as a result of the depletion of high grade ores and the corresponding high operating costs that may be associated with using tank bioleaching for low grade ores operations, bioleaching is performed on a large scale in both heaps and dumps of low grade ores. Heap bioleaching has become an attractive, well established technology for the extraction of copper from low-grade copper sulphide ores. The modelling of heap-bioleaching is often extremely complex as a result of the number of factors involved, including temperature, pH, oxygen and carbon dioxide concentration, and dissolved solids. It is not possible to control these conditions in a heap situation, while conditions may vary widely with time and locations within the heap bed.

Microbial ferrous-iron oxidation is an important subprocess in the bioleaching of sulphide minerals. The main role played by the microorganisms is to facilitate the oxidation of ferrous-iron (Fe^{2+}) to ferric-iron (Fe^{3+}) and the oxidation of sulphur compounds to sulphur or sulphates (Schippers and Sand, 1999; Boon, 1996; Sand *et al.*, 1995). The ferric-iron produced in this process is a critical reagent for the oxidation of many sulphide minerals which are industrially relevant. Accordingly, the microbial ferrous-iron oxidation is extremely

important in heap bioleaching. It has been shown that a wide variation in heap bioleach operating conditions (e.g. temperature, pH, etc.) will have implications for microbial ferrous-irons oxidation in heap systems (Ojumu and Petersen, 2011; Ojumu *et al.*, 2009; Dopson *et al.*, 2007; Ojumu *et al.*, 2006).

Ojumu (2008) has noted that several studies have been carried out on microbial ferrous-iron oxidation kinetics (Ojumu *et al.*, 2008; Boon *et al.*, 1999b; Boon *et al.*, 1999a; Breed and Hansford, 1999; Harvey and Crundwell, 1997). Most of these studies were conducted in conditions which were near optimum for microbial performance (Boon *et al.*, 1999b; Boon *et al.*, 1999a; Breed and Hansford, 1999). Previous studies were carried out in a stirred tank and a shake flask and these studies contributed to the success of tank bioleaching, i.e., operating conditions may be controlled and managed for maximum productivity. Recently, some studies were conducted to investigate the effects of a wide variation in operating conditions on microbial ferrous-iron oxidation kinetics (Ojumu and Petersen, 2011; Ojumu *et al.*, 2009; Ojumu *et al.*, 2008). Although the operating parameters chosen by these authors were similar to a typical heap bioleach situation, these studies were performed in a stirred tank reactor, although, given the difference in hydrodynamics of tank and heap systems, the kinetics may not represent those of microbial ferrous-iron oxidation in a heap situation. It is, therefore, important to investigate the kinetics of microbial ferrous-iron oxidation in a system similar to a heap situation.

Nevertheless, some studies have focused on the rapid generation of ferric-iron, which is a critical reagent responsible for the leaching of sulphide minerals. These studies (Jensen and Webb, 1994; Armentia and Webb, 1992; Carranza and Garcia, 1990; Grishin and Tuovinen, 1988; Lancy and Tuovinen, 1984) were carried out in column reactor systems with different types of support for immobilisation. More recently, in the last decade, column systems have been explored further with the aim of improving ferric-iron generation (Mazuelos *et al.*, 2010; Alemzadeh *et al.*, 2009; Long *et al.*, 2004; 2003; Mazuelos *et al.*, 2002; Mazuelos *et al.*, 2000). The kinetics of microbial ferrous-iron oxidation increased significantly in these systems as compared to the stirred tank bioreactor. However, it is not certain whether these systems are capable of describing the kinetics of microbial ferrous-iron oxidation in the context of bioleach heap operation. These studies were carried out in a fluidised or flooded column conditions i.e., the feed was from the bottom-up, while the effluent streams were taken from the overflow at the top of the reactors. It is not possible for the solution flow dynamics in such systems to describe heap operation, where the reagent/feed is supplied from a sprinkler at the top of the heap and the effluent, i.e., the pregnant leach solution (PLS), is collected from the bottom of the heap. It is hoped that this study will provide an

understanding of ferrous iron biooxidation under heap conditions, which may then be used in either the design of a typical heap bioleach plant or in the assessment of any existing design.

1.2 Objectives of the study

The objective of this study is to investigate the kinetics of ferrous-iron biooxidation using a strain of mesophilic bacteria *Leptospirillum ferriphilum* in a temperature controlled packed column reactor with the view to understanding the kinetics in a typical heap bioleach system. In specific terms, this study will investigate:

- The effect of changes in temperature on the kinetics of ferrous-iron biooxidation in a packed column bioreactor, with a top-down feed.
- The effect of ferric-iron precipitate on the kinetics of this subprocess in a top-down feed bioreactor system, which represents the hydrodynamic movement of the liquid phase in a large-scale bioleaching operation.

1.3 Research design and methodology

This study involved experiments on microbial ferrous-iron biooxidation using a temperature controlled packed-column bioreactor in a continuous mode. The experimental set up was air-tight when assembled. The column was packed with inert materials to simulate inert mineral ore (represented by glass marbles). An inoculum containing predominantly *Leptospirillum ferriphilum* was used for this study. The substrate concentration in the growth medium was chosen to simulate a real heap bioleach situation (5 $g.L^{-1}$ Fe^{2+} as $FeSO_4$. $7H_2O$). The packed column reactor was fed with the growth medium from the top of the column at the desired flow rate, and aerated from the bottom to simulate the solution flow dynamic in a real heap situation. Effluent was collected from the bottom of the reactor and analysed (according to Ojumu, (2008)) in order to determine the biooxidation kinetics, the effect of temperature on the biooxidation of ferrous-iron and also the contribution of ferric precipitate to the kinetics of this subprocess.

1.4 Delineation of the study

This research will be limited to microbial ferrous-iron oxidation by *Leptospirillum ferriphilum* in a packed column reactor. In this study, the inert mineral particles will be represented by glass marbles in the reactor to simulate a heap system. An industrial heap system is extremely complex and the following was assumed not to affect the oxidation kinetics:

- Intra and inter particle diffusion between the fed solution and ore particles
- Oxidation of other minerals by ferric-iron

1.5 Significance of the study

It is expected that the results of this research project will provide an insight into the kinetics of microbial ferrous-iron oxidation in a heap bioleach environment, especially with respect to changes in temperature as well as the accumulation of ferric-iron precipitate (i.e. jarosite accumulation) inside the heap. This will contribute to efforts to predict heap bioleach performance. The results will also serve to provide a database for the validation of relevant kinetic equations for ferrous iron biooxidation under packed column conditions.

1.6 Thesis outline

This thesis is divided into seven chapters (including chapter 1) and is structured as follows:

Chapter 1 includes a brief summary of the background to this research project, a summary of the problems arising from previous work as well as a brief discussion of the research design and methodology and significance of the study.

Chapter 2 presents a brief historical background about heap bioleaching, and a literature review which covers both the accepted mechanisms of bioleaching and the characteristics of the microorganisms involved. Chapter 2 also covers the kinetics of microbial ferrous-iron oxidation with reference to the effects of temperature, pH, jarosite, packing height and packing size in the context of heap bioleaching.

Chapter 3 describes the detailed experimental methods and materials used in this study. The theoretical calculations involved in substrate utilisation are also described in detail. Chapters 4 and 5 present the experimental results of the study as well as a discussion of these results. The effects of changes in temperature are discussed in chapter 4 while the effect of ferric-iron precipitate in the packed column is discussed in chapter 5. The experimental data obtained was correlated to an appropriate rate equation arising from previous studies, as well as from rate equations reviewed in chapter 2. The kinetic constants are presented and discussed in chapters 4 and 5.

Chapter 6 summarising the main points of the study, highlighting the unique aspects of the study, drawing conclusions as well offering recommendations for future work to complement the insights gleaned from this research study. Chapter 7 lists the references cited in the thesis.

Chapter 2

Literature review

Literature pertinent to this research project, including the historical background to heap bioleaching, the microorganisms involved in bioleaching and the general mechanisms of bioleaching, will be discussed in this chapter. Thereafter, a detailed discussion of bioleaching techniques and microbial ferrous-iron oxidation in the context of heap bioleaching will be reviewed in order to understand the status quo with respect to this subject and to identify the gaps existing in the literature which justify the need for this study.

2.1 Historical background: Heap bioleaching

Copper recovery by sulphide ore biooxidation has been practised for centuries in Spain, Sweden, Germany and China through the use of biohydrometallurgy (Ehrlich, 2001). The Rio Tinto mines in Spain are among the ancient mines where biohydrometallurgy is considered to have played a critical role. According to Lugaski (1997), these mines have been exploited since pre-Roman times for their copper, gold and silver deposits. Bioleaching at the Rio Tinto mines was believed to be a natural phenomenon and, hence, the name Rio Tinto, meaning dark coloured, was given to the river because of its reddish colour which resulted from the high concentration of dissolved ferric iron (Rossi, 1990).

Since 1980, when copper leaching from heaps was first initiated, numerous copper heap bioleach operations have been set up (Brierley and Brierley, 2001). The first industrial scale copper heap bioleaching operation was commissioned at the Lo Aguirre copper mine in Chile, which produces 14 000 tonnes of fine copper per year from an ore containing 1 to 2% copper. The commercial application of biohydrometallurgy was designed to facilitate the activity of microorganisms (Brierley and Brierley, 2001). The minerals industry is pressurised to process low grade ores, overburden and the waste from current mining operations as the world demand for copper increases. Accordingly, in order to extract copper economically from low-grade ores, low-cost processing methods such as in-situ, dump and heap leaching, are required. Copper was the first metal to be extracted in 1950 from run-of-mine materials,

through the commercial application of biohydrometallurgy and using a dump leaching technique (Olson *et al.*, 2003; Brierley and Brierley, 2001; Acevedo, 2000). However, as a result of poor aeration, the design of dump leaching did not promote bacterial growth and activity, thus culminating in the development of heap leaching during the 1960s (Rossi, 1990). Heaps were specifically designed to provide for good aeration and other parameters that facilitated the activity of the bacteria to ensure better metal recovery (Olson *et al.*, 2003; Rawlings *et al.*, 2003).

The most successful copper heap leaching processes have been those which extract copper from both copper oxides and secondary copper sulphides − see Table 2.1. During bioleaching processes chalcocite (Cu_2S) is the main copper sulphide mineral mined. Initially, some of the chalcocite heap operations started out as chemical leaching processes and were converted to bioleaching processes via heap aeration and/or inoculation, when the oxidised ore had become depleted. However, if sulphide minerals are present in the heap, then the microbial assisted air oxidation of iron(II) as well as sulphur will contribute to copper extraction even if bacterial activity is not facilitated (Watling, 2006).

Table 2.1: Commercial copper heap bioleaching plants (Historical and current)

Region/mine	Operation reserves (t)	Ore processed (t/day)	Cu production (t/year)
Lo Aguirre, Chile, 1980–1996	Heap bioleach 12×10^{6} at 1.5% Cu	Oxides/chalcocite 16×10^{3}	14-15×10³
Cerro Colorado, Chile, 1993–	Heap bioleach 80×10^{6} at 1.4% Cu	Chalcocite, covellite 16×10^{3}	100×10³
Ivan Zar, Chile, 1994–	Heap bioleach 5×10^{6} at 2.5% Cu	Oxides/sulphides 1.5×10^{3}	12×10³
Quebrada Blanca, Chile, 1994–	Heap/dump bioleach 85×10^{6} at 1.4% Cu 45×10^{6} at 0.5% Cu	Chalcocite 17.3×10³	75×10³
Punta del Cobre, Chile, 1994–	Heap (bio)leach 10×10^{6} at 1.7% Cu	Oxides/sulphides –	7-8×10³
Andacollo, Chile, 1996–	Heap/dump bioleach 32×10^{6} at 0.58% Cu	Chalcocite 15×10³	21×10³
Dos Amigos, Chile, 1996–	Heap bioleach 2.5%	Chalcocite 3×10³	
Zaldivar, Chile, 1998–	Heap/dump bioleach 120×10^{6} at 1.4% Cu 115×10^{6} at 0.4% Cu	Chalcocite 20×10³	150×10³
Lomas Bayas, Chile, 1998–	Heap/dump 41×10^{6} at 0.4% Cu	Oxides/sulphides 36×10³	60×10³
Cerro Verde, Peru, 1977–	Heap bioleach —at 0.7% Cu	Oxide/sulphide 32×10³	54.2×10³
Escondida, Chile	Heap bioleach 1.5×10^{9} at 0.3–0.7%	Oxides, sulphides	200×10³
Lince II, Chile, 1991–	Heap leach 1.8% Cu	Oxides, sulphides	27×10³
Toquepala, Peru	Heap leach	Oxides, sulphides	40×10³
Morenci, Arizona, 2001–	Mine for leach 3450×10^{6} 0.28% Cu	Chalcocite, pyrite 75×10³	380×10³
Equatorial Tonopah, Nevada, 2000–2001	Heap bioleach 0.31% Cu	25×10³	25×10³
Gunpowder Mammoth Mine, Australia, 1991–	In situ (bio)leach 1.2×10^{6} at ~1.8% Cu	chalcocite and bornite –	33×10³
Girilambone, Australia, 1993–2003	Heap bioleach — at 2.4% Cu	Chalcocite/chalcopyrite 2×10^{3}	14×10³
Nifty Copper, Australia, 1998–	Heap bioleach — at 1.2%	Oxides/chalcocite 5×10³	16×10³
Whim Creek and Mons Cupri, Australia, 2006–	Heap bioleach 900×10³ at 1.1% Cu 6×10^{6} at 0.8% Cu	Oxides/sulphides	17×10³
Mt Leyshon, Australia, 1992–1997	Heap bioleach — 0.15%	Chalcocite 1.3×10³	750
S&K Copper, Monywa, Myanmar, 1999–	Heap bioleach 126×10^{6} at 0.5% Cu	Chalcocite 18×10³	40×10³
Phoenix deposit, Cyprus, 1996–	Heap (bio)leach 9.1×10^{6} at 0.78% Cu 5.9×106 at 0.31% Cu	Oxide/sulphide –	8×10³
Jinchuan Copper, China, 2006–	240×10^{6} at 0.63% Cu	Chalcocite, covellite, enargite	10×10³

Source: Watling (2006)

Large volumes of low-grade ore and copper-rich tailings containing chalcopyrite ($CuFeS_2$) await the development of an efficient and economic bioleach process which is capable of extracting copper from chalcopyrite (Watling, 2006). At present dump, heap and tank reactors are well-established processes which are applied to large-scale commercial bioleaching operations for copper and refractory gold concentrates around the world (Rawlings *et al.*, 2003). Considerable progress has been made in the commercial application of bioleaching for metal recovery, especially for both copper extraction and in the treatment of arsenopyrite gold-bearing concentrate (Brierley and Brierley, 2001). The in-situ and dump bioleaching of chalcopyrite is a practical option because the low, slow recovery rates are countered by the low processing costs (Schnell, 1997).

A developing technology is the bacterially assisted heap leaching of low-grade copper sulphides which has been successfully applied to the extraction of copper from secondary sulphide minerals such as chalcocite. Most of the technological developments have occurred in the bioleaching of chalcocite and other, less refractory, sulphide minerals. The increased demand for copper has meant that the focus of heap bioleaching has shifted from the extraction of copper from secondary sulphide minerals to extraction from refractory primary copper sulphide minerals. As a result, the bioleaching of chalcopyrite, the most abundant and refractory copper sulphide, is the process in heap bioleaching which is, at present, receiving the most attention. However, according to Watling (2006), heap bioleaching of the refractory primary copper sulphide, chalcopyrite, has not been successful on a commercial scale. Recent studies have, thus, been directed towards understanding the principles, mechanisms and dynamics of heap bioleaching (Petersen *et al.*, 2011; Petersen and Dixon, 2007; Petersen and Dixon, 2007; Petersen and Dixon, 2006) with a view to designing an efficient heap bioleaching system.

2.2 Microbial bioleaching

The concept of bioleaching sulphide minerals was first proposed by Silverman and Ehrlich (1964). Bioleaching was described as a combined chemical and microbial process, with ferric-iron and/or protons as the fundamental reactants in the leaching reaction. The main role of the microorganisms is both to regenerate the leaching agents (Fe^{3+}) and to facilitate the reaction by creating a reaction space in which the leaching process occurs. It has been reported that, when microorganisms attach on the metal surface, the bioleaching reactions occur most rapidly and most efficiently within the exopolysaccharide (EPS) layer, which serves as the reaction zone (Rohwerder *et al.*, 2003; Sand *et al.*, 2001; Tributsch, 2001).

According to Ojumu (2008), the bioleaching of sulphide minerals occurs via three main subprocesses. These subprocesses are illustrated in Figure 2.1:

- Chemical attack of the sulphide mineral by ferric-iron and/or protons, subsequently releasing the metal cations (e.g. copper) and sulphur species into solution, and the reduction of ferric-iron to ferrous-iron,
- Microbial Fe-oxidation of reduced ferrous-iron to ferric-iron,
- Microbial S-oxidation of the sulphur moiety to elemental sulphur and/or sulphate ions, respectively.

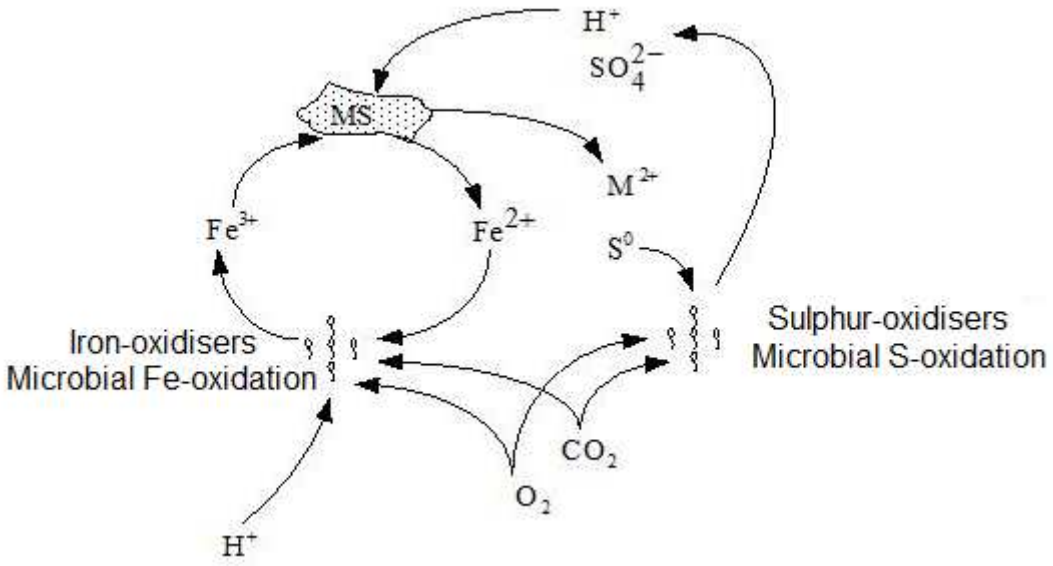

Figure 2.1: A schematic representation of the bioleaching mechanism (Hansford and Vargas, 2001; Breed and Hansford, 1999)

Despite the fact that elemental sulphur is relatively stable, it may be oxidised to sulphate by sulphur-oxidising microoganisms such as; *At. thioxidans* or *At. caldus (*Rawlings*,* 2007*)*. The three bioleaching subprocess may be represented by equations 2.1, 2.2 and 2.3:

$$MS + 2Fe^{3+} \rightarrow 2Fe^{2+} + M^{2+}S^{0}\downarrow \qquad 2.1$$

$$2Fe^{2+} + \frac{1}{2}O_2 + 2H^{+} \xrightarrow{Iron-oxidising\ Bacteria} 2Fe^{3+} + H_2O \qquad 2.2$$

$$S + \frac{3}{2}O_2 + H_2O \xrightarrow{Sulphur-oxidising\ Bacteria} H_2SO_4 \qquad 2.3$$

The ferric-iron reacts chemically with the sulphide mineral to produce ferrous-iron − see Equation 2.1. The ferric-iron is regenerated by iron-oxidising microorganisms through the oxidation of ferrous-iron to ferric-iron (Equation 2.2), thus allowing the leaching reaction in Equation 2.1 to continue in a cyclic manner. The sulphur species are oxidised to sulphuric acid by sulphur-oxidising microbes − see Equation 2.3. Accordingly, as illustrated by both Equations 2.1 to 2.3, it may be concluded that the role of the microorganisms in the

dissolution of metal sulphides is not only to provide sulphuric acid for a proton attack, but also to keep iron in the oxidised ferric state so as to enable an oxidative action on the sulphide minerals. As a result, microbial ferrous-iron oxidation to ferric-iron is a critical sub-process in the bioleaching of sulphide minerals. A similar reaction to that illustrated in Equation 2.1 also occurs for chalcopyrite, whereby, the ferric ions chemically oxidise the mineral, thus producing Cu^{2+} and elemental sulphur, as illustrated in Equation 2.4.

$$CuFeS_2 + 4Fe^{3+} \rightarrow 5Fe^{2+} + Cu^{2+} + 2S^0 \downarrow \qquad 2.4$$

The reaction is known to be sensitive to redox potential. Nevertheless, higher leaching rates have been measured at lower potentials, in the range 0.45 to 0.65 V SHE (standard hydrogen electrode) (Hiroyoshi *et al.*, 2001; Third *et al.*, 2000; Hiroyoshi *et al.*, 1997; Peters, 1976).

2.3 The category of microorganisms involved in bioleaching

Various microorganisms found in bioleaching systems have been reported (Franzmann *et al.*, 2005; Rawlings *et al.*, 2003). However, microoganisms in heap or dump leaching processes are similar to those found in stirred tank processes. The types of microoganisms in a leaching process depend on the properties of the mineral and the conditions under which the processes are operated. Conditions in bioleaching heaps are complex than those in stirred tank reactors as a result of the fact that it is not possible to control various parameters, such as temperatures, solution pH, aeration, mineral type, nutrient availability and so forth in a heap. The existence of several potential ecological regions for the different kinds of microbes have been reported (Rawlings, 2007). It is, therefore, important to study the diversity of microorganisms with respect to the various operating parameters (Rawlings, 2007) − see Table 2.2 and Figure 2.2.

The most important microorganisms are considered to be a consortium of Gram-negative bacteria for heap or tank leaching processes, which operate at temperatures between ambient to approximately 40 °C (Rawlings, 2005). In addition Gram-positive iron and sulphur-oxidising bacteria have also been identified (Foucher *et al.*, 2003). According to the type of species oxidised, microorganisms may be divided into the following three groups: (1) iron-oxidisers, (2) sulphur-oxidisers, and (3) iron or/and sulphur oxidisers. Most of the research conducted into bioleaching has made extensive use of *Leptospirillum ferrooxidans* (*L. ferroxidans*), *L. ferriphilum*, *L. thermoferrooxidans, Acidimicrobium ferrooxidans* and *Ferroplasma acidiphilum* as iron-oxidisers; *Acidothiobacillus thiooxidans*, *At. caldus* and *Acidianus infernus* as sulphur-oxidisers; and *At. ferrooxidans*, *Sulfobacillus acidophilus*,

S. thermosulfidooxidans, *S. metallicus*, *Metallosphaera sedula* and *Acidianus brierleyi* as iron and/or sulphur oxidisers (Rawlings, 2005; Kinnunen, 2004; Rawlings, 2002).

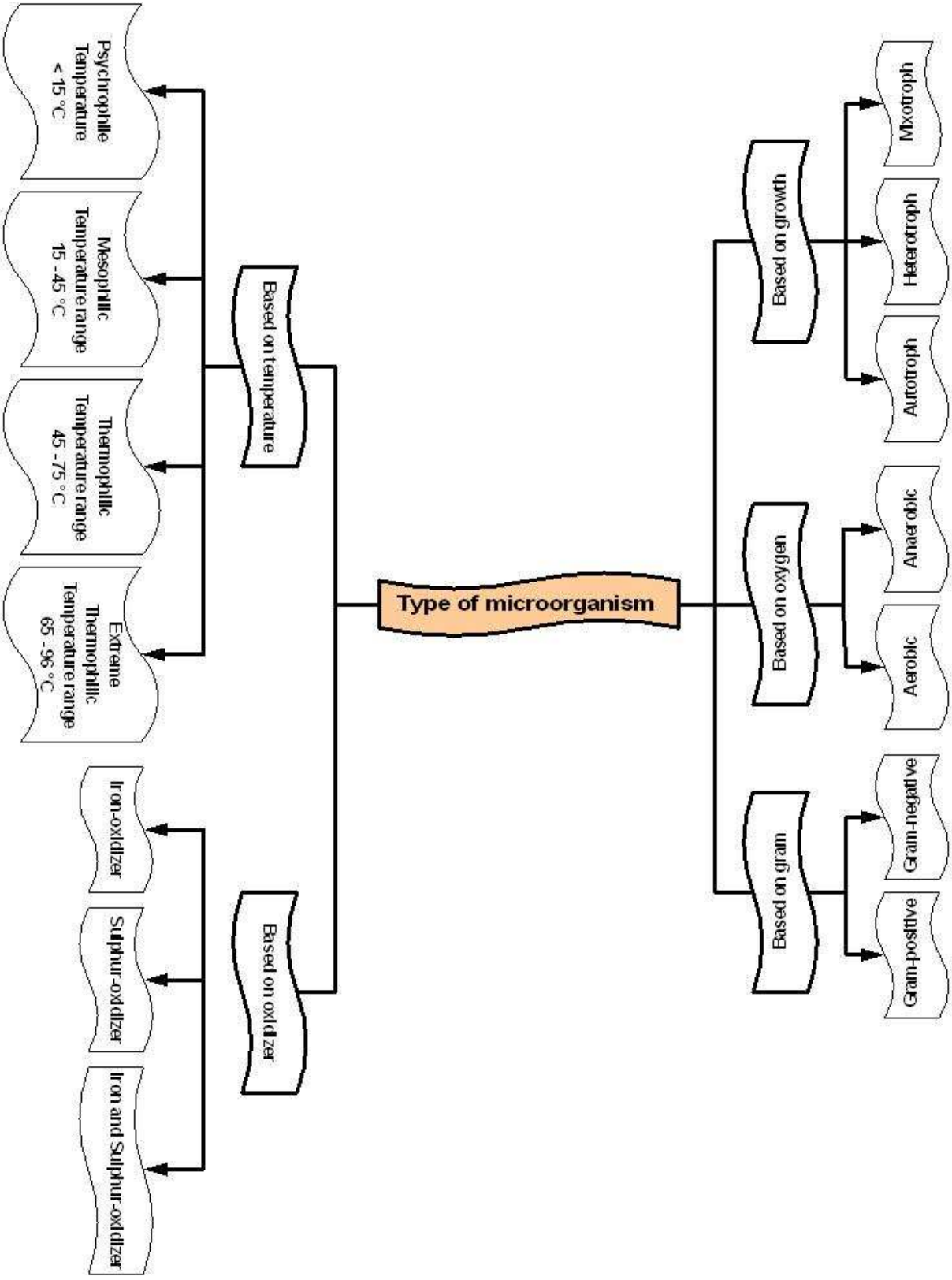

Figure 2.2: Classification of the microorganisms involved in bioleaching

In addition, microorganisms may also be separated into four groups according to their optimum temperature for growth. *Acidothiobacillus*, *Leptospirillum* and *Acidiphilum* may be classified as mesophiles with an optimum growth temperature between 15 and 45 °C; *Sulfobacillus*, *Ferroplasma*, *Sulfolobus*, *Metallosphaera* and *Acidianus* are classified as thermophiles with an optimum growth temperature between 45 and 75 °C; and *Acidianus* (*Acidianus infernos*) are classified as extreme thermophiles with an optimum growth temperature between 65 and 96 °C. Psychrophilic bacteria are defined as having an optimum growth temperature below 15 °C (Plumb *et al.*, 2008; Rohwerder and Sand, 2007; Rawlings, 2005; Kinnunen, 2004; Rawlings, 2002). Several of these microorganisms are recognised as autotrophs and heterotrophs, while one is a facultative mixotroph, obtaining its electrons from either an inorganic electron source (Fe^{2+}) or an organic source, but using organic matter as a carbon source. As depicted in Figure 2.3 the distribution of these autotrophic and heterotrophic bioleaching microorganisms as graphically represented in Figure 2.3 to illustrate their optimum growth temperature and time required for their development in an idealised bioleaching heap.

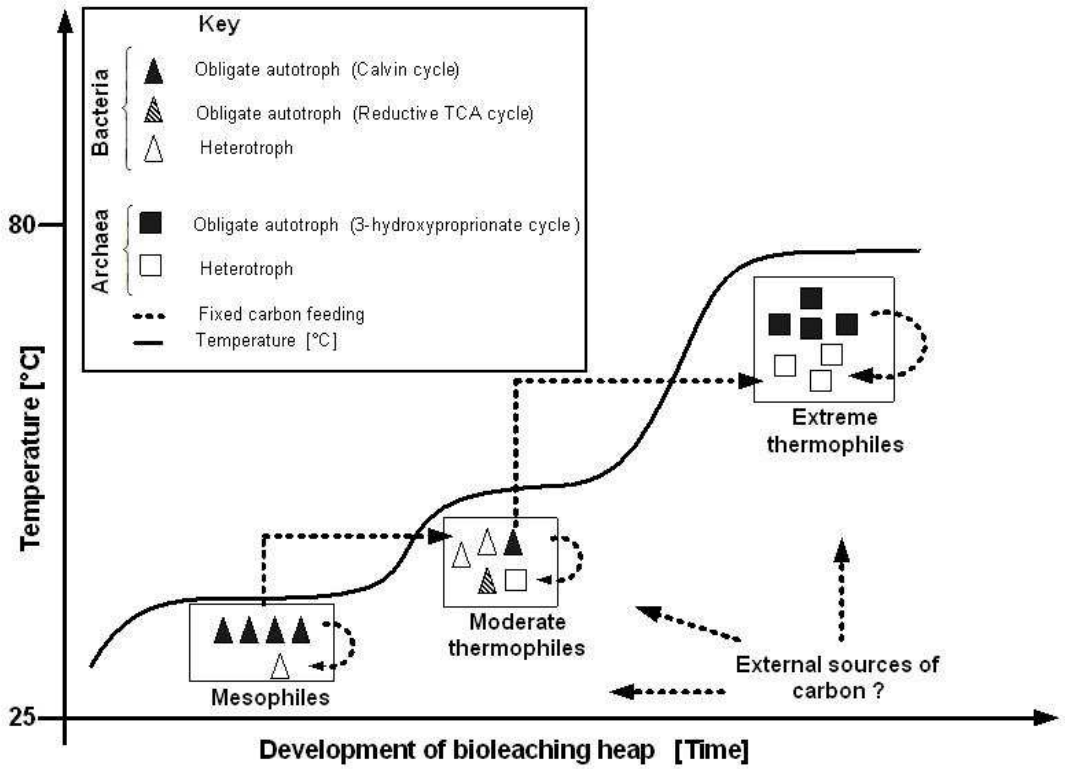

Figure 2.3: Distribution of microorganisms as a function of temperature and the development of an idealised bioleaching heap, distinguishing bacteria and archaea, autotrophs and heterotrophs and the different pathways of CO_2 fixation used by the autotrophs (Valdés *et al.*, 2010)

Table 2.2: The characteristics of the most popular microorganisms used in bioleaching and microbial process activation energies derived from Arrhenius plots for temperatures below optimum microbial growth temperature

Microorganisms	Classification	Oxidation	Growth	Temperature (°C)		pH		Carbon assimilation pathway	E_a(kJ.mol^{-1})
				Range	Optimum	Range	Optimum		
At. Ferrooxidans	M, G-	Iron, sulphur	A	15–35	31	1.4–6.0	1.8–2.0	Calvin cycle (6, 4)	32±3
At. Thiooxidans	M, G-	Sulphur	A	10–37	28–30	0.5–6.0	2.0–3.5	Calvin cycle (5)	47±2
L. ferrooxidans	M, G-	Iron	A	< 10–45	30–37	1.1–4.0	1.6–2.0	na	80±7
L. ferriphilum	M, G-	Iron	A	< 45	30–37	0.5–>3.5	1.4–1.8	Reverse TCA (8)	89±5
F. acidiphilum	M	Iron	F	15–45	35	1.3–2.2	1.7	na	79±19
F. cyprexacervatum	T	Iron		na	55.2	na	na	na	65±3
F. acidiphilum	na	Iron	H	< 10–45	37	1.3–4.8	2.0–2.5	na	na
At. Caldus	MT, G-	Sulphur	F	< 52	45	1.0–3.5	2.0–2.5	Calvin cycle (5)	26±3
A. ferrooxidans	MT	Iron	F	< 30–55	45–50	na	2.0	Calvin cycle (4)	62±5
L. thermoferrooxidans	MT	Iron	na	30–55	45–50	> 1.3	1.7–1.9	na	na
S. acidophilus	MT	Iron, sulphur	F	30–55	45–50	na	2.0	na	na
S. thermosulfidooxidans	MT, G+	Iron, sulphur	F	30–60	45–48	1.5–5.5	2.0	Calvin cycle (11)	51±7
S. metallicus	T	Iron, sulphur	A	50–75	65	1.0–4.5	1.3–1.7	na	50±8
M. sedula	T	Iron, sulphur	F	50–80	75	1.0–4.5	2.0–3.0	na	na
A. brierleyi	T	Iron	F	45–75	70	1.0–6.0	1.5–2.0	3-hydroxypropinate cycle (3)	na
A. brierleyi	T	Sulphur	F	na	78.1	na	na	3-hydroxypropinate cycle (3)	72±4
A. infernos	ET	Sulphur	A	65–96	90	1.0–5.5	2.0	na	na

Listed in alphabetical order: A = autotroph; F = facultative autotroph and/or mixotroph; ET = extreme thermophilic; G+ = Gram-positive; G- = gram-negative; H = heterotroph; M = mesophilic; MT = moderate thermophilc; T = thermophiles and na = data not available.

Source: Adapted from Rohwerder and Sand (2007); Franzmann *et al.* (2005); Rawlings (2005); Kinnunen (2004); Rawlings (2002)

The group *Acidithiobacillus* was described by Kelly and Wood (2000) after the reclassification of some species of the genus *Thiobacillus*. *Acidithiobacillus* as acidophilic (pH < 4.0), Gram-negative, motile rods. The genus includes the following species: *At. ferrooxidans, At. thiooxidans* and *At. caldus*. *At. ferrooxidans* is an obligate autotroph and obtains energy from the oxidation of ferrous-iron (Fe^{2+}) and various sulphur compounds such as elemental sulfur, thiosulfate, trithionate, tetrathionate, sulphide and hydrogen. This microorganism also grows anaerobically with elemental sulphur and hydrogen as electron donors. *At. thiooxidans* and *At. caldus* grow autotrophically with various sulphur compounds (e.g. elemental sulphur, thiosulfate and tetrathionate). *At. thiooxidans* does not oxidise pyrite (Bacelar-Nicolau and Johnson, 1999). These microorganisms, *At. Thiooxidans* and *At. Caldus*, have been found in tank bioleaching operations together with Fe^{2+} oxidisers (Rawlings, 2005; Rzhepishevska *et al.*, 2005; Okibe *et al.*, 2003; Rawlings, 2002; Battaglia *et al.*, 1994; Goebel and Stackebrandt, 1994).

The genus *Leptospirillum (L.)* was described by Hippe (2000), although the first bacteria of this genus were isolated and described by Markosyan (1972). *Leptospirillum* are acidophilic (pH < 4.0), aerobic, gram-negative, grow chemolithoautotrophically and derive energy only from the oxidation of Fe^{2+} ions, and not from sulphur compounds. The genus includes the following species: *L. ferrooxidans, L. ferriphilum, L. ferrodiazotrophum* and *L. Thermoferrooxidans, L. ferrooxidans* and *L. ferriphilum* are acid-tolerant and iron-oxidising autotrophs. *L. ferrooxidans* is able to oxidise Fe^{2+} ions at a high redox potential, i.e., of 550 to 700 mV (Rawlings, 2005; Rohwerder *et al.*, 2003; Rawlings *et al.*, 1999), while *L. ferriphilum* is able to oxidise Fe^{2+} ions at a high rate under acidic solution conditions, i.e., pH < 1 (Kinnunen and Puhakka, 2005).

Acidimicrobium ferrooxidans, as described by Clark and Norris (1996), is acidophilic, gram-positive, moderately thermophilic and iron-oxidising. Autotrophic growth occurs on Fe^{2+} ions, but not on sulphur compounds. *Acidimicrobium ferrooxidans* is also a heterotroph when growth occurs on yeast extracts. Facultative anaerobic growth via the reduction of Fe^{2+} has been described by Bridge and Johnson (1998). *Sulfobacillus acidophilus* was described by Norris *et al.* (1996) as a moderately thermophilic organism. It exhibits facultative anaerobic growth by reduction of ferric-iron (Fe^{3+}), as described by Bridge and Johnson (1998). *Sulfobacillus thermosulfidooxidans* was described by Golovacheva and Karavaiko (1978) as the first species of the genus *Sulfobacillus*. *Sulfobacillus thermosulfidooxidans* is a moderately thermophilic, gram-positive and iron or sulphur oxidising bacteria. Facultative anaerobic growth via the reduction of Fe^{3+} has also been described by Golovacheva and Karavaiko (1978).

The genus *Ferroplasma* was first described by Golyshina *et al.* (2000) as acidophilic archaea that oxidise Fe^{2+}, pyrite and other metal sulphides and are acid-tolerant, aerobic and obligatory chemolithoautotrophically bacteria. Growth may also be mixotrophic or organotrophic and facultatively anaerobic via Fe^{2+} reduction (Dopson *et al.*, 2004). Aerobic growth may be lithoautotrophic on Fe^{2+} ions and CO_2, organoheterotrophic on yeast extract or mixotrophic on Fe^{2+} and on organic carbon sources. Anaerobic growth also occurs on Fe^{3+} in the presence of yeast extract as an electron donor (Dopson *et al.*, 2004). A fluidised-bed reactor operating at 37°C and pH 1.4 was dominated by *L. ferriphilum* with a small proportion of acidophilic heterotrophic *Ferroplasma*-like archaea. The *Ferroplasma*-like archaea are not directly involved in bioleaching, but have been found to assist the growth of iron-oxidising bacteria such as *At. ferrooxidans* and *L. ferriphilum* (Hallberg and Barrie Johnson, 2001; Johnson, 1998; Goebel and Stackebrandt, 1994; Hallmann *et al.*, 1992).

Acidianus brierleyi and *Acidianus infernus* were described by Segerer *et al.* (1986). Both are facultative anaerobic and chemolithoautotrophic organisms, which use metal sulphides, elemental sulphur, hydrogen and organic compounds as substrates. *Sulfolobus metallicus,* described by Huber and Stetter (1991), is an acidophilic, aerobic, thermophilic, iron or sulphur oxidising microorganism. *Sulfolobus metallicus* is also an obligate chemolithoautotrophic organism which uses metal sulphides and elemental sulphur as substrates.

The activation energy for each of the strains for iron or sulphur oxidation is presented in Table 2.2. The activation energy was derived from the correlation of the Arrhenius equation to the temperature-oxidation rate data and were estimated for iron and sulphur oxidation using several common bioleaching strains (Franzmann *et al.*, 2005). Oxidation rate data at temperatures less than optimum temperature for microbial growth may be used in these estimates. It is important to note that the activation energy for sulphur oxidation are for zeroth-order reaction kinetics and first-order reaction kinetics for iron oxidation with the exception of the *Ferroplasma* spp., which portrayed zeroth-order reaction kinetics for iron oxidation (Franzmann *et al.*, 2005).

The selection of microorganisms is extremely important in a commercial bioleaching process. The selection of commercial bioleaching bacteria is made based on the ability of these bacteria to use the energy generated from the oxidation of elemental ferrous iron, inorganic reduced sulphur compounds and other elements in their reduced states, to catalyse and enhance the mineral ore dissolution process (Rawlings, 2005; Rawlings *et al.*, 1999; Rossi, 1990).

2.4 The application of bioleaching techniques

The industrial application of bioleaching technique falls into three main categories, namely, stirred tank, irrigated heap and dump processes. In stirred tank processes highly aerated, continuous-flow reactors placed in series are used to treat the minerals − see Figure 2.4a. The first commercial stirred tank bioleaching plant was commissioned in 1986 at Fairview, South Africa (Brierley and Briggs, 2002). Finely milled mineral concentrate is added to the first tank or make-up tank together with optimum inorganic nutrients and acid solution. The mineral suspension flows through a series of highly-aerated tanks that are able to maintain optimum pH and temperature (Rawlings, 2002; Dew *et al.*, 1997).

The main restriction as regards the operation of a stirred tank reactor is the quantity (i.e. pulp density) of solids that can be maintained in suspension. This is limited to approximately 20% (w/v) of the mineral suspension. In instances where the solids percentage in the mineral suspension is more than 20% (w/v), both physical mixing and the inhibition of microbial growth occurs. The mineral suspension becomes thick for efficient gas transfer and the shear force produced by the impellers in the continuous stirred tank reactor physically damages the microbial cells (Rawlings, 2005). However, stirred tank bioleaching allows for good control of the relevant operational parameters and it may be operated under optimum conditions for microbial activity, resulting in an improved performance and high productivity. However, limitations as a result of the tank reactor volume restrict the application of this process to the treatment of moderate volumes of ore or minerals. In addition, tank bioleaching processes have the highest capital and running costs when compared with heap bioleaching processes and, thus, tank reactors are used only for the leaching of high grade ores.

Heap bioleaching is a mineral processing technology whereby low grade ores are crushed, agglomerated, arranged in layers and placed on an impermeable pad, which serves as the base of the heap. The pad not only prevents the loss of leach solution, but it also prevents contamination of both the leaching solution and the ground. The pad comprises clay as the bedding layer and a permeable drainage system consisting of a drainage pipe network. The heaps are irrigated from the top with sulphuric acid and/or a suitable irrigation solution to prevent the segregation of particles of different sizes, prior to the mounting of ores on the prepared pad for leaching (Brierley and Brierley, 2001).

The treatment of ore requires the assistance of biocatalysts (i.e. microorganisms) that enhance the leaching rate under controlled conditions. The leaching solution which passes downwards through the heap and dissolves the elemental metals from the ore is known as the pregnant leach solution (PLS), and it is recovered at the bottom on the pad. As illustrated

in Figure 2.4b, air is supplied continuously from the bottom of the heap. This ensures an aerobic environment in which microbes are able to thrive, generating ferric-iron and acid. This increases the rate of copper recovery that is associated with sulphide minerals (Rawlings *et al.*, 2003; Brandl, 2001; Montealegre *et al.*, 1993). The target metal is removed from the PLS using a series of technologies, including solvent extraction, cementation or adsorption. The barren solution is then returned to the top surface of the heap for reuse (Petersen and Dixon, 2007; Petersen and Dixon, 2007). This technique is applied mainly to the bioleaching of copper and refractory gold-bearing ores (Rohwerder *et al.*, 2003; Rawlings, 2002).

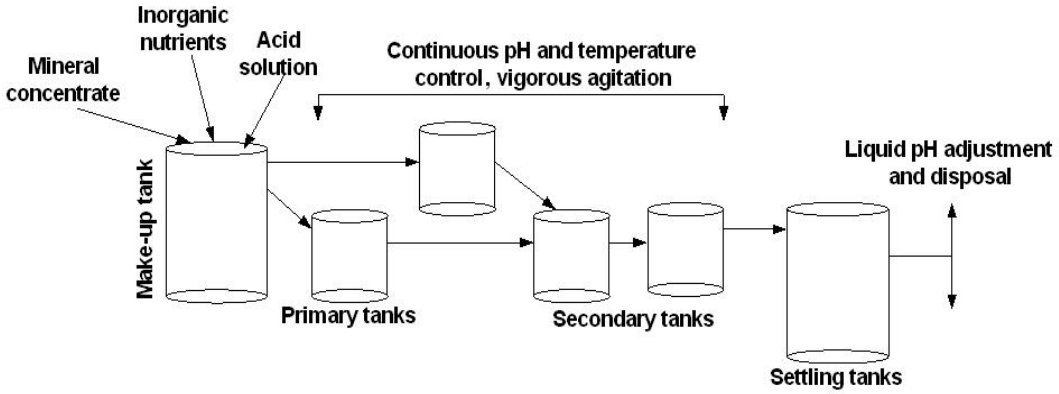

a. Tank bioleaching

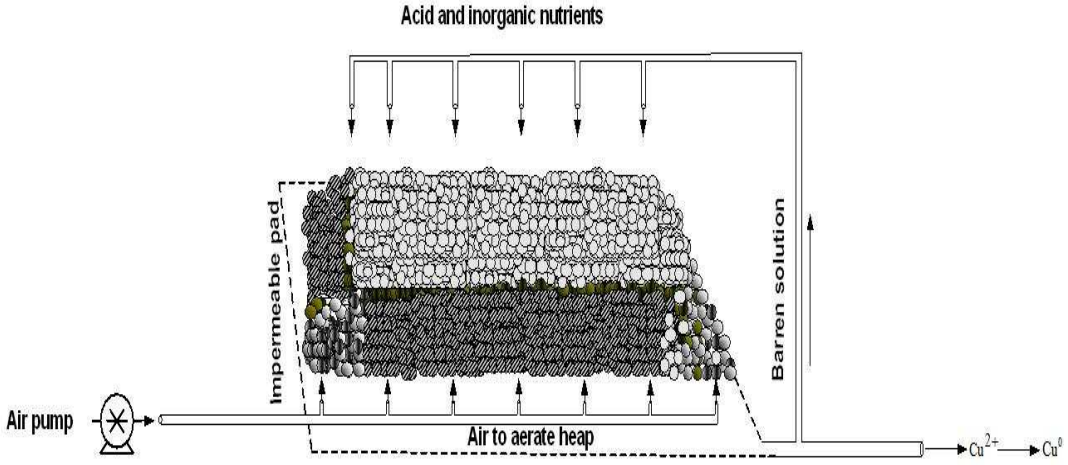

b. Heap bioleaching

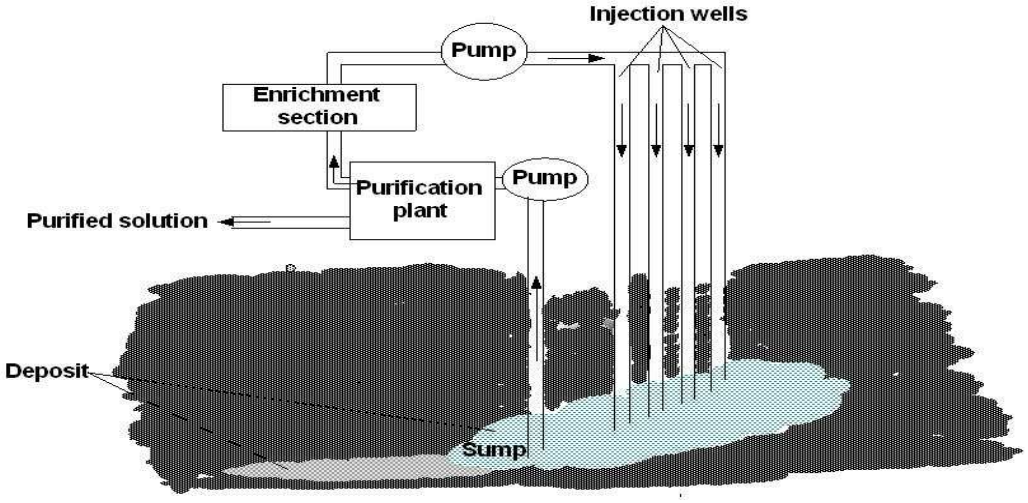

c. In-situ bioleaching

Figure 2.4: Schematic diagram of a) tank (modified from Rawlings (2002)), b) heap, and c) in-situ bioleaching processes

Heap processes offer a number of advantages, including low construction and operational costs, simplicity of operation, suitability for the treatment of lower grade ores and reasonable yields over a set period of recirculation (Pradhan *et al.*, 2008; Rawlings, 2005). However,

when compared to tank reactors, the complexity and heterogeneous nature of heap processes render certain of the operating conditions uncontrollable which results, in turn, in the occurrence of phenomena such as hot spots, regions of high concentration of total dissolved solids (TDS), poor nutrient solution distribution, low rate of oxygen including carbon dioxide transfer and/or varying undesirable pH levels (Ojumu *et al.*, 2006; Petersen and Dixon, 2004).

Heap, dump and in-situ bioleaching are examples of irrigation-based leaching processes. In dump leaching, waste rock and low grade ore are leached at the place of disposal. The fundamental difference between dump and heap bioleaching is the fairly uniform particle sizes and the introduction of aeration from underneath the heap. In-situ leaching or in-place leaching, as depicted in Figure 2.4c, the minerals are leached directly from the ore, without excavation. The process initially involves the drilling of holes into the ore deposit. Leaching reagents that dissolve the desired metals are pumped into the deposit through injection wells. The solution bearing the dissolved ore content is subsequently recovered by pumps to the surface through recovery wells and then processed further downstream. The permeability of the ore body is important and, thus, if the ore does not have sufficient porosity, it must be fractured by explosives so that the injected solution may flow through the deposit unhindered. This technique is applied mainly to the bioleaching of low-grade ore (Brandl, 2001; Schnell, 1997; Murr and Brierley, 1978).

In-situ bioleaching processes offer a number of advantages, including the possibility of mining inaccessible sites, shorter mine development times, no excavating costs, lower mining and infrastructure costs, a reduction in the visual impact of the mining operation and the isolation of personnel from both broken ore and other radiation hazards. However, this process also offers a number of disadvantages, including permeability problems, the precipitation of secondary minerals, the leaching liquor streaming downwards without penetration of the entire ore body and the risk of contamination of ground water (i.e. acid rock generation) because of poor solution control (Brandl, 2001; Schnell, 1997; Murr and Brierley, 1978).

The commercial application of in-situ, dump and heap bioleaching for the recovery of metals has been widely reported (Domic, 2007; Du Plessis *et al.*, 2007; Kinnunen, 2004; Brierley and Brierley, 2001; Brierley, 1999). Recent studies on the application of heap bioleaching to various other metals appear to be promising for the near future as a result of the cheap operational and construction costs associated with these processes and its ability to handle a substantial amount of ore.

2.5 General characteristics of bioleaching microorganisms

The microorganisms involved in the bioleaching of sulphide minerals are responsible for producing the ferric-iron and sulphuric acid required for the bioleaching reactions. Bioleaching microorganisms include iron and sulphur-oxidising chemolithotrophic bacteria and archaea (Rawlings, 2002). Although, these microorganisms are employed in different types of processes at different temperatures intended for optimum performance, they have a number of features in common that render them particularly suited to their role in mineral solubilisation. Four of the most important microbial characteristics are the following:

- They grow autotrophically by fixing carbon dioxide from the atmosphere,
- They obtain their energy by using either ferrous iron or reduced inorganic sulphur compounds. However, they may use both ferrous iron and reduced inorganic sulphur compounds as an electron donor, while they also use oxygen as an electron acceptor,
- They are acidophiles. This means that they grow in a low pH environments, typically pH 1.4 to 1.6,
- They are remarkably tolerant to a wide range of metal-ion concentration, although there is considerable variation within and between the species (Dopson *et al.*, 2003; Rawlings, 2002; Rossi, 1990).

2.6 Microbial ferrous-iron oxidation

Microorganisms that play a major role in the leaching of metals from minerals are either iron or sulphur oxidising organisms, with the iron and sulphur serving as electron donors during microbial respiration. Accordingly, the mechanisms of iron oxidising bacteria and their effectiveness in bioleaching operations, depend on the rate of the oxidation process. The mechanism of ferrous iron oxidation was described by Ingledew (1982) and applied to the bioenergetics of the growth of *At. ferrooxidans* on ferrous-iron. It was also assumed that the same mechanism applies for other iron-oxidising bacteria and archaea.

Microorganisms obtain their energy from ferrous oxidation by using oxygen as the oxidising agent. In the study conducted by Ingledew (1982), it was reported that various functions performed by *At. ferrooxidans* ensured that the internal cell pH was maintained close to neutrality, with the cytoplasmic pH being reported to be between pH 6.5 to 7.

The cells obtain their energy by using ferrous iron as an electron donor and oxygen as an electron acceptor under acidic conditions. The transfer of electrons occurs through an electron-transport chain which mediates between two half cell reactions:

Oxidation: $2Fe^{2+} \xrightarrow{At.ferrooxidans} 2Fe^{3+} + 2e^{-}$ $E_h^0 = +770\,mV$ 2.5

Reduction: $2e^{-} + \frac{1}{2}O_2 + 2H^{+} \rightarrow H_2O$ $E_h^0 = -1120\,mV$ 2.6

Overall reaction: $2Fe^{2+} + \frac{1}{2}O_2 + 2H^{+} \rightarrow 2Fe^{3+} + H_2O + Energy$ $E_h^0 = -350\,mV$ 2.7

The overall reaction consumes Fe^{2+}, O_2 and H^+ to generate H_2O and energy for carbon dioxide (CO_2) fixation and cell growth (Ingledew, 1982). The Fe^{2+}/ Fe^{3+} redox couple has a high positive standard electrode potential (+770 mV) at pH 2. Accordingly, only oxygen is able to act as a natural electron acceptor and, in the presence of protons (H^+), this results in the formation of water as the product of the reaction. Ferrous iron may serve as an electron donor only during aerobic respiration. However, under aerobic conditions ferrous iron spontaneously oxidises to ferric iron unless the pH is low. Therefore, extremely acidophilic bacteria are able to use ferrous iron as an electron donor in a manner that is not possible for bacteria that are able to grow at a neutral pH (Rawlings, 2005). This oxidation occurs in the periplasmic space and is facilitated by some enzyme complexes constituting the electron transport chain (Cavazza *et al.*, 1995).

The reduction of oxygen is promoted by the electrons that are transferred across the cell membrane. This reduction process requires a pair of protons, which must be brought from outside the cell membrane, as depicted in Figure 2.5. As a result of the difference between the cytoplasmic and bulk solution pH, a proton electrochemical gradient develops. The proton electrochemical gradient catalyses the conversion of adenosine diphosphate (ADP) and inorganic phosphate (P) to adenosine triphosphate (ATP). One molecule of ATP is synthesised per electron pair translocated to the oxygen from the oxidation of two Fe^{2+} ions. As a result, the energy carried by ATP in the cell is then transferred for oxygen reduction to form water (Nemati *et al.*, 1998; Rossi, 1990; Ingledew, 1982). It is, therefore, clear that ferrous-iron oxidation is an energy generating process for the bacteria and, thus, forms the basis for their survival and growth.

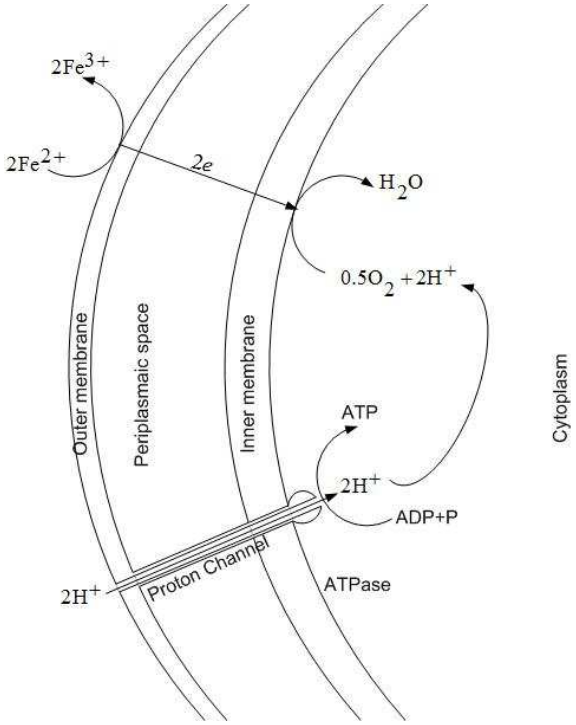

Figure 2.5: Schematic representation of the proton circuit and ferrous-iron oxidation by *At. ferrooxidans* (modified from Ingledew (1982) and Crundwell (1997))

According to Rawlings (2005), the proton electrochemical gradient is controlled by the available channels which are associated with ATPase on the cell membrane. The cell membrane is impermeable to protons and, therefore, proton transfer occurs only through the channels coupled to ATPase. It has been shown that the outer cell membrane of the cell wall of *At. ferrooxidans* contains high molecular weight c-type cytochrome-c2 (Cyc2), which acts as the primary electron acceptor. The electron is then passed to cytochrome-c1 (Cyc1) and cytochrome-cA1 (CycA1) in the periplasm, possibly via rusticyanin, and then to c-cytochrome oxidase (Rawlings, 2005; Yarzabal *et al.*, 2002) − see Figure 2.6.

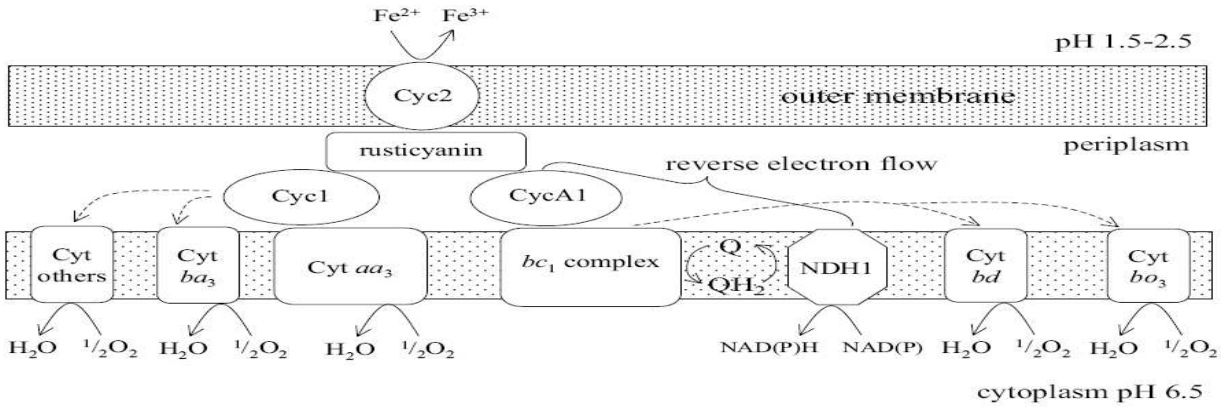

Figure 2.6: Schematic representation of the iron oxidation electron transport pathway of *At. ferrooxidans* showing the electron transfer generating proton gradient and reverse electron transport for nicotinamide adenine dinucleotide (NADH) formation (Rawlings, 2005)

The energy released in the ferrous oxidation process is used in the fixation of dissolved CO_2 through the Calvin reductive pentose phosphate cycle that was reported by Maciag and Lundgren (1964). Studies have shown that at least 2 moles of Fe^{2+} must be oxidised to provide sufficient redox potential energy ($\Delta G \approx -8.1$ kcal.mol^{-1}) needed for the phosphorylation of ADP to ATP (ΔG needed ≈ -8.9 to 16 kcal.mol^{-1}) (Ingledew, 1982; Tuovinen and Kelly, 1972). Ferrous-iron oxidation is also needed to produce nicotinamide adenine dinucleotide phosphate (NAD(P)H) for CO_2 fixation and other anabolic processes by the transfer of electrons from Fe^{2+}. Ss reported by Silver (1978), in the Calvin-Bensen cycle, three molecules of ATP and two molecules of NAD(P)H are required to fix one molecule of CO_2.

2.7 The kinetics of microbial ferrous-iron oxidation

During the leaching of sulphide minerals the role of microorganisms is to oxidise ferrous-iron to ferric-iron. The microbial growth kinetic equation proposed by Monod (1942), and reported by Rossi (1990), has its foundation in the Michaelis-Menten model for enzyme-substrate interaction kinetics. According to this model the enzyme (E) combines with the substrate (S) to form an enzyme-substrate complex (ES). The enzyme-substrate complex subsequently decomposes to form both the product (P) and free enzyme (E). The basic assumption behind Michaelis-Menten enzyme kinetics is that the formation of the enzyme-substrate complex is reversible, while the formation of the product and the free enzyme is irreversible. Equation 2.8 represents the chemical reactions for both the formation of the enzyme-substrate complex and the product.

$$E + S \underset{K_{2,ES}}{\overset{K_{1,ES}}{\rightleftarrows}} ES \xrightarrow{K_{3,ES}} P + E \qquad 2.8$$

Where $K_{1,ES}$ is the rate constant for enzyme-substrate complex formation, $K_{2,ES}$ is the rate constant for reverse enzyme-substrate complex formation, and $K_{3,ES}$ is the rate constant for product formation. Equation 2.8 may be written separately as Equations 2.9, 2.10 and 2.11.

$$E + S \xrightarrow{K_{1,ES}} ES \qquad 2.9$$

$$ES \xrightarrow{K_{2,ES}} E + S \qquad 2.10$$

$$ES \xrightarrow{K_{3,ES}} P + E \qquad 2.11$$

The corresponding rate laws for Equations 2.9, 2.10 and 2.11 are:

$$r_{2.9(S)} = K_{1,ES}[E][S] \qquad 2.9a$$

$$r_{2.10\,(S)} = -K_{2,ES}[ES] \quad 2.10a$$

$$r_{2.11\,(P)} = K_{3,ES}[ES] \quad 2.11a$$

The net rate of disappearance of the substrate, $-r_{(ES)}$, is represented by Equation 2.12 (Fogler, 2006).

$$-r_{(ES)} = K_{1,ES}[E][S] - K_{2,ES}[ES] \quad 2.12$$

According to the Pseudo-Steady-State Hypothesis (PSSH), the enzyme adsorption and desorption of the substrate are assumed to occur so rapidly that the rate of formation of the enzyme-substrate complex is zero at equilibrium. Equation 2.13 represents the net rate of formation of the enzyme-substrate complex (Fogler, 2006).

$$r_{(ES)} = K_{1,ES}[E][S] - K_{2,ES}[ES] - K_{3,ES}[ES] \quad 2.13$$

Using the PSSH, $r_{(ES)}$ = 0, therefore:

$$[ES] = \frac{K_{1,ES}[E][S]}{K_{2,ES} + K_{3,ES}} \quad 2.14$$

Substituting Equation 2.14 into Equation 2.12 and, after simplification, Equation 2.15 is obtained.

$$-r_{(ES)} = \frac{K_{1,ES}\,K_{3,ES}[E][S]}{K_{1,ES} + K_{3,ES}} \quad 2.15$$

In the absence of enzyme denaturisation, the total concentration of the enzyme in the system [E_T] is constant and equal to the sum of the concentrations of the free, unbonded enzyme [E] and the enzyme-substrate complex [ES] such that:

$$[E_T] = [E] + [ES] \quad 2.16$$

Substituting Equation 2.14 into Equation 2.16 and, after simplification, Equation 2.17 is obtained.

$$[E] = \frac{[E_T](K_{2,ES} + K_{3,ES})}{K_{2,ES} + K_{3,ES} + K_{1,ES}[S]} \quad 2.17$$

Substituting for Equation 2.17 into Equation 2.15, the rate Equation for a single substrate enzymatic reaction is obtained (Equation 2.18).

$$-r_{(ES)} = \frac{K_{1,ES}\, K_{3,ES}[E_T][S]}{K_{1,ES}[S] + K_{2,ES} + K_{3,ES}} \qquad 2.18$$

The division of the numerator and denominator of Equation 2.18 by $K_{1,ES}$, results in Equation 2.19, a form of the Michaelis–Menten equation.

$$-r_{(ES)} = \frac{K_{3,ES}[E_T][S]}{K_m + [S]} \qquad 2.19$$

Where, $K_m = \frac{K_{2,ES} + K_{3,ES}}{K_{1,ES}}$, $K_{3,ES}$ is the number of substrate molecules converted to product during a given time period on a single-enzyme molecule when the enzyme is saturated with substrate. It is also referred to as the turnover number. K_m is the Michaelis-Menten constant, also termed the affinity constant. The constant K_m (mmol.L^{-3}) is a measure of the attraction of the enzyme to its substrate.

Let $V_{\max} = K_{3,ES}[E_T]$, where V_{max} represents the maximum rate of reaction for a known enzyme concentration. When substituted into Equation 2.19, the common form of the Michaelis–Menten equation is obtained, as seen in Equation 2.20.

$$-r_{(ES)} = \frac{V_{\max}[S]}{K_m + [S]} \qquad 2.20$$

If the substrate concentration [S] is sufficiently small (K_m >> [S]), its contribution to the denominator is negligible:

$$-r_{(ES)} \cong \frac{V_{\max}[S]}{K_m} \qquad 2.21$$

The kinetics, therefore, become first order with respect to the limiting substrate concentration. At high substrate concentrations ([S]) >> K_m), the reaction rate becomes zero order:

$$-r_{(ES)} \cong V_{\max} \qquad 2.22$$

The most commonly used microbial growth rate expression in a batch system is the Monod equation (Equation 2.23).

$$r_X = \frac{dX}{dt} = (\mu - K_d)X \qquad 2.23$$

If $\mu >> K_d$ then Equation 2.23 can be simplified to Equation 2.24.

$$r_X = \frac{dX}{dt} = \mu X \qquad 2.24$$

The proportional constant μ is known as the specific cell growth rate (s^{-1}). A suitable method to determine the kinetic parameters for a microbial culture is to run a one stage, continuous stirred tank bioreactor at steady-state with different dilution rates (Doran, 1995). If the bioreactor is fed with sterile nutrients under steady-state conditions, cell death and accumulation of cells may be assumed to be negligible compared to the growth rate. Thus, it may be shown that the specific microbial growth rate is equal to the dilution rate because, in a bioreactor, cells are removed at a rate equivalent to the growth rate and the cell growth rate is equal to the dilution rate. Therefore, any specific growth rate may be determined for different feed substrate concentrations by changing the feed flow rate of the bioreactor. The specific cell growth rate may be expressed in the form of Equation 2.25 for a continuous stirred tank reactor (CSTR), only if the microorganism's growth is described by Monod kinetics.

$$\mu = \frac{\mu_{\max}[S]}{K_m + [S]} \qquad 2.25$$

Where μ_{max} is the maximum specific growth rate (s^{-1}), K_m is the Monod constant ($mmol.L^{-3}$), similar to and based on the Michaelis–Menten kinetics for enzymes. Monod kinetics assumes that bacteria cells may be considered as a group of enzymes to which Michaelis–Menten kinetics may be applied.

However, Equation 2.25 cannot be used for a batch culture CSTR and therefore Equation 2.26 must be utilised instead.

$$V_r \frac{dX}{dt} = \mu X V_r - K_d X V_r + F X_0 - F X \qquad 2.26$$

If at steady state μ >> K_d then $V_r \frac{dX}{dt}$=0 with a sterile feed and X_0=0. Therefore, $0 = \mu X - \frac{FX}{V_r}$ and since $\frac{F}{V_r} = D$ then:

$$D = \mu = \frac{\mu_{\max}[S]}{K_m + [S]} \quad 2.27$$

The stoichiometry for cell growth is extremely complex due to the variety of microorganisms, nutrient media used and environmental conditions, including pH, aeration rate, temperature and redox potential. In general, the stoichiometric growth equation may be expressed in the form highlighted in Equation 2.28.

$$Cells + Substrate \longrightarrow More\ cells + \text{Pr}oduct \quad 2.28$$

Monod proposed a microbial yield coefficient which is defined as the ratio of the cell growth rate to the substrate consumption rate. The yield coefficient for cells and substrate is:

$$Y_{X/S} = \frac{Cell\ growth\ rate}{Substrate\ consumption\ rate} = \frac{dX/dt}{dS/dt} \quad 2.29$$

The kinetics of microbial ferrous-iron oxidation are derived from the Monod equation. For the limiting substrate concentration, the specific growth rate kinetics of ferrous-iron oxidation may be expressed according to Equation 2.30 (Monod, 1942).

$$\mu = \frac{\mu_{\max}[Fe^{2+}]}{K_{Fe^{2+}} + [Fe^{2+}]} \quad 2.30$$

Where the specific growth rate, (μ), and maximum specific growth rate, (μ_{max}), for the limiting substrate (i.e. ferrous iron) have the units (h^{-1}), [Fe^{2+}] is the concentration of the limiting substrate (mmol.L^{-1}) and $K_{Fe^{2+}}$ is the affinity constant (mmol.L^{-1}). The microbial cell growth rate, r_X (mmol C.$L^{-1}h^{-1}$), is directly proportional to the microbial population, C_X, as shown in Equation 2.31.

$$r_X = \frac{dC_X}{dt} = \mu C_X \quad 2.31$$

Equation 2.31 and the yield coefficient have been previously defined in Equations 2.24 and 2.29, respectively. If the microbial yield is based on the amount of ferrous-iron consumed,

(i.e. oxidation of [Fe^{2+}]), the yield coefficient may be obtained from the ratio of cell growth rate to the rate of ferrous-iron oxidation $r_{Fe^{2+}}$. Similar equations for cell yield based on oxygen consumption are shown in Equations 2.32 and 2.33.

$$-r_{Fe^{2+}} = \frac{1}{Y_{Fe^{2+}X}} r_X \qquad 2.32$$

$$-r_{O_2} = \frac{1}{Y_{O_2X}} r_X \qquad 2.33$$

Where r_{O_2} is the rate of oxygen utilisation and Y_{O_2X} is the cell yield per mole of oxygen consumed. Both Equations 2.32 and 2.33 have been found to be inadequate for explaining the observed microbial cell growth rate. Thus, Herbert (1958) suggested that the presence of endogenous metabolisms in growing bacteria, which is equivalent to a maintenance energy requirement, may account for the yield variation in the growth rate. As a result, the endogenous metabolism was accounted for by a modification of the growth rate law. According to Pirt (1965), the two main causes of energy consumption by microbes during substrate utilisation are (1) energy required for maintenance processes within the microbes, and (2) energy required for microbial growth. Maintenance energy is utilised in non-growth associated processes, including turnover of cell material, cell motility, adjustment of cell membrane potential and other endogenous metabolisms. Therefore, the rate of substrate utilisation or consumption by microbes was modified by Pirt to incorporate the maintenance term as shown in Equation 2.34. Pirt's concept was first applied to microbial ferrous-iron oxidation by Boon (1995).

$$-r_{Fe^{2+}} = \frac{1}{Y^{\max}_{Fe^{2+}X}} r_X + m_{Fe^{2+}} C_X \qquad 2.34$$

Simplifying,

$$\frac{-r_{Fe^{2+}}}{r_X} = \frac{1}{Y^{\max}_{Fe^{2+}X}} + m_{Fe^{2+}} \frac{C_X}{r_X} \qquad 2.35$$

Substitution of Equations 2.31 and 2.32 into Equation 2.35, followed by simplification, results in Equation 2.36.

$$\frac{1}{Y_{Fe^{2+}X}} = \frac{1}{Y^{\max}_{Fe^{2+}X}} + \frac{m_{Fe^{2+}}}{\mu} \qquad 2.36$$

Furthermore, by substituting the value of r_X from Equation 2.31 into Equation 2.34, Equations 2.37 and 2.38 can be derived.

$$-r_{Fe^{2+}} = C_X\left(\frac{1}{Y^{\max}_{Fe^{2+}X}}\mu + m_{Fe^{2+}}\right) \quad 2.37$$

$$q_{Fe^{2+}} = \frac{-r_{Fe^{2+}}}{C_X} = \frac{\mu}{Y^{\max}_{Fe^{2+}X}} + m_{Fe^{2+}} \quad 2.38$$

Where $Y_{Fe^{2+}X}$ is the observed growth yield (i.e. mass of cell per mass of substrate consumed $^{-1}$), $Y^{\max}_{Fe^{2+}X}$ is the maximum microbial yield or true growth yield (i.e. mass of cell per mass of substrate consumed^{-1}), μ is the specific microbial growth rate (h^{-1}), $q_{Fe^{2+}}$ is the specific rate of substrate utilisation (i.e. mol of substrate consumed per mol of cell per hour), and $m_{Fe^{2+}}$ is the maintenance coefficient, which is the specific substrate utilisation rate for maintenance activities (i.e. mass of substrate consumed per mass of cell per hour).

However, for a continuous culture at steady state, the parameters, μ_{max}, $K_{Fe^{2+}}$, $Y^{\max}_{Fe^{2+}X}$ and $m_{Fe^{2+}}$, are characterised under a continuous mode at various dilution rates. These values may be calculated if the steady state substrate (i.e. Fe^{2+}) and cell concentrations (C_X) are known at different dilution rates because, as explained in Section 2.9, for a continuous culture at steady state, μ is equal to the dilution rate (D). The kinetic parameters, μ_{max} and $K_{Fe^{2+}}$, may be determined graphically by linearising the appropriate governing equation. For example, using the Monod type Equation 2.30, the Lineweaver-Burk, Eadie-Hofstee and Langmuir plots may be plotted to obtain the required kinetic parameters. Linearisation of the Monod-type Equation 2.30 by the Lineweaver-Burk method (Lineweaver and Burk, 1934) is given by Equation 2.39.

$$\frac{1}{D} = \frac{K_{Fe^{2+}}}{\mu_{\max}}\left(\frac{1}{[Fe^{2+}]}\right) + \frac{1}{\mu_{\max}} \quad 2.39$$

Thus, by plotting 1/D versus $1/[Fe^{2+}]$, μ_{max} may be obtained from the intercept and $K_{Fe^{2+}}$ from the slope of the resulting straight line, as depicted in Figure 2.7a. Linearisation of the Monod type Equation 2.30 by the Eadie-Hofstee method (Hofstee *et al.*, 1959) is given by Equation 2.40.

$$\frac{D}{[Fe^{2+}]} = \frac{\mu_{max}}{K_{Fe^{2+}}} - \frac{D}{K_{Fe^{2+}}} \qquad 2.40$$

Plotting D/[Fe^{2+}] versus D gives a straight line with a slope of $-1/K_{Fe^{2+}}$ and an intercept of $\mu_{max}/K_{Fe^{2+}}$, as shown in Figure 2.7b. Using the Langmuir method (Verger and De Haas, 1976), linearisation of the Monod equation is given by Equation 2.41.

$$\frac{[Fe^{2+}]}{D} = \frac{K_{Fe^{2+}}}{\mu_{max}} + \frac{[Fe^{2+}]}{\mu_{max}} \qquad 2.41$$

Plotting [Fe^{2+}]/D versus [Fe^{2+}] gives a straight line with the slope $1/\mu_{max}$ and intercept $K_{Fe^{2+}}/\mu_{max}$, as shown in Figure 2.7c.

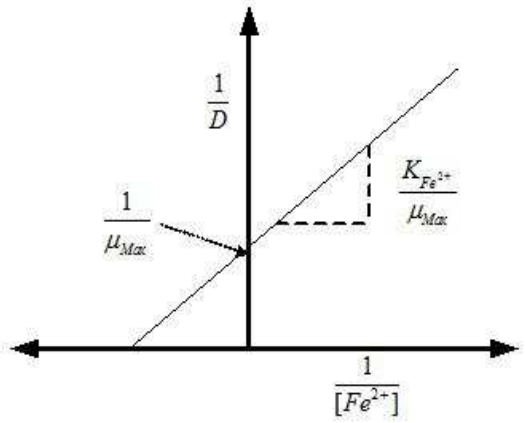

a. Lineweaver-Burk plot

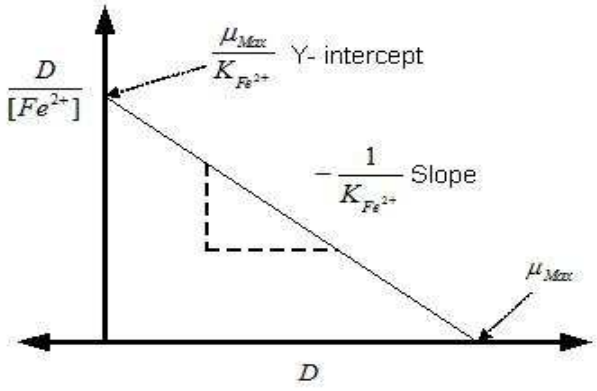

b. Eadie-Hofstee plot

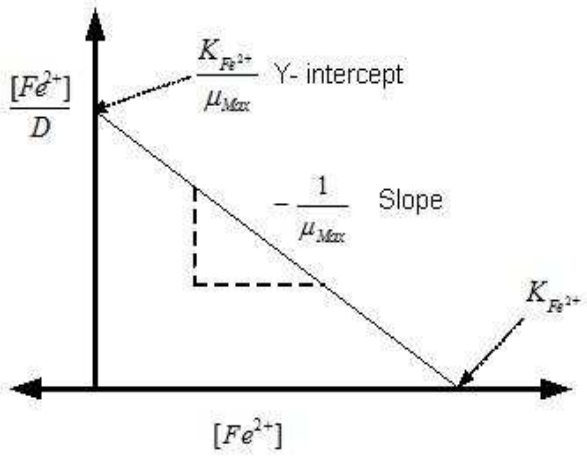

c. Langmuir plot

Figure 2.7: Linearised Monod equation using (a) the Lineweaver-Burk method, (b) the Eadie-Hofstee method, and (c) the Langmuir method

2.8 Development of the fundamental rate equation for microbial ferrous-iron oxidation

Various kinetic equations for microbial ferrous-iron oxidation have previously been proposed (Ojumu *et al.*, 2006; Nemati *et al.*, 1998; Boon *et al.*, 1995; Kelly and Jones, 1978; Lacey and Lawson, 1970). A number of published rate equations for ferrous-iron biooxidation are presented in Table 2.3. As reported by Ojuma *et al*. (2006), most of these kinetic equations may be applied to the same set of experimental data while most of these kinetic equations have been developed from the basic enzymatic equation for growth rate based on the limiting substrate concentration, which is a Monod-type model:

$$-r_{Fe^{2+}} = \frac{r_{Fe^{2+}}^{\max}[Fe^{2+}]}{K_{Fe^{2+}} + [Fe^{2+}]} \qquad 2.42$$

Table 2.3: Selected published kinetic models for ferrous-iron oxidation with *At. ferrooxidations*

Model	Conditions
$\mu = \frac{\mu_{max}[Fe^{2+}]}{Y_{SX}K_m + [Fe^{2+}]}$	Batch STR, T = 25–30 °C, pH = 2–2.3, Fe_T = 6 g.L^{-1}
$\mu = \frac{\mu_{max}[Fe^{2+}]}{K_m + [Fe^{2+}]}$	Continuous, T = 28 °C, pH = 2.2
$\mu = \frac{\mu_{max}[Fe^{2+}]}{[Fe^{2+}] + K_m\left(1 + \frac{[Fe^{3+}]}{K_i}\right)}$	Continuous, T = 30 °C, pH = 1.6, Fe_T = 5–400 mM
$\mu = \frac{\mu_{max}\left([Fe^{2+}] - [Fe^{2+}]_t\right)}{K_m + \left([Fe^{2+}] - [Fe^{2+}]_t\right)}$	Continuous, T = 22 °C, Fe_T = 9–22 mM, Isolate AKI
$\mu = \frac{\mu_{max}[Fe^{2+}]}{[Fe^{2+}] + K_S\left(1 + K_i[Fe^{3+}]\right)}$	Continuous, T = 35 °C, pH = 1.8, Fe_T = 0.52–3.29 g.L^{-1}
$-r_{O_2} = \frac{k_3'[X][Fe^{2+}]}{[Fe^{2+}] + K_m\left[1 + \frac{[X]}{K_i'} + \frac{[Fe^{3+}]}{K_{if}} + \frac{[X][Fe^{3+}]}{\alpha K_i' K_{if}}\right]}$	Initial Rate, T = 29 °C, pH = 1.8–2.0, Fe_T = 0.25–26 mM
$\mu = \frac{\mu_{max}[Fe^{2+}]}{[Fe^{2+}] + K_S + [Fe^{3+}]\frac{K_S}{K_i} + \frac{([Fe^{2+}])^2}{K_{Si}}}$	Continuous, T = 29 °C, pH = 1.8–2.0, Fe_T = 2–70.8 g.L^{-1}
$-r_{Fe^{2+}} = a_1\left(\frac{\rho O_2}{k_B + \rho O_2}\right)\left(\frac{[Fe^{2+}]}{[Fe^{2+}] + K_{Fe^{2+}}\left(1 + \frac{[Fe^{3+}]}{K'}\right)}\right)$	Continuous, T = 30 °C, pH = 2.0, *Leptospirillum ferrooxidans*
$-r_{Fe^{2+}} = k\left(\frac{[Fe^{2+}]/[H^+]}{K_{Fe^{2+}} + [Fe^{2+}]/[H^+] + K_i[Fe^{3+}]}\right)^{0.5}\left(\frac{\rho O_2}{k_B + \rho O_2}\right)^{0.5}$	Theoretical, fitted to data from Huberts (1994)
$q_{Fe^{2+}} = \frac{q_{Fe^{2+}}^{max}}{1 + K_{Fe^{2+}}\frac{[Fe^{3+}]}{[Fe^{2+}]}}$	Only *Leptospirillum* fitted to data
$\frac{d[Fe^{2+}]}{dt} = \frac{K_0 e^{-\frac{E_a}{RT}}[X][Fe^{2+}]}{\left(1 + \frac{[Fe^{3+}]}{K_i}\right)\left(K_m + [Fe^{2+}]\right)}$	Initial Rate, T = 29 °C, pH = 2.0, Fe_T = 0.45–31.5 Kg.m^{-3}
$q_{O_2} = \frac{q_{O_2}^{max}}{1 + \frac{K_S}{[Fe^{2+}] - [Fe^{2+}]_t} + \frac{K_S}{K_i}\cdot\frac{[Fe^{3+}]}{[Fe^{2+}] - [Fe^{2+}]_t}}$	Continuous, T = 30 °C, pH = 1.8–1.9, Fe_T = 0.05–0.36 M
$q_{Fe^{2+}} = \frac{K_1^* \exp\left[\frac{nF}{2RT}\left(E^m - E_h^0\right)\right]\left\{1 - \exp\left[\frac{nF}{RT}(E^m - E)\right]\right\}}{1 + \frac{K_2^*}{[Fe^{2+}]} + K_3^* \exp\left[\frac{nF}{RT}\left(E_h - E_h^0\right)\right]}$	Electrochemical cell, T = 30 °C, pH = 1.8, Fe_T = 0.05–1 g.L^{-1}

Source: Adapted from Ojumu *et al.*(2006)

A simplified version of the Jones and Kelly model (1983), and presented by Boon, Hansford and co-workers (Hansford and Vargas, 2001; Hansford, 1997; Boon *et al.*, 1995) has been suggested as appropriate to describe the microbial ferrous-iron oxidation kinetics in terms of the ferric-to-ferrous ratio − see Equation 2.43.

$$q_{Fe^{2+}} = \frac{q_{Fe^{2+}}^{\max}}{1 + K'_{Fe^{2+}} \dfrac{[Fe^{3+}]}{[Fe^{2+}]}} \qquad 2.43$$

Where $q_{Fe^{2+}}$ is the specific ferrous-iron oxidation rate, $q_{Fe^{2+}}^{max}$ is the maximum specific ferrous-iron oxidation rate, and $K'_{Fe^{2+}}$ the apparent affinity constant for the Hansford model. These parameters may be determined by fitting an experimental set of data to the equation using the least squares method, or from the corresponding Lineweaver–Burk plot.

2.9 A theoretical development of the kinetic model of microbial ferrous-iron oxidation

In order to determine the kinetic and yield parameters for a Fe^{2+} oxidising culture, the overall cell and substrate mass balances must be established for a packed reactor at different residence times. The following general assumptions are must considerate:

- As a result of high aeration within the bioreactor, intensive mixing occurs and, therefore, homogeneous mixing of the liquid in the bioreactor is achieved.
- The reaction is carried out at constant temperatures and constant substrate concentration.
- The total active reactor volume remains constant.
- In a packed bioreactor the micro-organisms grow in the liquid within the bioreactor and are uniformly immobilised on the surface of the inert matrix (i.e. packing) in the bioreactor as a monolayer of constant thickness.
- The process is a continuous and steady-state regime is maintained.
- The death cell rate is negligible, when compared to the growth rate.
- At steady state conditions, the cell concentration is constant since the rate of cell removal is equal to the rate of cell growth. The growth rate is significantly lower than the rate of biochemical reaction and, therefore, this assumption is valid for a small time period in biofilm reactors.
- The culture is substrate-limited with respect to Fe^{2+}.
- The feed solution is sterile, free of microbial biomass and no growth inhibition compounds are present.

- There is no diffusion limitation of the substrate. In a thin biofilm, the limiting substrate concentration drop across the film is negligible and, therefore, has a negligible effect on diffusion.
- Limited kinetic changes occur in the reactor after fixation of the micro-organisms.

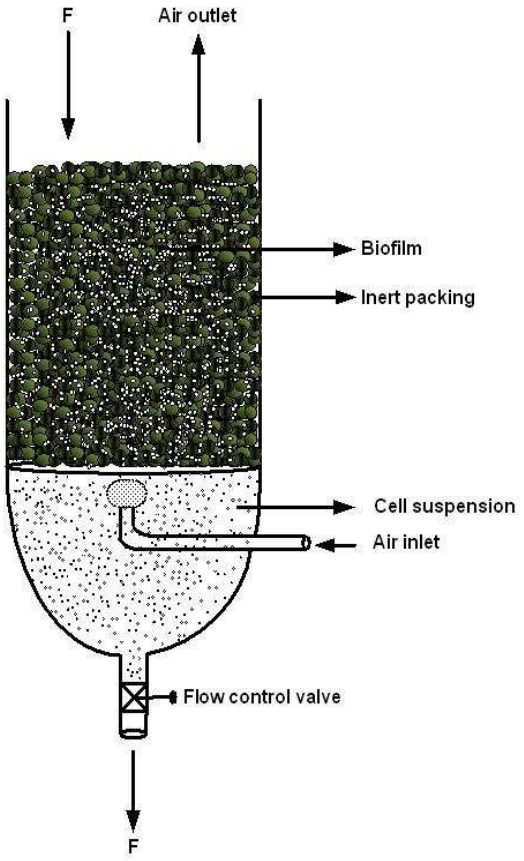

Figure 2.8: Schematic diagram of ideal pack bioreactor

Figure 2.8 is a schematic diagram representing an ideal packed bioreactor. F is the inlet and outlet flow rate. Based on the assumptions listed above, a mathematical model has been developed for the packed bioreactor. The kinetics of the ferrous-iron oxidising culture may be determined by performing a mass balance for the cell and substrate over the bioreactor at different residence times (Sundkvist *et al.*, 2007; Boon *et al.*, 1995). If the bioreactor, which is being operated under steady-state conditions, is fed with sterile nutrient medium, both the cell death and accumulation of cell are negligible when compared to the growth rate. Accordingly, it may be shown that the specific microbial growth rate is equal to the dilution rate, since the cell is removed at a rate equal to the growth rate and the growth rate is equal to the dilution rate. At steady state conditions, the material balance equation for any reactor is described by Equation 2.44.

Accumulation = In – Out + Generation 2.44

The overall cell balance for an active microbial cell in a packed bioreactor over time is given by the following Equation 2.45:

$$V_{AR}\frac{dC_X}{dt} = FC_{X_0} - FC_X + \mu C_X V_{AR} - K_d C_X V_{AR} \quad 2.45$$

Where V_{AR} is the reactor active volume (L), (V_{AR} = Volume of the reactor – Total volume of the inert packing), F is the inlet and outlet flow rate, ($L.h^{-1}$); C_X is the bacterial concentration, (mmol $C.L^{-1}$), and μ and K_d are the specific growth and death rate constants, respectively, (h^{-1}). K_d implies that cell death and lysis are the primary mechanisms of mass reduction. Assuming that the feed is sterile, (C_{X_0}=0), then the death rate negligible, (K_d=0), and, if the system is at steady state, ($\frac{dC_X}{dt}$=0), then Equation 2.45 is converted to Equation 2.46.

$$\mu = \frac{F}{V_{AR}} = D = \frac{1}{\tau} \quad 2.46$$

Where D is the dilution rate and τ (h) the residence time.

However, for the overall substrate balance, the amount of Fe^{2+} in the packed bioreactor at a given time is represented by Equation 2.47.

$$\tau = \frac{V_{AR}}{v_0} = [Fe^{2+}]_{In}\int_0^X \frac{dX}{-r_S} = \int_{[Fe^{2+}]_{Out}}^{[Fe^{2+}]_{In}} \frac{d[Fe^{2+}]}{-r_{Fe^{2+}}} \quad 2.47$$

The Monod Equation 2.30 may further be simplified by substituting for μ as follows:

$$[Fe^{2+}]_{In} - [Fe^{2+}]_{Out} = [Fe^{2+}] = \frac{DK_{Fe^{2+}}}{\mu_{\max} - D} \quad 2.48$$

The Monod equation, indicated by Equation 2.42, may be simplified by substituting as follows $r_{Fe^{2+}} = q^{\max}_{Fe^{2+}} C_X$:

$$-r_{Fe^{2+}} = \frac{q^{\max}_{Fe^{2+}} C_X [Fe^{2+}]}{K_{Fe^{2+}} + [Fe^{2+}]} \quad 2.49$$

Cell concentration, (C_X), in the packed reactor may be determined by Equation 2.47, but it may be further simplified by substituting Equations 2.48 and 2.49:

$$C_X = \frac{D}{q_{Fe^{2+}}^{\max}}\left(K_{Fe^{2+}} \log[Fe^T] + [Fe^T] - K_{Fe^{2+}} \log\frac{DK_{Fe^{2+}}}{\mu_{\max} - D} - \frac{DK_{Fe^{2+}}}{\mu_{\max} - D}\right) \quad 2.50$$

The Hansford Equation 2.43 may be further simplified by substituting $q_{Fe^{2+}} = D$ and $q_{Fe^{2+}}^{\max} = D^{\max}$:

$$[Fe^{2+}] = \frac{DK'_{Fe^{2+}}[Fe^T]}{D^{\max} - D\left(1 - K'_{Fe^{2+}}\right)} \quad 2.51$$

At steady state conditions, the Hansford Equation 2.43 may be further simplified to Equations 2.52 and 2.53 by multiplying Equation 2.43 with the cell concentration (C_X). This is approached by minimising the ferric-iron precipitation in the packed column.

$$-r_{Fe^{2+}} = \frac{q_{Fe^{2+}}^{\max} C_X}{1 + K'_{Fe^{2+}} \dfrac{[Fe^{3+}]}{[Fe^{2+}]}} \quad 2.52$$

$$-r_{Fe^{2+}} = \frac{r_{Fe^{2+}}^{\max}}{1 + K'_{Fe^{2+}} \dfrac{[Fe^{3+}]}{[Fe^{2+}]}} \quad 2.53$$

Where $-r_{Fe^{2+}}$ is the ferrous-iron oxidation rate and $r_{Fe^{2+}}^{max}$ is the maximum overall ferrous-iron oxidation rate. Cell concentration, (C_X), in the packed reactor may be determined from Equations 2.47, 2.51 and 2.52 for a packed-bed system,

$$C_X = \frac{D}{q_{Fe^{2+}}^{\max}}\left[[Fe^T]\left\{K'_{Fe^{2+}}\left(\log[Fe^T] - \log\frac{DK'_{Fe^{2+}}[Fe^T]}{D^{\max} - D(1 - K'_{Fe^{2+}})} - 1\right) + 1\right\} + \log\frac{DK'_{Fe^{2+}}[Fe^T]}{D^{\max} - D(1 - K'_{Fe^{2+}})}(1 - K'_{Fe^{2+}})\right] \quad 2.54$$

The detailed derivation of Equations 2.50 and 2.54 is shown in Appendix A1.1. Figure 2.9 depicts the variation of cell concentration with dilution rate for a packed bioreactor as predicted by Equations 2.50 and 2.54. The parameters, μ_{max}, $K_{Fe^{2+}}$, $K'_{Fe^{2+}}$, $q_{Fe^{2+}X}^{max}$ and D^{max}, are established by reasonable assumption. This plot (Figure 2.9) shows that, initially, the cell concentration increased with increasing dilution rate and then declined sharply as the system approached the washout region.

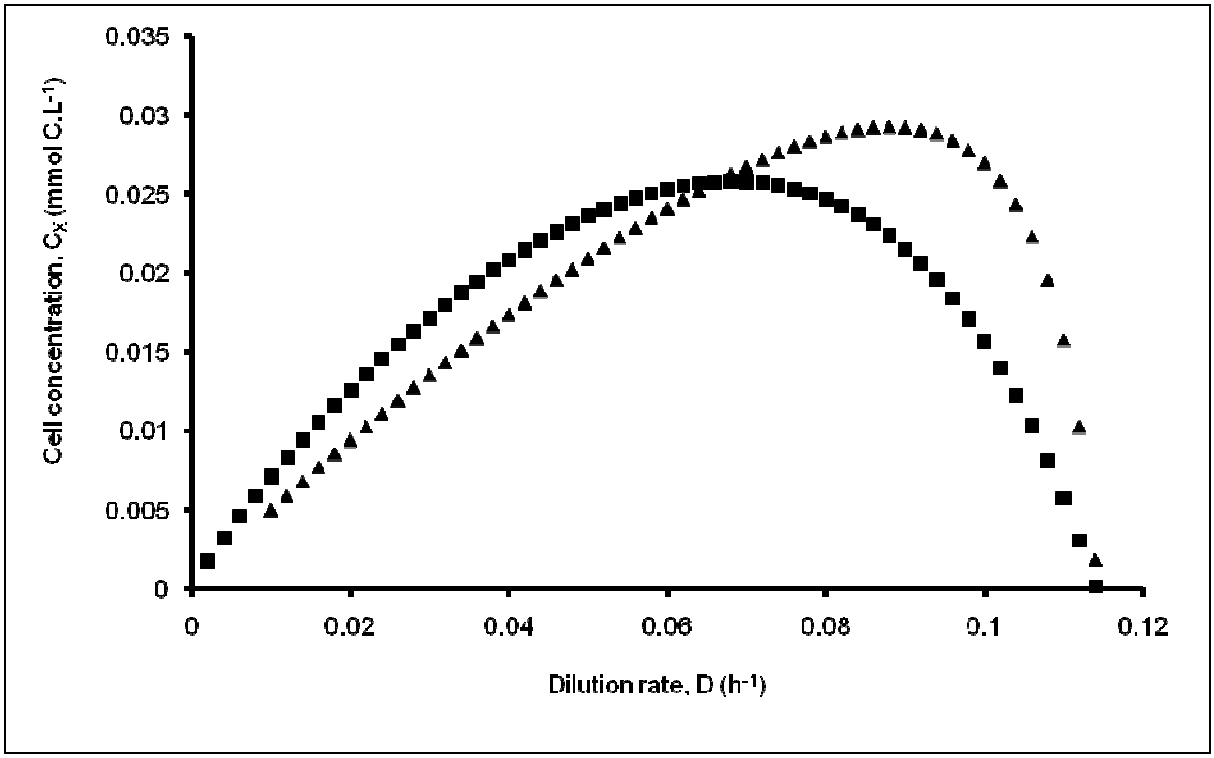

Figure 2.9: Predicted cell concentration as a function of the dilution rate based on both the Hansford model (▲) and the Monod model (■)

2.10 Effects of relevant parameters on microbial ferrous-iron oxidation

Various parameters affect the rate of ferrous iron biooxidation. Thus, several parameters, including temperature (Ojumu *et al.*, 2009; Franzmann *et al.*, 2005), solution pH (Ojumu and Petersen, 2011; Plumb *et al.*, 2008; Özkaya *et al.*, 2007), accumulation of jarosite (Daoud and Karamanev, 2006; Pogliani and Donati, 2000; Grishin *et al.*, 1988), and the effect of packing height and size (Mazuelos *et al.*, 2001) have been the subject of previous studies. Nevertheless, the parameters affecting the rate of ferrous iron bio-oxidation are not limited to those mentioned above and there are other factors that may have a significant effect on ferrous iron bio-oxidation. These factors have, however, received considerably less attention than those listed previously. The following subsections will provide as much as possible a brief discussion of parameters affecting ferrous iron bio-oxidation.

2.10.1 Effect of operating temperature

Ferrous-iron oxidation rates are affected by temperature which is, in turn, a major selective operating parameter for the organisms and which may inhabit a bioleaching operation. Microorganisms are classified in terms of the temperature range in which they are able to survive, namely, mesophiles within the temperature range of 15 to 40 °C, moderate thermophiles between 45 and 50 °C, thermophiles at approximately 65 °C and extreme thermophiles at above 65 °C. Microorganisms subjected to temperatures below their optimum operating temperature become inactive, and are destroyed rapidly when subjected

to temperatures above their optimum operating temperatures − see Figure 2.10 for the iron oxidising microorganisms. Franzmann *et al*. (2005) have indicated the physiological operating window of common bioleaching organisms found in bioleach heaps.

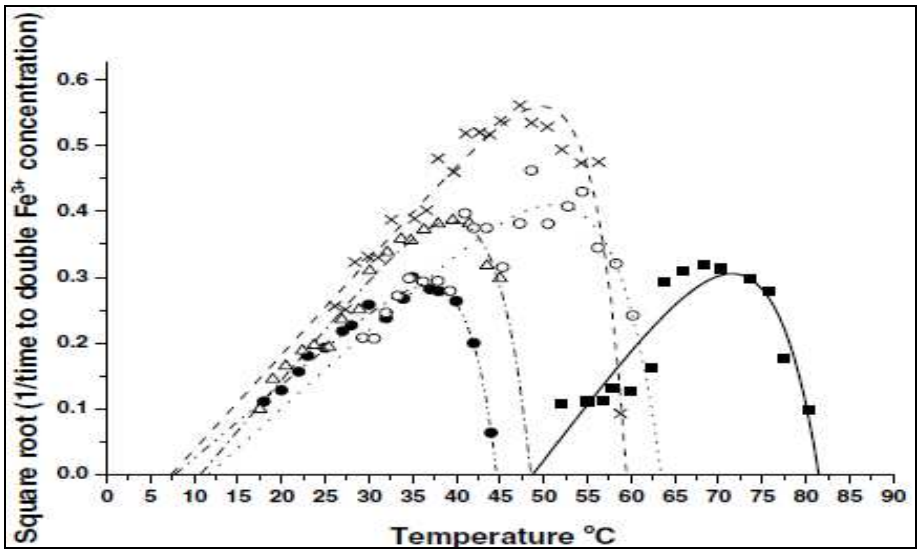

Figure 2.10: Ratkowsky plots showing the relationship of temperature to the oxidation of iron for a range of common bioleaching organisms *L. ferrooxidans* (●), *L. ferriphilum* (∆), *Acidimicrobium ferrooidans* (X), *Sulfobacillus thermosulfidooxidans* (O), *Acidianus brierleyi* (■) (Franzmann *et al.*, 2005)

If any commercial bioleaching process is to achieve the full bioleaching capability of a particular organism, it is important that the temperature is maintained within its physiological operating range, and preferably near is optimal temperature. Temperature has a profound effect on the bioleaching rate of primary and secondary sulphides ores (Stott *et al.*, 2003; Dixon, 2000). It is a well known phenomenon that higher temperatures increase the chemical reaction rates. The maximal measured rates of iron or sulphur oxidation for each of the organisms, and the temperature at which each rate was achieved, are presented in Table 2.4.

Table 2.4: Measured reaction rates for sulphur oxidation and iron oxidation by common bioleaching organisms and the temperature at which those rates were measured (Franzmann *et al*., 2005)

Organism	Substrate	Fastest observed reaction rate [a]	Temperature (°C)
L. ferrooxidans	Fe^{2+}	0.06 (h^{-1})	35.0
L. ferriphilum	Fe^{2+}	0.10 (h^{-1})	39.6
Ferroplasma acidiphilum	Fe^{2+}	44 (mg $Fe^{2+}.L^{-1}h^{-1}$)	35.5
Acidmicrobium ferrooxidans	Fe^{2+}	0.22 (h^{-1})	47.3
Sufobacillus thermosulfidooxidans	Fe^{2+}	0.15 (h^{-1})	48.6
Ferroplasma cyprexacervatum	Fe^{2+}	115 (mg $Fe^{2+}.L^{-1}h^{-1}$)	51.6
Acidianus brierleyi	Fe^{2+}	0.07 (h^{-1})	68.3
At. Ferrooxidans	S^0	6.1 (mg SO_4–S.L^{-1} h^{-1})	31.0
At. Thiooxidans	S^0	39.3 (mg SO_4–S.L^{-1} h^{-1})	32.4
At. Caldus	S^0	25.4 (mg SO_4–S.L^{-1} h^{-1})	45.9
Sulfolobus metallicus	S^0	35.9 (mg SO_4–S.L^{-1} h^{-1})	71.0
Acidianus brierleyi	S^0	20.5 (mg SO_4–S.L^{-1} h^{-1})	79.3

[a] S^0 was oxidised in a reaction with zeroth-order kinetics while Fe^{2+} was oxidised in a reaction with first-order kinetics, with the exception of Fe^{2+} oxidation by *Ferroplasma* spp.

According to Fogler (2006), the effect of temperature on a reaction rate may be described using Arrhenius Equations 2.55 and 2.56. Several researches have shown that, for most of the microbial species found in tank and heap bioleaching environments, the effect of temperature on the maximum oxidation rate. ($r_{Fe^{2+}}^{max}$), may be described using these equations (Ojumu *et al*., 2009; Franzmann *et al*., 2005; Breed *et al*., 1999; Nemati and Webb, 1997).

$$r_{Fe^{2+}}^{\max} = K_0 \exp\left(-\frac{E_a}{RT}\right) \qquad 2.55$$

$$\ln r_{Fe^{2+}}^{\max} = -\frac{E_a}{R}\left(\frac{1}{T}\right) + \ln K_0 \qquad 2.56$$

The activation energy (E_a) and the frequency factor (K_0) for microbial ferrous-iron oxidation kinetics may be obtained from the plot of $ln\, r_{Fe^{2+}}^{max}$ versus1/T. The plot should give a straight line with a slope of $-E_a/R$ and an intercept of $ln\, K_0$, from which the E_a and K_0 values may be established, given that R is the gas constant (8.314 $J.mol^{-1}K^{-1}$). It should be noted that the Arrhenius equation was developed to describe the effect of temperature on the rates of purely chemical reactions, not biologically catalysed reactions that are subjected to enzyme denaturisation with increasing temperatures. Accordingly, it is not possible to fit the Arrhenius equation to oxidation rate data at temperatures above the optimum temperature for microbial growth. Different values of activation energy, ranging from 20 to 96 $kJ.mol^{-1}$, have been reported in the literature (De *et al.*, 1996; Leduc *et al.*, 1993; Ahonen and Tuovinen,

1989; Ferroni *et al.*, 1986; Guay *et al.*, 1977; Lundgren, 1975; Lacey and Lawson, 1970; MacDonald and Clark, 1970). The variation in reported values may have resulted from different monitoring approaches, while differences in microbial strain and experimental conditions may also be responsible for the variations.

Higher values of activation energy indicate a limitation in the biochemical reaction at low temperatures and not diffusion control, which is associated with lower values of activation energy. Ahonen and Tuovinen (1989) obtained an activation energy of 83 kJ.mol^{-1}, which is suggestive of biochemical limitation at low temperatures. Similarly De (1993) and De *et al*. (1996) reported a value of 49.82 kJ.mol^{-1} for the activation energy (E_a) in the temperature range of 5 to 18°C, which was suggestive of a chemical controlled reaction.

In contrast, another study carried out by De (1993) and De *et al*. (1996) in the temperature range of 5 to 25 °C reported a value of 20.93 kJ.mol^{-1} for the activation energy, which suggested that the reaction was diffusion controlled (De *et al.*, 1996; De, 1993). The range of activation energies summarised from previous studies may be represented by: Diffusion ≤ 20 kJ.mol^{-1} < Both Biochemical and Diffusion < 42 kJ.mol^{-1} ≤ Biochemical/Chemical (De *et al.*, 1997; 1996; De, 1993; Leduc *et al.*, 1993; Ahonen and Tuovinen, 1989; Ferroni *et al.*, 1986; Verbaan and Crundwell, 1986; Chmielewski and Charewicz, 1984; Guay *et al.*, 1977; Lundgren, 1975; Lacey and Lawson, 1970; MacDonald and Clark, 1970).

2.10.2 Effect of solution pH

The solution pH greatly affects the availability of the ferric ion reagent for the leaching of most sulphide minerals. A high solution pH not only inhibits the acidiophilic microorganisms but may also lead to ferric-ion precipitation within the heap bed, thus reducing heap permeability. In bioleaching, it is also important to keep iron in solution by preventing the precipitation of ferric ion as either hydroxyl and/or sulphate complexes, as the latter may reduce the amount of ferric ion in the leaching medium. Researchers have shown that variations in the pH of the solution in the bioreactor, with a pH of 0.9 - 1.7, have no significant effect on the microbial growth and ferrous-iron oxidation by iron oxidizing microbes when operated under normal conditions (Kinnunen and Puhakka, 2005; Breed and Hansford, 1999). According to Kinnunen and Puhakka (2005), the ferrous-iron oxidation rate by *L. ferriphilum* is significantly inhibited at pH ≤0.7. However, Breed and Hansford (1999) reported that the kinetic constant increases linearly with an increase in pH from 1.10 to 1.70.

According to Coram and Rawlings (2002), the optimum pH for growth of *L. ferriphilum* is between pH 1.4 and 1.8. However, the study conducted by Plumb *et al*. (2008) focused on the measurement of microbial activity rather than on microbial growth. Plumb *et al*. (2008)

reported that *L. ferriphilum* exhibited a broad optimum pH range, peaking at pH 2.0. Plumb *et al.* (2008) also noted that a moderate Fe^{2+} oxidation rate occurred at pH 3.0 and pH 3.5. However, at pH 3.0 and pH 3.5 the precipitation of jarosite made the quantification of the cell impossible. Other studies have shown that the microbial growth on ferrous-iron is negatively affected at pH greater than 2.0 (Du Plessis *et al.*, 2007; Van Aswegen *et al.*, 2007). At a higher pH, ferric iron readily precipitates, and this has a negative effect on bioleaching application (Halinen *et al.*, 2009; Meruane *et al.*, 2002). On the other hand, Crundwell (1997) postulated that the effect of a higher pH on ferrous ion results in the formation of an insoluble $Fe(OH)^{+}$ complex, which is pH dependent and which adsorbs onto the microbes. In contrast, several studies have shown that microbial ferrous iron oxidation may be achieved at pH 0.9 (Özkaya *et al.*, 2007; Kinnunen and Puhakka, 2005) and that this phenomenon of increased tolerance at lower pH may be attributed to the adaptation of the microbial species. Although there seems to be no definite optimum pH, the resistance of iron oxidising microbes to low pH was attributed to the composition of the cell walls of the iron oxidising microorganisms. At extremely low pH the cell may require more energy to maintain proton gradient, since the cell cytoplasm must be maintained at or near neutral values, thus cell maintenance may be at the expense of cell growth.

2.10.3 Accumulation of jarosite

It should be recalled that an acidic environment is critical to ferrous-iron biooxidation. However, the acidic dissolution of gangue minerals may lead to an increase in the solution pH within the heap. Consequently, the condition of high pH in high ferric iron solution favours the formation of ferric-iron precipitate, as hydroxides, oxyhydroxides and hydroxylsulphate (i.e. jarosite) within the heap (Watling, 2006). The formation of insoluble hydroxyl compounds by the hydrolysis of ferric iron is depicted in Equation 2.57.

$$Fe^{3+} + 3H_2O \Leftrightarrow Fe(OH)_3 + 3H^+ \qquad 2.57$$

The reaction occurs in the presence of suitable mono-valent cations, such as K^+, Na^+, Ag^+, NH_4^+ and H_3O^+ and excess sulphate (Jensen and Webb, 1995), forming products of basic ferric hydroxysulphates with the formula $MFe_3(SO_4)_2(OH)_6$. The nature of the precipitate depends on the type of mono-valent cation (represented by the symbol M). These hydroxysulphate precipitates are known as jarosites. Equations 2.58 and 2.59 represent the formulae for jarosite precipitation.

$$3Fe^{3+} + M^+ + 2HSO_4^- + 6H_2O \Leftrightarrow MFe_3(SO_4)_2(OH)_6 + 8H^+ \qquad 2.58$$

$$3Fe^{3+} + SO_4^- + 14H_2O \Leftrightarrow Fe_8O_8(OH)_6 + 22H^+ \qquad 2.59$$

The nature of the jarosite percipitate also depends on the pH, temperature, ionic composition and concentration of the bioreactor medium (Daoud and Karamanev, 2006; Dutrizac, 1984). Eneroth and Koch (2004) observed that at pH 1.6 ammonium jarosite was predominant in ferrous-iron oxidation by *At. ferrooxidans* and at pH 3.2 schwertmannite was observed. Kupka *et al.* (2007) also reported that at low temperature schwertmannite was dominant in ferrous-iron oxidation by *At. ferrooxidans*. Daoud and Karamanev (2006) observed that at temperatures of 35 and 40 °C, both the oxidation rate and jarosite mass increased as the pH increased. Several studies have been conducted in order to determine the importance of jarosite formation in bioreactors. Jensen and Webb (1995) and Pogliani and Donati (2000) observed that the formation of jarosite precipitation is directly related to the number of attached cells. During bioleaching of chalcopyrite a layer of jarosite may hinder chalcopyrite leaching by restricting the mass transfer of ions into solution (e.g. Cu^{2+}, Fe^{2+}) and by preventing bacterial and iron(III) access to the mineral sulphide surface (Nemati *et al.*, 1998; Hackl *et al.*, 1995; Boon and Heijnen, 1993). It has been reported that several moderately thermophilic iron-oxidising bacteria (e.g. *S. thermosulfidooxidans*, *Sulfobacillus acidophilus* and *Acidimicrobium ferrooxidans*) are capable of reducing jarosite and ferric-iron in anoxic environments. Although the loss of jarosite precipitates from the surface of the chalcopyrite occurs under this condition, bioreduction did not significantly increase the copper extraction when compared with the non-treated controls (Stott *et al.*, 2000).

2.10.4 Effect of packing height on ferrous-iron biooxidation

Oxygen (O_2) and carbon dioxide (CO_2) transfer is of paramount importance in ferrous-iron biooxidation processes. This is as a result of the fact that O_2 acts as an electron acceptor in ferrous-iron biooxidation (Ojumu, 2006) while CO_2 serves as a source of the carbon needed for cell generation (Pradhan *et al.*, 2008) − See discussion in section 2.6. Ojumu (2008) reported that the CO_2 requirement relative to the O_2 consumption during ferrous-iron biooxidation in tank bioreactor is substantially larger than the molar ratio of CO_2 to O_2 in air. Since the aeration rate in tank systems is considerably larger than the minimum air supply required, this does not become problematic. On the other hand, there is no agitation in a packed column while microorganisms colonise mostly on the packing rather than in the aqueous solution. Accordingly, continuous cell regeneration is not as necessary as one would expect in a tank system. CO_2 is, thus, required for ferrous-iron biooxidation in a packed column only during initial colonisation. Petersen *et al*. (2011) reported that CO_2 is consumed rapidly as air moves upwards in a packed column, resulting in complete exhaustion at 3 to 4 m. This, in turn, caused a gradual decline of both the microbial population and the ferrous-iron biooxidation rate. If CO_2 is available in abundance near the base of the packed column, more rapid CO_2 consumption will occur, regardless of the oxygen

consumption, indicating microorganisms would potentially consume the available excess CO_2 for storage and not only use it as needed. Petersen *et al*. (2011) observed that O_2 and CO_2 consumption rates are directly linked and that O_2 consumption proceeded slowly where little or no CO_2 was available. Petersen *et al*. (2011) also showed that a narrow peak of activity travels from the bottom segment upwards through the column over time. Accordingly, an understanding of the O_2 and CO_2 transfer phenomenon in a packed column reactor is essential.

2.10.5 Effect of packing size

The size of the packing in the reactor has been found to have a significant effect on the microbial growth and ferrous iron oxidation by iron oxidising microorganisms, under normal operating conditions. The study conducted by Mazuelos *et al.* (2001) revealed that ferric iron productivity increased with an increase in particle size if the particle size were smaller than 4 mm. Mazuelos *et al.* (2001) also reported that, when the bioreactor packing size was smaller than 4 mm, the bed underwent a rearrangement that produced flow channelling, resulting in low ferric iron productivity. Poor channelling, in turn, hindered the biofilm development and consolidation within the spaces between the particles (Nikolov *et al.*, 1988) as a result of the limitations of the oxygen/carbon dioxide concentrations and nutrient solution in the bioreactor. Mazuelos *et al.* (2001) also reported that ferric iron productivity decreased with an increase in particle size, if the particle size were larger than 7 mm. If the particle size increased with a decrease in the average surface area, a significant decrease in the number of attached microorganisms in the bioreactor was observed and this, in turn, resulted in low ferric iron productivity (Mazuelos *et al.*, 2001).

2.11 Gas-liquid mass transfer in packed column

Cells in aerobic cultures take up oxygen from the liquid. The rate of O_2 and CO_2 transfer from the gas phase to the liquid phase is given by Equation 2.60.

$$N_A = K_L a(C^*_{AL} - C_{AL}) \qquad 2.60$$

Where, K_L is the liquid-phase mass transfer coefficient ($m.s^{-1}$), a is the gas-liquid interfacial area per unit volume of fluid ($m^2.L^{-1}$), C^*_{AL} is the oxygen concentration in the liquid phase in equilibrium with the gas phase ($gmol.m^{-3}$), and C_{AL} is the oxygen concentration in the liquid phase ($mmol.L^{-1}$). C^*_{AL} is also known as the solubility of oxygen in the liquid phase.

Oxygen and carbon dioxide molecules are transferred from the interior of the gas bubble to the gas-liquid interface. These molecules diffuse through a relatively stagnant liquid film

surrounding the gas bubble and are then transported through the liquid phase. The transfer of oxygen and carbon dioxide from the interior of gas bubbles to the liquid phase is represented schematically in Figure 2.11.

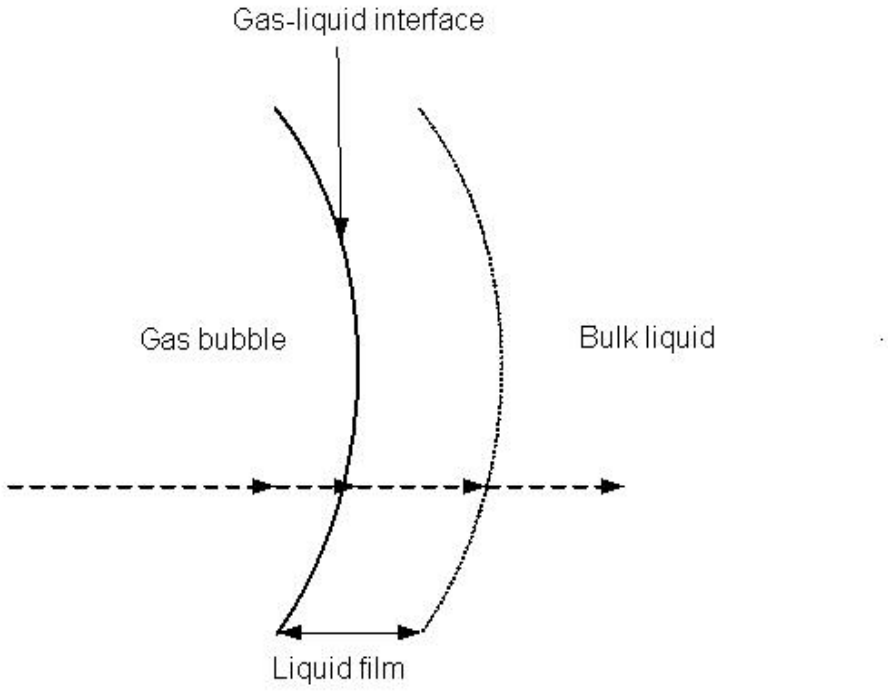

Figure 2.11: Oxygen and carbon dioxide transfer from a gas bubble to the liquid phase

The effectiveness of gas-liquid mass transfer depends on the characteristics of the bubbles in the liquid medium. Bubble behaviour significantly affects the value of $K_L a$. The total interfacial area for oxygen transfer is the gas-liquid interfacial area, which is a function of the total volume of the gas in the system, as well as of the bubble size distribution. The gas-liquid interfacial area at a height (h) is calculated using Equation 2.61 (Mazuelos *et al.*, 2002):

$$A_h = a_h V_{Gh} \qquad 2.61$$

Where a_h is the specific interfacial area and V_{Gh} is the average volume of gas bubbles at height h.

The specific interfacial area at a height (h) is given by Equation 2.62.

$$a_h = \frac{S_h}{V_{Gh}} = \frac{6\pi \quad n_{Th}\sum d_{ih}^2 f_{ih}}{\pi \quad n_{Th}\sum d_{ih}^3 f_{ih}} = 6\left(\frac{\sum d_{ih}^2 f_{ih}}{\sum d_{ih}^3 f_{ih}}\right) = \frac{6}{\sum d_{in}} \qquad 2.62$$

Where S_h is the average surface area of bubbles at height h, n_{Th} is the total number of bubbles at height h, d_{ih} is the average diameter of the bubbles, and f_{ih} is the bubble number fraction.

2.12 Oxygen and carbon dioxide uptake rate in cells

The specific oxygen utilisation rate is a function of the ferrous/ferric iron ratio (Boon, 1996):

$$q_{O_2} = \frac{-r_{O_2}}{C_X} = \frac{q_{O_2}^{\max}}{1 + K\frac{Fe^{3+}}{Fe^{2+}}} \qquad 2.63$$

The stoichiometric formula for bacteria has been described in detail in literature (Jones and Kelly, 1983; Roels and Kossen, 1978). Using the stoichiometric formula, bacteria may be approximately represented by $CH_{1.8}O_{0.5}N_{0.2}$. Hansford (1997) has shown that, by using the degree-of-reduction balance, the rate of ferrous iron oxidation may be obtained from the rates of oxygen and carbon dioxide utilisation, as shown in Equation 2.64:

$$-r_{Fe^{2+}} = -4r_{O_2} - 4.2r_{CO_2} \qquad 2.64$$

Where $-r_{Fe^{2+}}$ is the ferrous iron oxidation rate (mol $Fe^{2+}.L^{-1}$ s^{-1}), $-r_{O_2}$ is the O_2 consumption rate (mol $O_2.L^{-1}$ s^{-1}), and $-r_{CO_2}$ is the CO_2 consumption rate (mol $CO_2.L^{-1}$ s^{-1}).

The carbon dioxide utilisation rate may also be used to estimate both the bacterial concentration and growth rate (Boon, 1996):

$$-r_{CO_2} = \mu C_X \qquad 2.65$$

Where C_X is the cell concentration (mmol $C.L^{-1}$).

2.13 Summary

Currently, bioleaching is an attractive technology in the metallurgical industries when compared to pyrometallurgical techniques, because of its simplicity, low cost, low lack of gaseous emissions and its applicability to low grade ore. Accordingly, various research efforts have been directed toward understanding the mechanisms of the reactions involved in the bioleaching process. The formulation of models is extremely important for the design of these operations.

Industrial applications of bioleaching fall into two categories, namely tank and heap bioleaching. Various rate equations have been developed in the context of tank bioleaching, where it is possible to control and manage operating conditions. This implies that parameters, such as temperature and pH, are maintained close to optimum values. The ferric to ferrous ratio prevailing in the system is governed primarily by the interaction between micro-organisms, mineral concentrate and tank residence times.

Alternatively, it may be inferred from section 2.4 that heap bioleach processes offer no control over the existing operating conditions. Furthermore, compared with tank reactors, the heterogeneous nature of heap processes render some of the operating conditions uncontrollable and this, in turn, results in the occurrence of phenomena such as wide temperature variations; regions with high concentrations of total dissolved solids (TDS); poor nutrient solution distribution; low rate of oxygen and carbon dioxide transfer and undesirable pH levels. While pyrite heaps are known to reach considerable temperatures, often into the thermophile range. Copper sulphide heaps are warm, however not as hot as pyrite heaps and are therefore considered cold in comparison. Initially the temperature of any heap situation is dependent on the temperature of the surrounding environment.

Numerous studies have been carried out on ferrous-iron biooxidation because it is such a critical subprocess in bioleaching. Recently several studies conducted in the context of heap bioleaching have investigated the effects of wide variation/changes in operating conditions. The operating parameters chosen by these researchers were similar to those possible in a typical heap bioleach situation while the fact that the experiments were performed in a stirred tank reactor show that the kinetics may not represent those of microbial ferrous-iron oxidation in a heap situation, given the differences in the hydrodynamics of tank and heap systems. Other studies have been carried out in a fluidised/flooded column system and have focused on the effect of changes in temperature on the kinetics of microbial ferrous-iron oxidation. However, these studies focused on the immobilisation of microorganisms where the system was fed from the bottom of the column and such operations are not relevant to heap bioleach systems. Therefore, it is important to investigate the kinetics of Fe^{2+} biooxidation in a system that may closely represent the heap situation, at least with respect to the solution flow in heap systems. The outcome of such an investigation may provide some understanding of the way in which the oxidation process may be adequately managed and predicted under heap conditions and outcome may also be used either in the design of a typical heap bioleach plant or in the diagnosis of any existing design.

Chapter 3

Materials and Methods

This chapter contains a detailed description of the materials used during the experiments, the experimental methods followed and the analytical techniques utilised. The theoretical calculation/formulation used for the analysis of the experimental data is also discussed.

3.1 Materials

3.1.1 Experimental rig

A schematic and photographic representation of the experimental set-up is depicted in Figures 3.1(a and b), respectively. The experimental rig consisted of a single jacket, an autoclaveable packed-bed bioreactor, made of borosilicate glass. The height-to-diameter ratio of the bioreactor was H/D ≈ 12.5 with a total volume of 750 mL. Attached to the bioreactor was a FMH model TR-E constant temperature water bath, which maintained the desired temperature within the bioreactor by circulating water through the bioreactor jacket. The column was packed with inert glass marbles (diameter 15 mm), to a height corresponding to 700 mL, and held in place above the bottom reservoir (volume 220 mL) by a 1 mm stainless steel sieve. The packing, i.e. 250 glass marbles, introduced an additional surface area of 0.18 m^2 to the bioreactor. The working liquid level within the packed-bed bioreactor was 500 mL, immersing approximately 40 % of the glass marble bed in solution before the sparger was turned on. However, during operation approximately 75 % of the marble bed was immersed in liquor. The feed was pumped into the bioreactor from the top of the column by a WATSON MARLOW 205S low-flow, multi-channel pump using 0.5 mm PVC (colour code orange/yellow) tubing. The liquid effluent was removed from the bottom of the column by using a separate pump (WATSON MARLOW 101U/R low-flow, single channel pump), using silicone tubing with an inner diameter of 5 mm. Air was supplied to the bottom of the column while the off-gas from the bioreactor was passed through a condenser in order to minimise evaporation. The gas flow rate to the bioreactors was controlled using a bubble air flow meter. The solution's reduction-oxidation (redox) potential and pH were analysed using a CRISON GLP 21 redox and pH meters.

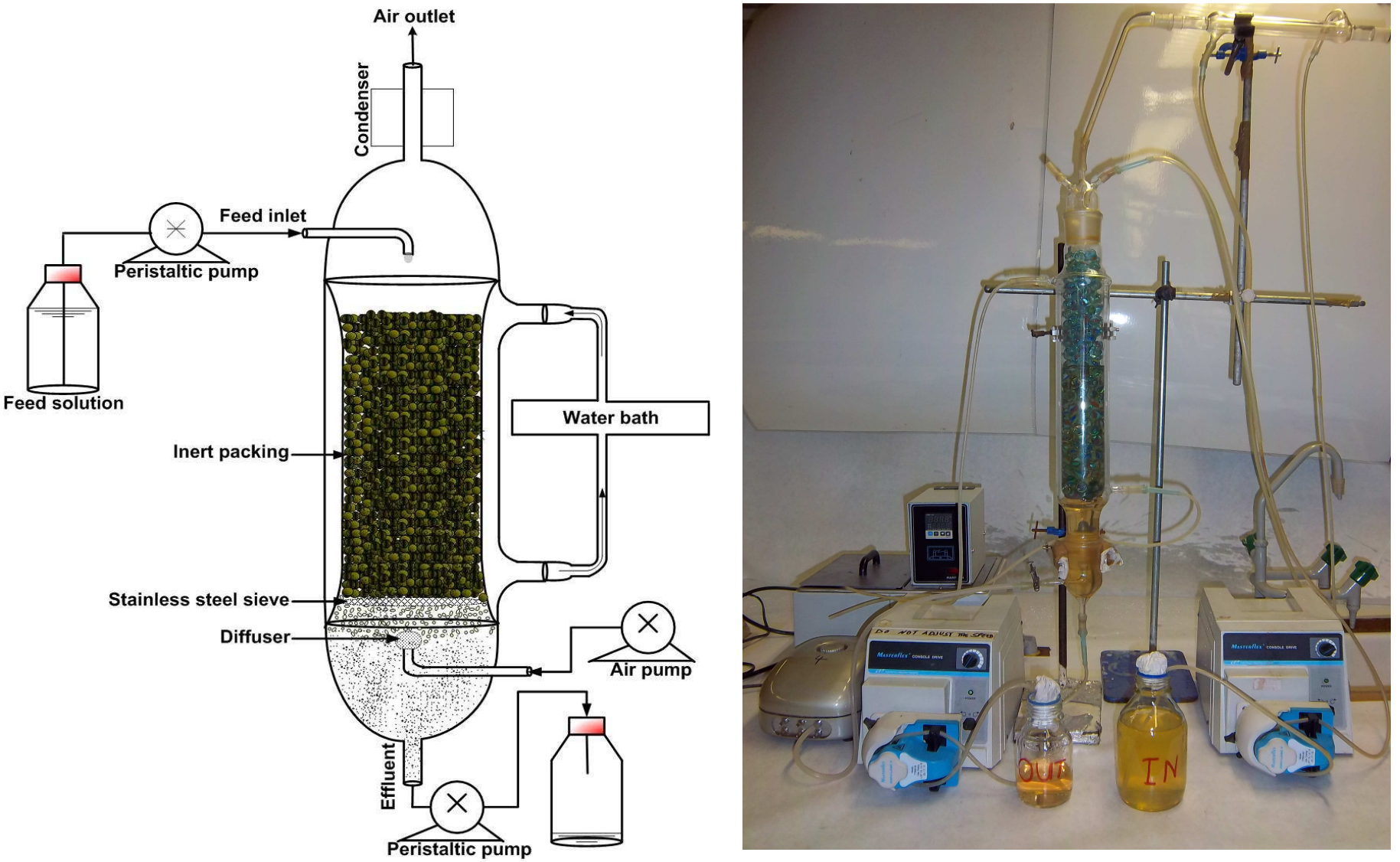

Figure 3.1: (a) Schematic representation of experimental rig; and (b) Photographic representation of the experimental set-up

3.1.2 Growth medium

Analytical-grade reagents were used for all the experiments. The ferrous-iron media consisted of 5 $g \cdot L^{-1}$ of Fe^{2+} (added as $FeSO_4$. $7H_2O$), 1.11 $g \cdot L^{-1}$ K_2SO_4, 0.53 $g \cdot L^{-1}$ $(NH_4)_2HPO_4$, 1.83 $g \cdot L^{-1}$ $(NH_4)_2SO_4$ and 10 mL of Vishniac trace element solution (Vishniac and Santer, 1957). The pH of the growth media was adjusted to the desired pH (1.20<pH<1.3) using concentrated (98%) H_2SO_4. No attempt was made to maintain sterile conditions. In order to prepare the Vishniac solution, 50 $g.L^{-1}$ EDTA ($C_{10}H_{14}N_2Na_2O_8.2H_2O$, M = 372.24 $g.mol^{-1}$) was dissolved in 200 mL of 6% (w/v) KOH solution. In a separate container, 22 g $ZnSO_4.7H_2O$, 9.24 g $CaCl_2.2H_2O$, 5.06 g $MnCl_2.4H_2O$, 5.0 g $FeSO_4.7H_2O$, 1.1 g $(NH_4)_6Mo_7O_{24}.4H_2O$, 1.58 g $CuSO_4.5H_2O$, 1.62 g $CoCl_2.6H_2O$ were added to 400 mL dH_2O. Each component had to be completely dissolved before the addition of the EDTA solution and the Vishniac solution and made up to 1 L with sterile distilled water (dH_2O).

3.1.3 Bacterial culture

The bacterial strain was originally obtained from a two-stage (2 x 20 L), continuous bioleaching mini-plant treating a pyrite-arsenopyrite concentrate in Gamsberg, South Africa. The isolated ferrous iron oxidising species, *Leptospirrillum ferriphilum* sp. nov., was found to be the only iron oxidising species (Coram and Rawlings, 2002). The stock culture was maintained in a continuous stirred tank reactor at 30 °C and a residence time of 30 hours on a feed solution containing 5 $g.L^{-1}$ total iron at pH 1.45±0.05 (adjusted with concentrated H_2SO_4).

3.2 Methods

3.2.1 Microbial ferrous-iron oxidation under continuous operation

Continuous culture experiments with *L. ferriphilum* were carried out in the packed-bed column double walled bioreactor, with a working volume of 500 mL. The bioreactor was maintained at the desired temperature using a constant temperature water bath. The cell suspension was aerated with dry air at a flow rate of 15 $mL.s^{-1}$ while the off-gas from the bioreactor was passed through a condenser to minimise the evaporation of the liquor within the bioreactor. During the continuous culture experiments the ferrous-iron medium was fed to and removed from the bioreactors as previously described.

The pH of the solution in the bioreactors was not controlled directly. However, it was maintained at the required pH by manipulating the pH of the feed to the bioreactors using a concentrated solution of sulphuric acid. The actual pH of the solution depended on both the desired solution pH and the prevailing dilution rate. The ferrous-iron oxidation kinetics were investigated for five different dilution rates ranging from 0.033 to 0.1 h^{-1} (See Appendix E).

The bioreactor was assumed to be in steady-state at a particular dilution rate after running the bioreactor for a period of at least three residence times. Steady-state was assumed only when the pH and redox potential in the culture liquor were stabilised. Steady-state was maintained for at least one residence time in order to allow for the chemical analysis of the influent and effluent samples.

A fresh experiment was started by mixing 50% of the stock solution with ferrous-iron feed, and allowing the solution potential to attain 600 mV (i.e., Ag/AgCl electrode) before changing into continuous mode. The ferrous and total iron determinations were performed regularly on the feed samples to correct any errors incurred during sample preparation. The bioreactor was cleaned after each specific dilution rate by scrubbing the walls and all available surfaces with concentrated HCl (32%). This ensured the complete removal of ferric precipitate and any wall growth. The bioreactor was then washed with diluted H_2SO_4 (≈50%) to remove the HCl, which is harmful to microorganisms. Finally, the bioreactor was rinsed with distilled water to neutralise the pH in the reactor.

3.2.2 Experimental study on the effects of operating temperature

Continuous culture experiments with *L. ferriphilum* were carried out in the packed bioreactors, as indicated in Figure 3.1. The cell suspension was aerated with dry air at a flow rate of 15 $mL.s^{-1}$. The growth medium was fed continuously at the desired dilution rate to the packed-bed bioreactor, and the effluent removed by means of variable-speed pumps. The growth medium (See section 3.1.2) contained 5.0±0.05 $g.L^{-1}$ of Fe^{2+} added as $FeSO_4.7H_2O$. The pH of the solution in the bioreactors was maintained at pH 1.45±0.05 by adjusting the feed pH using concentrated (98%) H_2SO_4. The microbial ferrous iron oxidation kinetics were investigated at 25, 30 and 35 °C for at least five different dilution rates ranging from 0.033 to 0.1 h^{-1}. The experimental data (ie. Fe^{2+}, total iron, pH and solution potential) was obtained from the steady state condition of the packed bioreactor. Regular bioreactor maintenance was observed.

3.2.3 Experimental study on the effects of ferric-iron precipitate

The experimental procedure for studying the effects of ferric-iron precipitation was similar to that described in section 3.2.2. This experiment was conducted at a bioreactor temperature of 30 °C. The growth medium contained 5.0±0.05 $g.L^{-1}$ of Fe^{2+} as $FeSO_4.7H_2O$ and aeration was maintained at 15 $mL.s^{-1}$. The pH of the solution in the bioreactors was maintained at pH 1.45±0.05 by adjusting the feed pH using concentrated (98%) sulphuric acid. The microbial ferrous-iron oxidation kinetics was determined for seven different dilution rates ranging from 0.03 to 0.1 h^{-1}. For the experiment in which jarosite was accumulated, the bioreactor was not

cleaned after each specific dilution rate. However, with the exception of the jarosite experiment, the bioreactor was cleaned after each specific dilution rate by scrubbing the walls and all available surfaces with concentrated HCl (32%) and distilled water as this ensured the complete removal of ferric precipitate and any wall growth.

3.3 Analytical procedure

3.3.1 Iron determination

The redox potential of the solution in both the feed and bioreactor were measured periodically using a redox electrode (Ag/AgCl). The redox probe was calibrated (Refer to section 3.3.2) regularly under the same conditions as the bioreactor operation prior to use. This allowed the determination of the ferric-to-ferrous iron ratio in both the bioreactor and feed solution. The total iron concentration in both the feed and bioreactor effluent was determined by titration with potassium dichromate using the BDS indicator (Vogel and Svehla, 1987). The difference between the total iron concentration in the feed entering the packed bioreactor and the total iron concentration in the effluent leaving the packed bioreactor enabled the determination of ferric iron precipitation in the effluent. The ferrous iron concentrations in both solutions were determined by titration with potassium dichromate (Vogel and Svehla, 1987). The ferric-iron concentrations were determined by subtracting the ferrous-iron concentration from the total iron concentration. Thus, it was possible to calculate the ferrous-iron utilisation rate, $-r_{Fe^{2+}}$, and the ferric-iron concentration using Equations 3.1 and 3.2, respectively.

$$-r_{Fe^{2+}} = D\left([Fe^{2+}]_{In} - [Fe^{2+}]_{Out}\right) \quad 3.1$$

Where $-r_{Fe^{2+}}$ represents the ferrous-iron utilisation rate (mmol $Fe^{2+}.L^{-1}h^{-1}$); D is the dilution rate (h^{-1}); $[Fe^{2+}]_{In}$ is the influent ferrous-iron concentration (mmol $Fe^{2+}.L^{-1}h^{-1}$) and $[Fe^{2+}]_{Out}$ is the effluent concentration (mmol $Fe^{2+}.L^{-1}h^{-1}$).

$$[Fe^{3+}] = [Fe^{T}] - [Fe^{2+}] \quad 3.2$$

Where $[Fe^{3+}]$ represents the ferric-iron concentration (mmol $Fe^{2+}.L^{-1}h^{-1}$); $[Fe^{2+}]$ is the total iron and $[Fe^{T}]$ is the ferrous-iron.

3.3.2 Redox probe calibration

The redox electrode (i.e., Ag/AgCl electrode) was calibrated against the half reaction of ferrous to ferric oxidation ($Fe^{2+} \rightarrow Fe^{3+} + e$) which was the only redox couple existing within the bioreactors. The calibration was performed at the specific temperature of the study and

the calibration curve was plotted using the Nernst equation shown in Equation 3.3. This enabled the determination of $[Fe^{3+}]/[Fe^{2+}]$ in the bioreactors.

$$E_h = E'_h + \frac{RT}{nF} \ln \frac{[Fe^{3+}]}{[Fe^{2+}]} \quad 3.3$$

Where E_h is the standard redox potential and $[Fe^{3+}]/[Fe^{2+}]$ is the ratio between the total concentration of ferric and ferrous ions. The term E'_h is defined as the solution potential measured at equal total ferric and ferrous-iron concentration, which accounts for the activity coefficient, formation of complexes, electrode type and fouling of the electrode. E'_h values may be determined from the intercept of the plot, E_h, versus $\ln([Fe^{3+}]/[Fe^{2+}])$, while the slope gives RT/nF. The theoretical aspect of the calibration using the Nernst equation is discussed in detailed in Appendix B1.2.

3.4 Analysis of kinetic data

3.4.1 Kinetic equation of microbial ferrous-iron oxidation

Both the apparent affinity constant for the Monod and Hansford models and the maximum overall ferrous-iron oxidation rate ($r_{Fe^{2+}}^{max}$) may be determined by rewriting Equations 2.42 and 2.53 in terms of $-r_{Fe^{2+}}$. These apparent affinity constants may be determined by either fitting the experimental data to Equations 2.42 and 2.53 using the least squares method, or from the corresponding Lineweaver–Burk plot.

$$-r_{Fe^{2+}} = \frac{r_{Fe^{2+}}^{max}[Fe^{2+}]}{K_{Fe^{2+}} + [Fe^{2+}]} \quad 2.42$$

$$-r_{Fe^{2+}} = \frac{r_{Fe^{2+}}^{max}}{1 + K'_{Fe^{2+}} \frac{[Fe^{3+}]}{[Fe^{2+}]}} \quad 2.53$$

3.4.2 The effect of temperature

The maximum microbial ferrous-iron utilisation rate, $r_{Fe^{2+}}^{max}$, and the operating temperature may be described by the Arrhenius equation which may, in turn, be rewritten from Equations 2.55 and 2.56 as:

$$r_{Fe^{2+}}^{max} = K_0 \exp\left(-\frac{E_a}{RT}\right) \quad 2.55$$

$$\ln r_{Fe^{2+}}^{\max} = -\frac{E_a}{R}\left(\frac{1}{T}\right) + \ln K_0 \qquad 2.56$$

The activation energy E_a and the frequency factor K_0 for microbial ferrous-iron oxidation kinetics may be obtained from the plot of $ln\, r_{Fe^{2+}}^{max}$ versus $1/\mathrm{T}$. The plot should give a straight line with a slope of - E_a/R and an intercept of $ln\, K_0$, from which the E_a and K_0 may be established. R is the gas constant (8.314 J mol^{-1} K^{-1}). After plotting the experimental data a trend-line must be inserted and the correlation coefficient (R^2) value determined to investigate the accuracy of the experimental data obtained. A correlation coefficient value above 0.90 was considered to be sufficient for the correlation of experimental data and mathematical models.

3.5 Conclusion

A summary of the conclusions is presented below:

- The test rig and experimental equipment used were described and proved to be reliable in measuring the kinetics of microbial ferrous-iron oxidation in a packed column reactor.
- Detailed dimensions of the packed column used were presented.
- A detailed description of the growth medium for the bacteria and bacterial culture used was presented.
- Detailed experimental procedures describing the effects of temperature and ferric-iron precipitation on microbial growth were presented.
- Procedures describing the kinetic analysis of microbial ferric-iron oxidation were presented.

Chapter 4

The effect of temperature on the kinetics of ferrous-iron biooxidation by *Leptospirillum ferriphilum* in a packed column bioreactor

4.1 Introduction

Microbial oxidation of ferrous iron is an important aspect in the bioleaching of sulphide minerals. The reaction mechanism is well understood, and there are several studies on the bacterial oxidation of ferrous-iron. Studies have also been conducted on various kinds of reactor systems in order to gain understanding of the reaction kinetics and to improve the rate of this subprocess (Ojumu and Petersen, 2011; Penev and Karamanev, 2010; Ojumu *et al.*, 2006; Meruane *et al.*, 2002; Breed *et al.*, 1999; Huberts, 1994; Boon and Heijnen, 1993). These studies have all contributed to the success of tank bioleaching, where it is possible to control and manage operating conditions.

The objective of this study was to investigate the kinetics of microbial ferrous-iron oxidation in a packed-bed column, which was operated in a mode similar to the heap operation. It has been shown that the operating temperature is critical to the oxidation process (Ojumu *et al.*, 2009). However, in a heap leach context, temperature variation is often common and difficult to control. While higher temperatures may be found in some regions of the heap, extremely cold conditions may exist in other parts. Hence, there is a need to investigate the kinetics of microbial ferrous-iron oxidation under such conditions. It has been shown that an Arrhenius equation may be used to describe the kinetics of microbial ferrous-iron oxidation at different temperatures (Ojumu *et al.*, 2009; Franzmann *et al.*, 2005; Breed *et al.*, 1999; MacDonald and Clark, 1970). The results of this study will be compared to previous studies with a view to provide an understanding of the kinetics of microbial ferrous-iron oxidation by *L. ferriphilum* in a bioleach heap system.

4.2 Methodology

Continuous culture experiments with *L. ferriphilum* were carried out in the packed column at 25, 30 and 35 °C and at a pH of 1.45±0.05, with feed substrate containing 5 $g.L^{-1}$ total iron concentration. The microbial ferrous iron oxidation kinetics were investigated at five different dilution rates, ranging from 0.033 to 0.1 h^{-1}. The experiment is described in detail in section 3.2.2.

4.3 Results and discussion

4.3.1 Variation of iron species concentrations, ferrous-iron biooxidationconversion rate, and solution redox potential with dilution rate

The residual ferrous iron concentration in the column increased with an increase in the dilution rate (Figure 4.1a) while the ferric iron concentration and the solution redox potential decreased (Figure 4.1b and c). The highest solution redox potential was observed at a temperature of 35 °C. At high dilution rates, minimal reaction time is allowed for the bio-oxidation process to occur within the reactor as a result of decreased residence time. Similarly, it was to be expected that the residual ferrous iron concentration would decrease and the ferric-iron concentration would increase with increasing temperature (Ojumu, 2008). However, the experimental data obtained in this study (Figure 4.1a) suggested that although, there was a decrease in ferric-iron concentration (Figure 4.1b) with increasing temperature, it was noted that the dilution rates were not constant at the various temperatures evaluated, and this may account for the trend observed with regards to the increasing temperature. It was observed from the results that ferric-iron precipitation was not related to the dilution rate and did not follow a definitive trend (refer to Table 4.1). It was also observed that, at higher temperature, higher ferric-iron precipitation of 9.33% occurred quantified in the effluent.

When the oxidation rate was calculated (refer to Table 4.2 for calculated values) it was noted that a maximum overall ferrous iron oxidation rate (average $r_{Fe^{2+}}^{max}$ = 15.10 mmol $Fe^{2+}.L^{-1}h^{-1}$) was observed at the highest temperature (i.e. 35 °C), indicating that the oxidation rate increased with increasing temperature (refer to Table 4.2). In addition, Figure 4.1d also illustrates that the ferrous iron bio-oxidation rate increased and the conversion decreased with both increasing dilution rate and temperature, as stated. The results showed conversion of approximately 96.5% at the highest dilution rate and 99.5% at the lowest dilution rate.

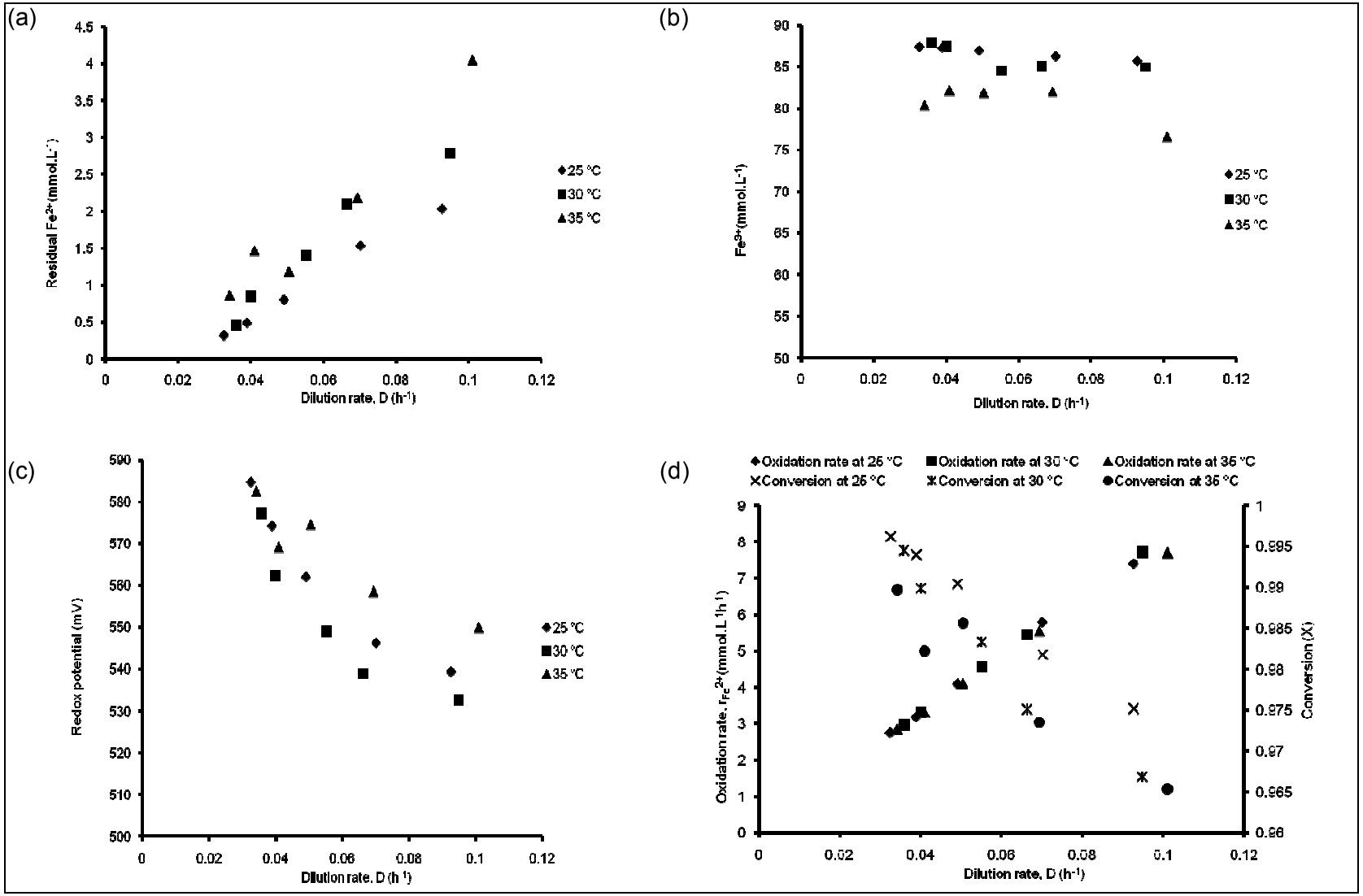

Figure 4.1: Dilution rate vs (a): residual ferrous-iron; (b): ferric-iron; (c): solution redox potential (Ag/AgCl); (d): ferrous-iron oxidation rate and conversion

Table 4.1: Precipitation ferric-iron at different dilution rates and different temperatures

Temperature	Dilution rate, D (h^{-1})	Total iron influent $[Fe^T]_{In}$ ($mmolL^{-1}$)	Total iron effluent $[Fe^T]_{Out}$ ($mmolL^{-1}$)	% of ferric-iron (Fe^{3+}) Precipitation
25 °C	0.033	89.53	87.74	2.00
	0.039	89.53	87.74	2.00
	0.049	89.53	87.74	2.00
	0.070	89.53	87.74	2.00
	0.093	89.53	87.74	2.00
30 °C	0.036	89.53	88.33	1.33
	0.040	89.53	88.33	1.33
	0.055	88.33	85.94	2.70
	0.066	88.33	87.14	1.35
	0.095	89.53	87.74	2.00
35 °C	0.034	89.53	81.17	9.33
	0.041	89.53	83.56	6.67
	0.050	89.53	82.96	7.33
	0.069	88.93	84.15	5.37
	0.101	88.33	80.54	8.82

4.3.2 The rate of microbial ferrous-iron oxidation, $-r_{Fe^{2+}}$

The Monod equation (Equation 2.42) and the Hansford equation (Equation 2.53) were used for the analysis of the experimental data. These two models have been shown to describe the same experimental data accurately (Ojumu *et al*., 2006).

$$-\mathrm{r}_{\mathrm{Fe}^{2+}} = \frac{\mathrm{r}^{\max}_{\mathrm{Fe}^{2+}}[\mathrm{Fe}^{2+}]}{\mathrm{K}_{\mathrm{Fe}^{2+}} + [\mathrm{Fe}^{2+}]} \qquad 2.42$$

$$-r_{Fe^{2+}} = \frac{r^{\max}_{Fe^{2+}}}{1 + K'_{Fe^{2+}}\dfrac{[Fe^{3+}]}{[Fe^{2+}]}} \qquad 2.53$$

The parameters of both equations, i.e. $r^{max}_{Fe^{2+}}$ and $K_{Fe^{2+}}$ for Monod, and $r^{max}_{Fe^{2+}}$ and $K'_{Fe^{2+}}$ for Hansford, were determined by fitting Equations (2.42) and (2.53) to the experimental data. Solver in Microsoft Excel was used to minimise the sum of the squared errors (SSE) (refer to Appendix C1.1) between the measured and predicted values of, $-r_{Fe^{2+}}$, as shown in Figures 4.2a and b, respectively.

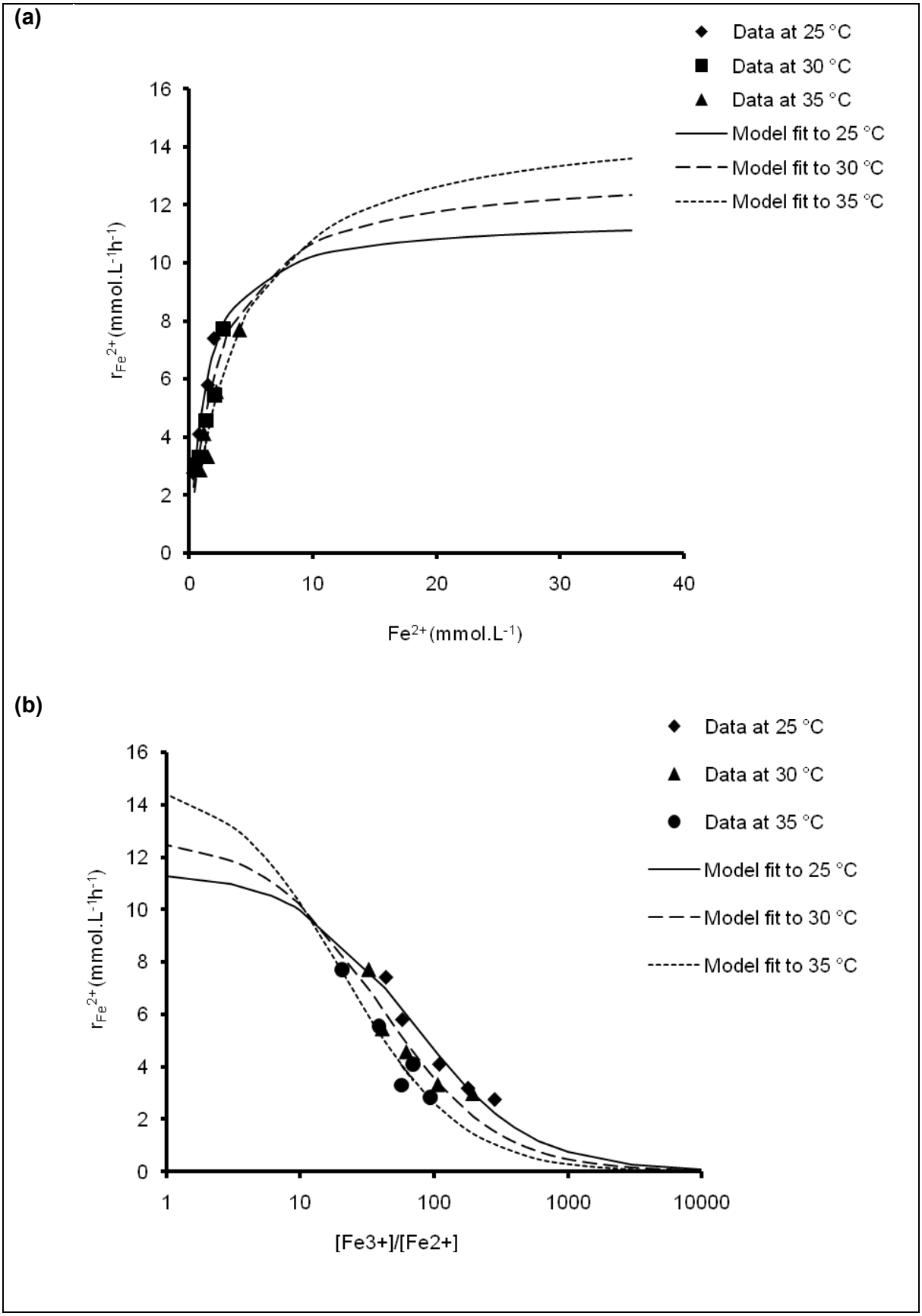

Figure 4.2: The effect of temperature on (a) the ferrous iron oxidation rate versus residual ferrous-iron concentration compared with the trend of the Monod model (Equation 2.42); (b) the fit of the rate data to the Boon and Hansford model, Equation 2.53

The maximum overall ferrous-iron oxidation rate, $r_{Fe^{2+}}^{max}$, increased significantly with an increase in temperature within the range studied (Table 4.2).

Table 4.2: Maximum overall ferrous-iron oxidation and kinetic constant, determined from the fit of rate data to the Hansford and Monod models

Temperature	Hansford model		Monod model		Average	Reference
	$r_{Fe^{2+}}^{max}$	$K'_{Fe^{2+}}$	$r_{Fe^{2+}}^{max}$	$K_{Fe^{2+}}$	$r_{Fe^{2+}}^{max}$	
25 °C	11.42	0.0146	11.51	1.30	11.47	This study
30 °C	12.80	0.0258	13.17	2.39	12.98	
35 °C	15.09	0.0474	15.10	3.91	15.10	
42 °C	10.10	0.0561	10.97	0.16	10.54	Data from Ojumu (2008)

Units: $r_{Fe^{2+}}^{max}$ (mmol $Fe^{2+}.L^{-1}h^{-1}$), $K_{Fe^{2+}}$ (mmol.L^{-1}), $K'_{Fe^{2+}}$ is dimensionless.

The microbial ferrous-iron oxidation rate was determined to be temperature dependent within the temperature range of 25 to 35 °C for *Leptospirillum*- like species. This temperature range is similar to that observed by Franzmann *et al.* (2005), who reported an optimum temperature of 38.6 °C for *L. ferriphilum*. It was not feasible to confirm an optimum temperature in this study as a result of the limited temperature resolution. The values of $r_{Fe^{2+}}^{max}$ obtained using both equations were found to be similar, thus an average was quantified as shown in Table 4.2. The results showed that the maximum overall ferrous-iron oxidation rate was greater in a packed-bed bioreactor when compared to a tank bioreactor. In previous work conducted by Ojumu (2008), a maximum rate of 10.54 mmol $Fe^{2+}.L^{-1}h^{-1}$, calculated by averaging $r_{Fe^{2+}}^{max}$ of both the Hansford and Monod model, was obtained in a tank reactor at a temperature of 42 °C. The value of 10.54 mmol $Fe^{2+}.L^{-1}h^{-1}$ being comparable to the rate obtained at 25 °C for this study in a packed-bed bioreactor, which was a non-optimum temperature condition for the growth of the microorganisms. This indicates that a much higher rate may be achieved if the packed-bed bioreactor was to be operated at 42 °C. The larger surface area available for microbial attachment in the packed-bed bioreactor may be responsible for the higher rate of oxidation. The value of $r_{Fe^{2+}}^{max}$ obtained was less than those reported in previous studies using fluidised and flooded columns. In previous studies conducted by Alemzadeh *et al.* (2009) and Long *et al*. (2003), the maximum oxidation was 141.42 and 55.50 mmol $Fe^{2+}.L^{-1}h^{-1}$ respectively. The higher value ($r_{Fe^{2+}}^{max}$) found in previous studies may be the result of the differently configured column reactor used. The kinetic constants for both the Hansford and Monod models increased with increasing temperature. However, the Monod constant reported by Ojumu (2008) was considerably less than that observed in the packed-bed.

Since the Monod constant is indicative of microbial substrate affinity, in relation to cell growth and substrate usage, a lower value indicates higher affinity (Kovárová-Kovardagger and Egli, 1998). Accordingly, the Monod constant values may suggest that the oxidation process is growth associated in a tank reactor and cell maintenance associated in the packed-bed column.

4.3.3 The activation energy determination

An increase in of ferrous-iron biooxidation rate with temperature may be described using the Arrhenius equation (Equation 2.56). The equation was used to assess the maximum overall oxidation rate data at the three temperatures investigated (Figure 4.3a). The values of the activation energy (E_a) and the frequency factor (K_0) for microbial ferrous-iron oxidation kinetics are 20.97 kJ.mol^{-1} and 5.42 mmol Fe^{2+}. $L^{-1}h^{-1}$, respectively. These were average values for the parameters obtained from correlating the experimental data to the Monod and Hansford equations (Figure 4.2). The E_a value falls in the lower end of the range (20 to 96 kJ.mol^{-1}) of E_a previously reported for acidophilic chemolithotrophs (De *et al.*, 1996; Ahonen and Tuovinen, 1989; Guay *et al.*, 1977; Lacey and Lawson, 1970; MacDonald and Clark, 1970). This suggests that the biooxidation rate was controlled both biochemically and by diffusion. A similar value (20.93 kJ.mol^{-1}) was reported by De *et al*. (1997) for a study in which *Acidothiobacillus ferrooxidans* was used in the temperature range of 5 to 25 °C. The activation energy obtained in this study was lower than the reported value for the same microorganisms in a tank bioreactor (34.46 kJ.mol^{-1}) (Ojumu *et al.*, 2009). This observation implies that the microbial ferrous-iron oxidation rate in the packed-bed column was higher in comparison to that observed in a continuous stirred tank bioreactor. The relationship between the apparent affinity constants ($K_{Fe^{2+}}$ and $K'_{Fe^{2+}}$) and temperature may be represented by a linear function, namely, Equations 4.1 and 4.2, as shown in Figure 4.3b. This linear dependency has also been shown in previous studies (Ojumu *et al.*, 2009; Breed *et al.*, 1999).

$$K_{Fe^{2+}} = 1.46\times10^{-2}T - 4.2731,\ R^2 = 0.99 \quad (4.1)$$

$$K'_{Fe^{2+}} = 3.30\times10^{-3}T - 0.9641,\ R^2 = 0.97 \quad (4.2)$$

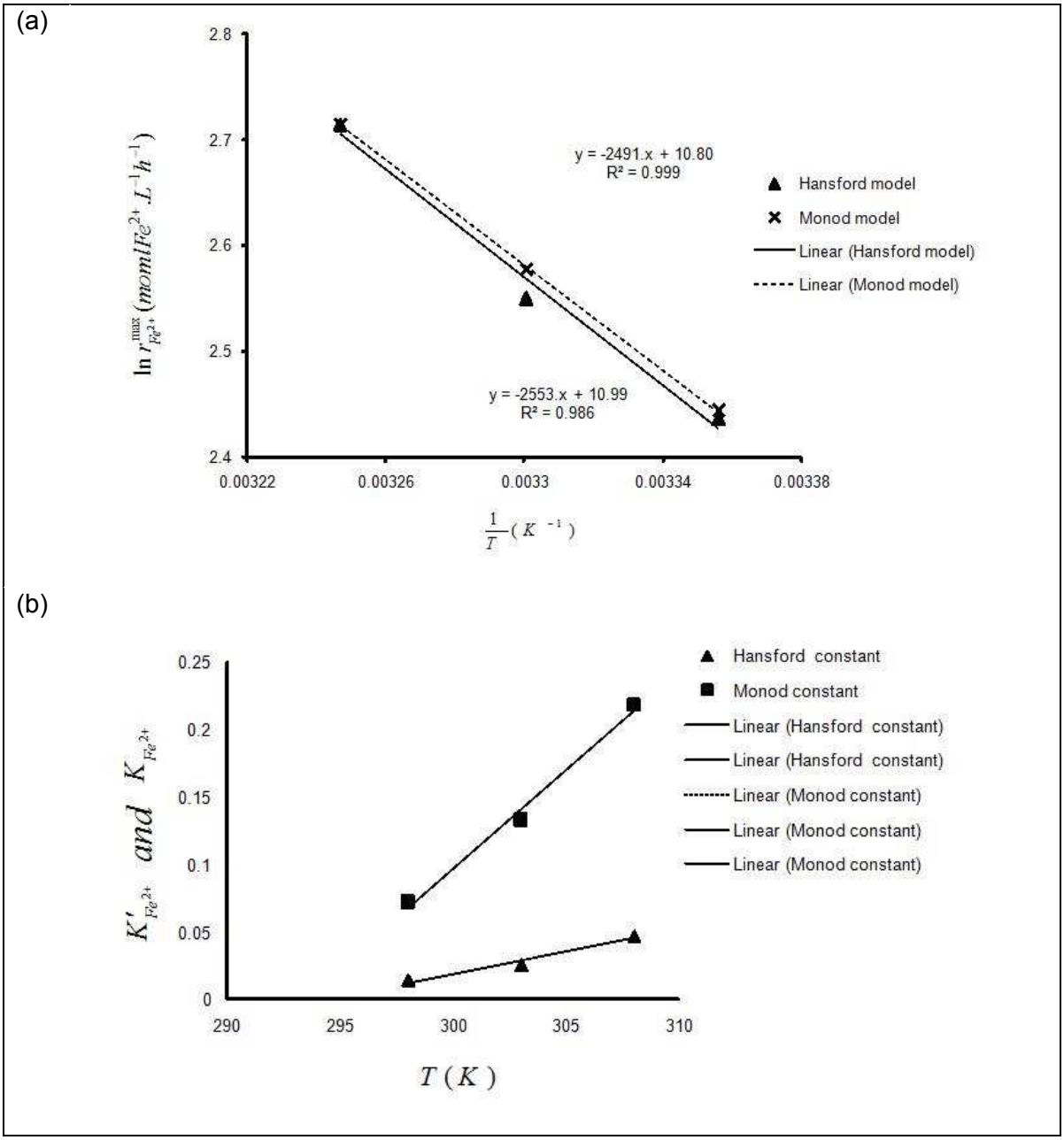

Figure 4.3: (a) Arrhenius plot to show the effect of temperature on the maximum overall ferrous-iron oxidation rate; (b) The effect of temperature on the kinetic constants $K_{Fe^{2+}}$ and $K'_{Fe^{2+}}$

By substituting the values of E_a and,K_0 as well as the expression for $K_{Fe^{2+}}$ and $K'_{Fe^{2+}}$, into the Monod and Hansford models (Equations 2.42 and 2.53), it is possible to obtain Equations 4.3 and 4.4 which, in turn, predict $r_{Fe^{2+}}^{max}$ as a function of the ferric to ferrous-iron ratio ($[Fe^{3+}]/[Fe^{2+}]$) across a range of temperatures. The error analysis of the predicted data based on the measured data suggests that the model may accurately predict the effect of temperature on microbial ferrous-iron oxidation (to 92%), as shown in Figure 4.1. See Appendices C1.1 and C1.2 for the statistical and error analyses.

$$-r_{Fe^{2+}} = \frac{K_0 \exp\left(-\frac{E_a}{RT}\right)[Fe^{2+}]}{(1.46\times10^{-2}T - 4.27) + [Fe^{2+}]} \quad 4.3$$

$$-r_{Fe^{2+}} = \frac{K_0 \exp\left(-\frac{E_a}{RT}\right)}{1 + (3.30\times10^{-3}T - 9.64\times10^{-1})\frac{[Fe^{3+}]}{[Fe^{2+}]}} \quad 4.4$$

4.4 Conclusion

Microbial ferrous-iron oxidation rate in a packed-bed bioreactor may be described accurately by means of the Monod and Hansford equations. The maximum overall rate increased with an increase in temperature within the range studied, while the data indicated that the values obtained in this study are higher than those obtained in a previous study in a continuous stirred tank bioreactor. The affinity constants, for both the Monod and Hansford models, increased significantly with an increase in temperature. The value of the activation energy obtained from the Arrhenius equation indicated that the biooxidation reaction is controlled biochemically and by diffusion. Furthermore, the rate of microbial ferrous-iron oxidation by *L. ferriphilum* in a packed-bed column, and also in the context of heap leaching, is likely to be lower than those reported in previous studies in fluidised and flooded columns. It is expected that the knowledge gained from this study will contribute towards the effort of predicting a heap bioleaching system performance accurately.

Chapter 5

Contribution of ferric-iron precipitate to the kinetics of microbial ferrous-iron oxidation by *Leptospirillum ferriphilum* in a packed column

5.1 Introduction

Research into microbial ferrous-iron oxidation focuses on increasing the oxidation rate, since ferric-iron reagent generation is critical to the lifespan of a bioleach operation. However, excess ferric-iron readily precipitates as hydroxides, oxyhydroxides and hydroxylsulphate (jarosite) compounds, depending on the solution pH (MacDonald and Clark, 1970). Jarosite precipitation is often perceived as an unwanted phenomenon; for example, it has been shown that the precipitation of a layer of Jarosite may hinder chalcopyrite leaching by restricting the mass transfer of ions in solution (Cu^{2+}, Fe^{2+}), by preventing bacterial including iron(III) access to the mineral sulphide surface (Nemati *et al.*, 1998; Boon and Heijnen, 1993). The number of attached cells in flow reactors has been directly linked to jarosite precipitation (Pogliani and Donati, 2000; Jensen and Webb, 1995). Immobilisation of relevant acidophilic microbes at lower pH values has been investigated with a view to enhancing the ferrous oxidation rate (Grishin *et al.*, 1988; Grishin and Tuovinen, 1988; Jones and Kelly, 1983).

This chapter presents the results for the rate of ferrous-iron biooxidation in a packed-bed column, with a view to identifying the input of jarosite precipitate to the rate of biooxidation for this subprocess of bioleaching.

5.2 Methodology

Studies were carried out in the packed column at 30 °C and at pH 1.45±0.05 with the feed substrate containing 5 $g.L^{-1}$ total iron concentration. The microbial ferrous iron oxidation kinetics were investigated at seven different dilution rates i.e. 0.033, 0.038, 0.044, 0.052, 0.062, 0.071 and 0.099 h^{-1}. The experimental approach was described in detail in Section 3.2.3.

5.3 Results and discussion

5.3.1 The effect of jarosite on microbial ferrous-iron oxidation and conversion

The rate of microbial ferrous-iron oxidation, $-r_{Fe^{2+}}$, and the conversion achieved from both experiments, namely, the limited jarosite and jarosite accumulated experiments, were plotted against dilution rates − see Figure 5.1. The $-r_{Fe^{2+}}$ increased linearly with the dilution rate for both the limited jarosite and jarosite accumulated experiments (Figure 5.1). This corresponds to results obtained previously by Ojumu *et al*. (2009) where $-r_{Fe^{2+}}$ increased linearly with the dilution rate. Figure 5.1 also shows that the data for ferrous-iron conversion to ferric-iron does not follow a definite trend with regards to the dilution rate for the experiment characterised by jarosite accumulation. Although, there was limited correlation between the dilution rate and ferrous-iron conversion, the conversion recorded (0.9979) at the lowest dilution rate studied (0.033 h^{-1}) was higher than that recorded (0.9861) at the highest dilution rate studied (0.099 h^{-1}). During the jarosite accumulation experiment, it was observed that, as the dilution rate increased from 0.038 to 0.044 h^{-1} and 0.062 to 0.071 h^{-1}, the ferrous-iron conversion increased from 0.9954 to 0.9955 and 0.9854 to 0.9895 respectively (see Table 5.1), respectively, instead of decreasing. A possible reason for the increase in the ferrous-iron conversion was attributed to significant jarosite accumulation observed inside the packed column between days 12 to 58 and days 65 to 70 (Table 5.1), respectively. Jarosite accumulated continuously inside the packed column over the period of experimentation. The increased conversion with increasing dilution rate may, therefore, be attributed to cell accumulation in the bioreactor as a result of microorganism attachment on the accumulated jarosite in the bioreactor. Although there was no significant difference between the minimum and maximum ferrous-iron conversion of 0.9854 and 0.9955 (Table 5.1), respectively, the fact that the column system did not washout even at a dilution rate of 0.1 h^{-1} suggested microbial accumulation within the bioreactor. Therefore, it was concluded from the high ferrous-iron conversion results (Figure 5.1 and Table 5.1) that it would be possible to maintain the bioreactor at a loading rate beyond 0.7 $g.L^{-1}h^{-1}$ without a washout. However, for both experiments, a conversion greater than 90% was obtained at the highest dilution rate investigated. The maximum ferrous-iron conversion in both experiments was above 99% at a dilution rate of 0.03 h^{-1}. The results indicated that the jarosite accumulation was not related to the dilution rate (refer to Table 5.2), with a maximum of approximately 4% of the jarosite obtained from the bioreactor effluent. Most of the jarosite which had accumulated within the bioreactors served as a support matrix for microbial attachment. Figure 5.2a depicts the experimental setup in which the jarosite accumulation was limited, while in Figure 5.2b,

jarosite was allowed to accumulate in the packed-bed bioreactor. However, jarosite accumulation was not quantified in this study.

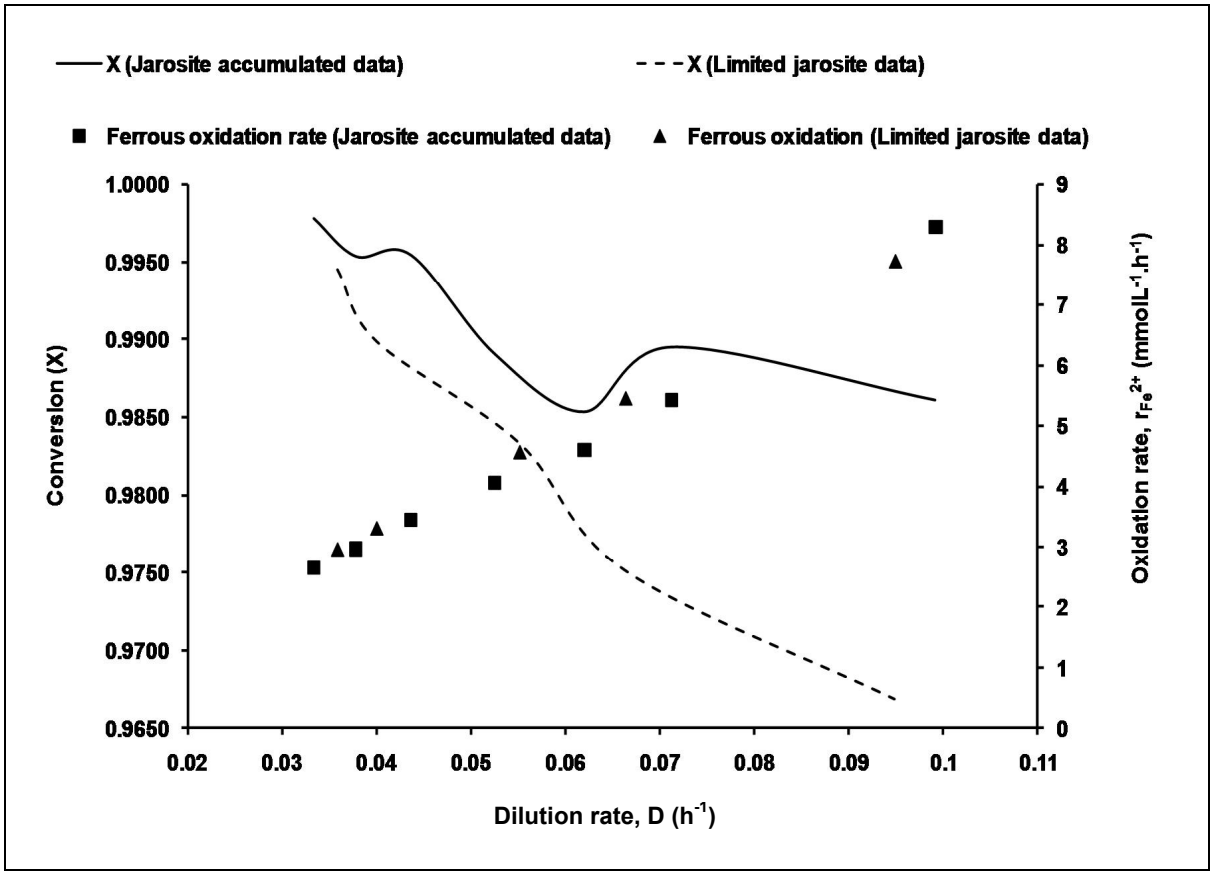

Figure 5.1: Steady-state ferrous iron conversion and oxidation rate as a function of dilution rate at 30 °C

Table 5.1: Jarosite accumulation data

Day	Dilution rate, D (h^{-1})	Ferrous iron conversion (X)
12	0.038	0.9954
58	0.044	0.9955
65	0.062	0.9854
70	0.071	0.9895
80	0.099	0.9861

Table 5.2: Percentage (%) of jarosite in the effluent stream at different dilution for jarosite accumulation experiment

Dilution rate, D (h^{-1})	Total iron influent $[Fe^{I}]_{In}$ ($mmolL^{-1}$)	Total iron effluent $[Fe^{I}]_{Out}$ ($mmolL^{-1}$)	% of jarosite
0.033	87.13817	87.13817	0.00
0.038	85.94449	85.94449	0.00
0.044	88.92868	85.34766	4.03
0.071	86.54133	84.75082	2.07
0.099	88.63026	86.83975	2.02

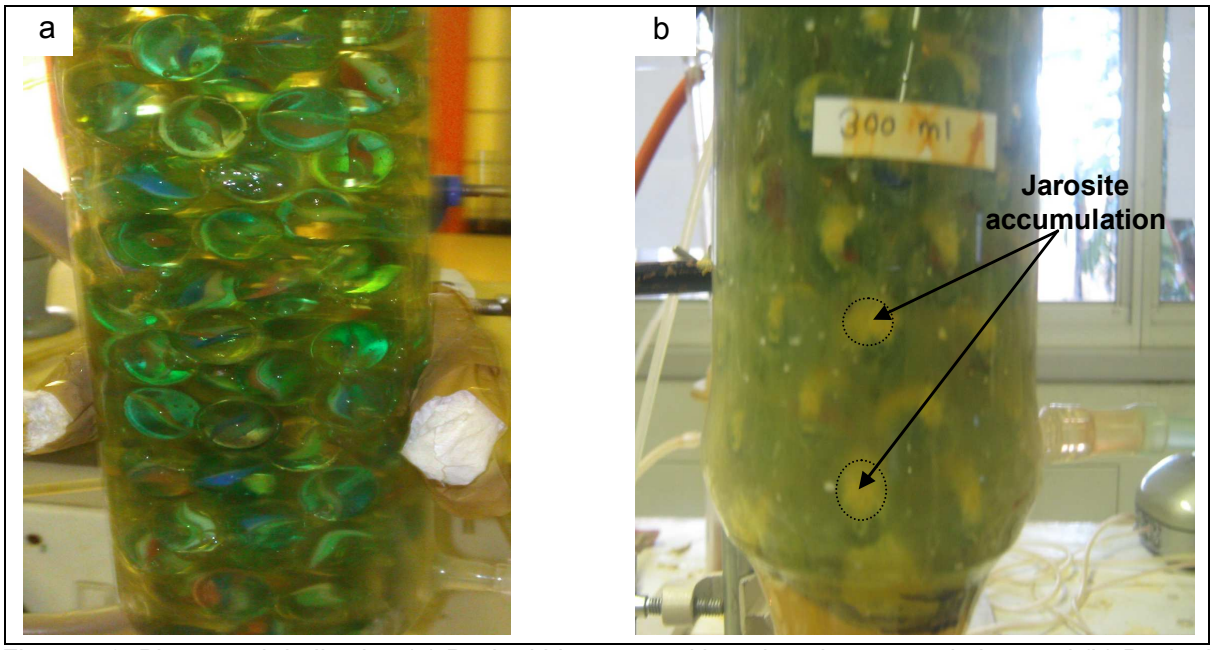

Figure 5.2: Photograph indicating (a) Packed bioreactor without jarosite accumulation; and (b) Packed bioreactor with jarosite accumulation on the packing material

The maximum overall rate of microbial ferrous-iron oxidation, $r'^{max}_{Fe^{2+}}$, the apparent affinity constant, $K'_{Fe^{2+}}$ and the Monod saturation constant, $K_{Fe^{2+}}$ were determined from correlating Equations 2.42 and 2.53 to the experimental data. Solver (Microsoft Excel) was used to minimise the sum of the squared errors (SSE) between the measured and the predicted values of $-r_{Fe^{2+}}$ − see Figures 5.3a and b.

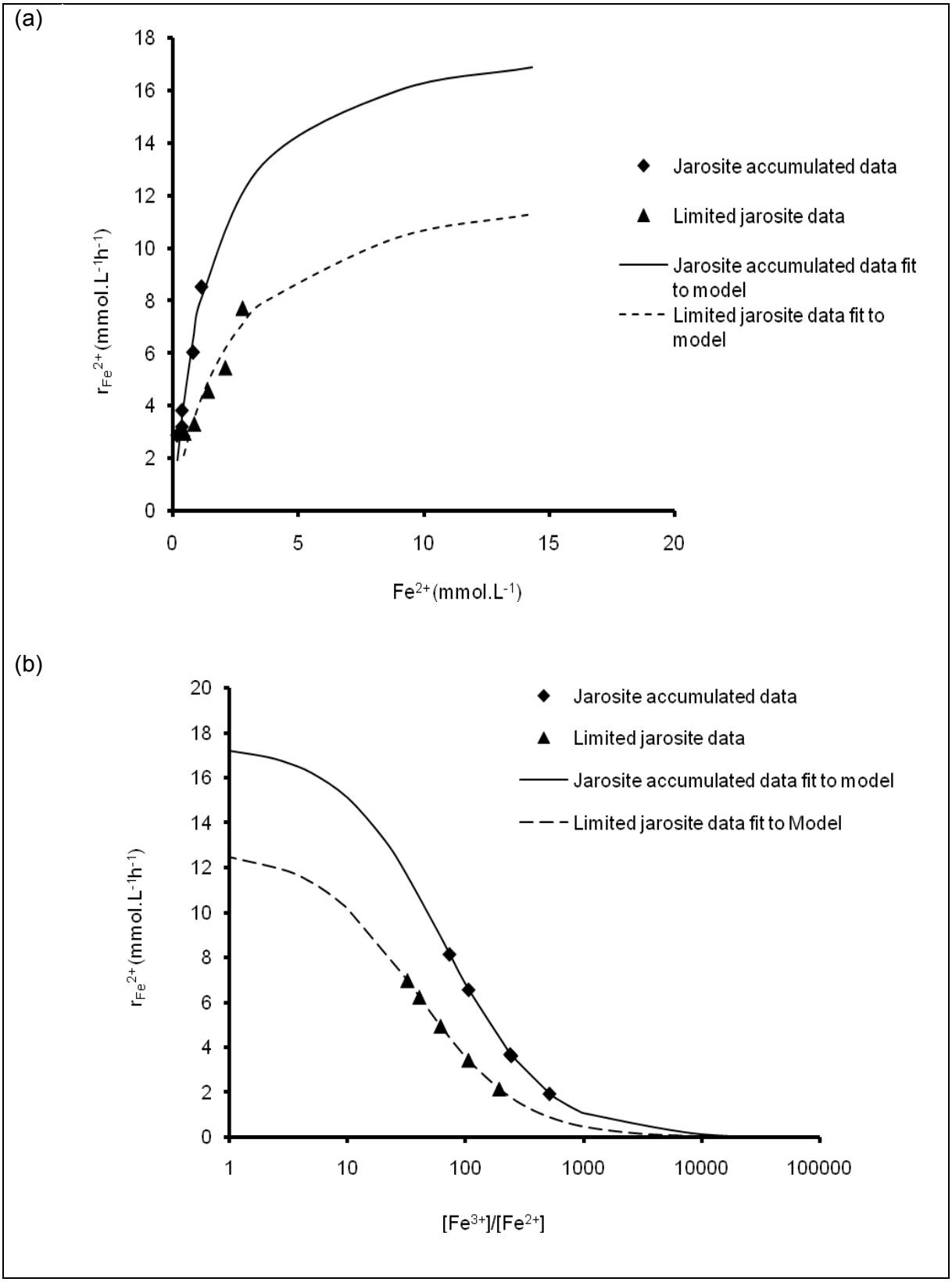

Figure 5.3: The effect of ferric-iron precipitate on (a) the ferrous iron oxidation rate versus residual ferrous-iron concentration compared with the trend of the Monod model (Equation 2.42); (b) the fit of the rate data to the Boon and Hansford model, Equation 2.53

Table 5.3 illustrates that a higher maximum overall microbial ferrous-iron oxidation rate was obtained in the jarosite accumulated experiment (average value of $r_{Fe^{2+}}^{max}$ = 18.03 mmol $Fe^{2+}.L^{-1}h^{-1}$) compared to the value obtained when the precipitate was minimised (average value of $r_{Fe^{2+}}^{max}$ = 12.99 mmol $Fe^{2+}L^{-1}h^{-1}$). This increase may only be the result of the increase in the microbial biomass attachment in the jarosite accumulated bioreactor. It was hypothesised that the precipitate provided support for microbial attachment and, thus, increased the ferrous-iron oxidation rate. This phenomenon has been reported previously (van der Meer *et al.*, 2007; Pogliani and Donati, 2000). These results showed significantly higher values when compared to values (10.97 mmol$Fe^{2+}.L^{-1}h^{-1}$) obtained during a recent study conducted in a continuous stirred tank bioreactor system (Ojumu, 2008). The study by Ojumu (2008) was conducted in conditions closer to the reported optimum for *L. ferriphilum*. However, this study showed that bioreactor configuration significantly influences the microbial ferrous-iron oxidation kinetics. Table 5.3, indicates the maximum overall rate of microbial ferrous-iron oxidation increased by 38.80% due to the accumulation of jarosite, while the Monod substrate affinity, $K_{Fe^{2+}}$, and the Hansford apparent affinity constant, $K'_{Fe^{2+}}$, decreased significantly with jarosite accumulation. The Monod substrate affinity, $K_{Fe^{2+}}$, measures the affinity of the microorganisms for ferrous-iron and/or the rate of conversion of the ferrous to ferric. The reduction of $K'_{Fe^{2+}}$ and $K_{Fe^{2+}}$ as a result of jarosite accumulation is indicative of increased microbial affinity for the substrate and may also be indicative of the reduced specific microbial ferrous-iron oxidation rate observed as a result of an increase in cell concentration, as suggested by Petersen and Ojumu (2007). However, this phenomenon was not investigated in this current study.

Table 5.3: Maximum ferrous-iron oxidation and kinetic constants at 30 °C, determined from the fit of rate data to the Hansford and Monod models

	Hansford model		Monod model		Average	Increase (%)
	$r_{Fe^{2+}}^{max}$	$K'_{Fe^{2+}}$	$r_{Fe^{2+}}^{max}$	$K_{Fe^{2+}}$	$r_{Fe^{2+}}^{max}$	$r_{Fe^{2+}}^{max}$
Jarosite accumulated data	17.47	0.016	18.57	1.47	18.03	38.80
Limited jarosite data	12.80	0.026	13.17	2.39	12.99	

Units: $r_{Fe^{2+}}^{max}$ (mmol $Fe^{2+}.L^{-1}h^{-1}$), $K_{Fe^{2+}}$ (mmol.L^{-1}), $K'_{Fe^{2+}}$ is dimensionless.

5.4 Conclusion

This study showed that the jarosite precipitate accumulated within the bioreactors served as a support for microbial attachment which, in turn, increased the cell concentration in the packed-bed bioreactor. Maximum of 4% for jarosite was obtained from the bioreactor effluent

at some of the dilution rates investigated, while the remainder of jarosite accumulated in the bioreactor. The data showed that a relatively high maximum overall oxidation rate, $r_{Fe^{2+}}^{max}$, may be achieved in the system as a result of jarosite accumulation. The value obtained in the jarosite-rich experiment corresponded to a 38.80% increase in $r_{Fe^{2+}}^{max}$ when compared to the jarosite limited study. Although jarosite is seen to be an undesirable product in the bioleach heap process, this study showed that it may be advantageous in the context of bioleaching or ferric-iron generation. However, the challenge is to manage its accumulation so that it does not create a mass transfer barrier to bioleaching. Further studies should be directed towards the management of jarosite precipitation in packed-bed column bioreactors.

Chapter 6

Conclusions and Recommendations

6.1 Conclusions

The objective of this study was to investigate the kinetics of microbial ferrous-iron oxidation by *L. ferriphilum* in a packed-bed column, with the view to providing an understanding of the effects of temperatures and ferric-iron precipitate on the kinetics in the context of a heap bioleach system. A similar study was conducted previously using various simplified Equations based on the Monod model, which were developed to describe the rate of microbial ferrous-iron oxidation by *At. ferrooxidans* and *Leptospirillum*–like mesophiles. The operating parameters reported in the literature were similar to those which are possible in a typical heap bioleaching operation. However, the experiments were performed in a stirred tank reactor and a fluidised/flooded column reactor, indicating that the kinetics may not represent those of microbial ferrous-iron oxidation in a heap operation, given the difference in hydrodynamics between tank and heap systems. Previous studies on microbial ferrous-iron oxidation kinetics of *L. ferriphilum* in a continuous culture had applied various kinetic equations to the data obtained, with a view to developing an integrated model to describe the kinetics over a wider range of conditions.

The microbial ferrous-iron oxidation was studied in a temperature controlled and well-aerated packed-bed bioreactor. The oxidation kinetics were monitored by measuring the redox potential in both the reactor feed and effluent. This allowed for the determination of the ferric-to-ferrous iron ratio in the reactor effluent and feed solution. The ferrous-iron oxidation rate was determined from the ferrous-iron balance around the bioreactor.

This study shows that the microbial ferrous-iron oxidation kinetics may be described accurately by both the Monod (Equation 2.42) and Hansford models (Equation 2.53).

$$-r_{Fe^{2+}} = \frac{r_{Fe^{2+}}^{\max}[Fe^{2+}]}{K_{Fe^{2+}} + [Fe^{2+}]} \quad 2.42$$

$$-r_{Fe^{2+}} = \frac{r_{Fe^{2+}}^{\max}}{1 + K'_{Fe^{2+}} \frac{[Fe^{3+}]}{[Fe^{2+}]}} \quad 2.53$$

Both models predicted the experimental data to an accuracy of approximately 92%. The effect of a change in temperature on the system showed that the maximum overall oxidation rate, $r_{Fe^{2+}}^{max}$, increased exponentially with temperature, as expressed by the Arrhenius equation (Equation 2.56) and described in chapter 4. The apparent affinity constant ($K_{Fe^{2+}}$ and $K'_{Fe^{2+}}$) values for the Monod and Hansford models increased significantly with an increase in temperature. However, the limitation of the Hansford's model is such that it is not possible to use it to predict microbial activity, since the apparent affinity constant values in the model are a combined parameter of ferric and ferrous inhibition on microbial growth kinetics, as proposed by the Jones and Kelly (1983). Therefore, by utilising all the kinetic parameters quantified into Equations 2.42 and 2.53, Equations 4.3 and 4.4 were obtained:

$$-r_{Fe^{2+}} = \frac{K_0 \exp\left(-\frac{E_a}{RT}\right)[Fe^{2+}]}{(mT - d) + [Fe^{2+}]} \quad 4.3$$

$$-r_{Fe^{2+}} = \frac{K_0 \exp\left(-\frac{E_a}{RT}\right)}{1 + (mT - d)\frac{[Fe^{3+}]}{[Fe^{2+}]}} \quad 4.4$$

For the Monod model,

K_0 = 4.90×10^4 mmol Fe^{2+}.$L^{-1}h^{-1}$

m = 0.0146 mmol Fe^{2+}.$L^{-1}K^{-1}$

d = 4.2731

For the Hansford model,

K_0 = 5.93×10^4 mmol Fe^{2+}.$L^{-1}h^{-1}$

m = 0.0033 K^{-1}

d = 0.9641

Equations 4.3 and 4.4 were suitable for predicting the effect of temperature change (25 to 35 °C) on microbial ferrous-iron oxidation kinetics by *L. ferriphilum*.

The study on the effect of ferric-iron precipitation showed that ferric-iron accumulation, as described in chapter 5, resulted in an increase in the maximum overall rate of microbial ferrous-iron oxidation ($r^{max}_{Fe^{2+}}$) and a significant decrease in the apparent affinity constant. In addition, the study showed that approximately 4% of the jarosite was obtained from the bioreactor effluent at some of the dilution rates investigated. Equations 2.42 and 2.53 were not capable of predicting the effect of ferric-iron precipitate on microbial ferrous-iron oxidation kinetics by *L. ferriphilum* in a packed column at 30 °C, after substituting the expression for the apparent affinity constants used in this current study. This limitation was as a result of the fact that this experiment did not quantify the relationship between the apparent affinity constants and the mass of ferric-iron precipitation in the packed bed reactor. This highlighted the difficulty in quantifying the relationship between the micro-organisms attached to the ferric iron precipitated on the packing, as well as determining the mass of ferric iron that had precipitated on the packing.

6.2 Recommendations for future studies

This study attempted to investigate the microbial ferrous-iron oxidation kinetics in the context of heap bioleach operations. One limitation of the study is that it did not represent the complexities of a real heap leaching process. It is noted that, apart from the changes in temperature and the precipitation of the ferric ions, there are various operating parameters within a heap operation, including packing height and size, solution pH, and various metals in the ore particles etc., which also contribute to the limitations on the microbial kinetics. Consequently, certain recommendations are suggested for future research.

- In this study, the investigation into the effect of temperature may not have portrayed a real heap situation. It must be noted that the temperature variation within a real heap does not include a range promoting mesophilic growth (15 to 40 °C) only. In industrial heaps, the temperature may range from a value as low as 10 °C on the surface, especially in areas where low ambient temperatures prevail, to values above 65 °C within the heap, which would promote the growth of extreme thermophiles. There is no doubt that this may lead to a decrease in the efficiency of the heap operation by reducing the rate of microbial ferrous-ion oxidation and, as a result, render the process less economical. In this study, the efforts were directed only towards a temperature range that promoted mesophilic growth. It is, thus, recommended that further studies relating to a

wide range of temperature should be undertaken, with a view to a better understand of microbial ferrous-iron oxidation in a real heap situation.

- The packed bed bioreactor was operated at a constant packing height and size. In the heap situation oxygen (O_2) and carbon dioxide (CO_2) transfer may be rate controlling, because O_2 is the electron acceptor in bacterial ferrous-iron oxidation and CO_2 serves as a source of the carbon needed for cell generation. At the bottom of the packed reactor, where air is forced into the packing, O_2 and CO_2 are close to their saturation concentrations. However, as the air flows upwards through the packing, the bacteria catalysing the oxidation of ferrous-iron and the continuous generation of new cells consume O_2 and CO_2, thus resulting in a degree of O_2 and CO_2 depletion near the top of the packed column reactor. Therefore, an understanding of the effect of packing height on the oxygen and carbon dioxide transfer phenomenon in a packed column reactor is essential.

- In addition, the size of the packing in the reactor has been found to have a significant effect on the microbial growth and ferrous iron oxidation by iron oxidising microbes during normal operating conditions. Small particle sizes in the packing allow for poor channelling which, in turn, decreases the mass transfer of nutrients to the bacteria, thus resulting in obstructed biofilm development. Conversely, large particle sizes result in improved channelling, but the surface area available for bacteria attachment decreases, thus leading to low ferric iron productivity. Accordingly, it is recommended that further studies relating to packing height should be performed with the view to a better understanding of the effect of this phenomenon on microbial ferrous iron oxidation.

- Microbial ferrous iron biooxidation is affected significantly by the operating pH. This study was carried out at a constant bioreactor pH of approximately 1.45. The pH was controlled by adjusting the pH of the feed stream, which was fairly challenging as the set point was also dependent on the current bioreactor residence time. The optimum pH for *L. ferriphilum* growth is known to occur in a range of between 1.4 and 1.8. Furthermore, *L. ferriphilum* growth is known to be inhibited at a pH below 1.00 and above 1.6. It is not possible to eradicate ferric-iron precipitation completely. Although jarosite has been shown to facilitate oxidation, it is recommended that the management of jarosite be considered for future studies.

Chapter 7

References

Acevedo, F. 2000. The use of reactors in biomining processes. *Electronic Journal of Biotechnology,* 3(3)**:** 184-194.

Ahonen, L. & Tuovinen, O. 1989. Microbial oxidation of ferrous iron at low temperature. *Applied and Environmental Microbiology,* 55: 312-316.

Alemzadeh, I., Kahrizi, E. & Vossoughi, M. 2009. Bio-oxidation of ferrous ions by Acidithioobacillus ferrooxidans in a monolithic bioreactor. *Journal of Chemical Technology and Biotechnology,* 84(4)**:** 504-510.

Armentia, H. & Webb, C. 1992. Ferrous sulfate oxidation using Thiobacillus ferrooxidans cells immobilised in polyurethane foam support particles. *Applied Microbiology and Biotechnology,* 36(5)**:** 697-700.

Bacelar-Nicolau, P. & Johnson, D. B. 1999. Leaching of Pyrite by Acidophilic Heterotrophic Iron-Oxidizing Bacteria in Pure and Mixed Cultures. *Applied and Environmental Microbiology,* 65(2)**:** 584-590.

Battaglia, F., Morin, D., Garcia, J.-L. & Ollivier, P. 1994. Isolation and study of two strains of Leptospirillum-like bacteria from a natural mixed population cultured on a cobaltiferous pyrite substrate. *Antonie van Leeuwenhoek,* 66(4)**:** 295-302.

Boon, M., Ras, C. & Heijnen, J. J. 1999b. The ferrous iron oxidation kinetics of *Thiobacillus ferrooxidans* in batch cultures. *Applied Microbiology and Biotechnology,* 51(6)**:** 813-819.

Boon, M., Meeder, T. A., Thöne, C., Ras, C. & Heijnen, J. J. 1999a. The ferrous iron oxidation kinetics of *Thibacillus ferrooxidans* in continuous cultures. *Applied Microbiology and Biotechnology,* 51(6)**:** 820-826.

Boon, M. 1996. *Theoretical and Experimental Methods in the Modelling of Biooxidation Kinetics of Sulphide Minerals.* Unpublished PhD Thesis, Technical University, Delft, Netherlands.

Boon, M., Heijnen, J. J. & Hansford, G. S. 1995. Recent developments in modelling bio-oxidation kinetics. Part I. Measurement methods. *In:* Holmes, D. S. & Smith, R. W. (eds.) *Proceedings of Engineering Foundation Conference, July 1994. Minerals Bioprocessing II* Salt Lake City, Warrendale, Pennsylvania: The Minerals Metals and Materials Society.

Boon, M., Hansford, G. S. & Heijnen, J. J. 1995. Recent developments in modelling bio-oxidation kinetics. Part II: Kinetic modelling of the bio-oxidation of sulphide minerals in terms of critical sub-processes involved. *In:* Holmes, D. S. & Smith, R. W. (eds.) *Proceedings of Engineering Foundation Conference, July 1994. Minerals Bioprocessing II.* Salt Lake City, Warrendale, Pennsylvania The Minerals Metals and Materials Society.

Boon, M. & Heijnen, J. 1993. Mechanisms and rate limiting steps in bioleaching of sphalerite, chalcopyrite and pyrite with *Thiobacillus ferrooxidans*. *The Minerals, Metals and Materials Society, Warrendale, PA*: 217-235.

Bosecker, K. 1997. Bioleaching: metal solubilization by microorganisms. *FEMS Microbiology Reviews,* 20(3 4)**:** 591-604.

Brandl, H. 2001. Microbial leaching of metals. *In:* Rehm, H.-J. (ed.) *Biotechnology.* Weinheim: Wiley-VCH: 191-224.

Breed, A., Dempers, C., Searby, G., Gardner, M., Rawlings, D. & Hansford, G. 1999. The effect of temperature on the continuous ferrous iron oxidation kinetics of a predominantly *Leptospirillum ferrooxidans* culture. *Biotechnology and bioengineering,* 65(1)**:** 44-53.

Breed, A. & Hansford, G. 1999. Modeling continuous bioleach reactors. *Biotechnology and bioengineering,* 64(6)**:** 671-677.

Breed, A. W. & Hansford, G. S. 1999. Effect of pH on ferrous-iron oxidation kinetics of *Leptospirillum ferrooxidans* in continuous culture. *Biochemical Engineering Journal,* 3(3)**:** 193-201.

Bridge, T. A. M. & Johnson, D. B. 1998. Reduction of soluble iron and reductive dissolution of ferric iron-containing minerals by moderately thermophilic iron-oxidizing bacteria. *Applied and Environmental Microbiology,* 64(6)**:** 2181-2186.

Brierley, C. 1999. Bacterial succession in bioheap leaching. *In:* Ballester, A. & Amils, R. (eds.) *Biohydrometallurgy and the Environment Toward the Mining of the 21st Century: Part A.* Amsterdam: Elsevier: 91-97.

Brierley, C. L. & Briggs, A. P. 2002. Selection and sizing of biooxidation equipment and circuits. *In:* Mular, A. L., Halbe, D. N. & Barret, D. J. (eds.) *Mineral processing plant design, practice and control.* Littleton, Colo.: Society of Mining Engineers: 1540-1568.

Brierley, J. A. & Brierley, C. L. 2001. Present and future commercial applications of biohydrometallurgy. *Hydrometallurgy,* 59(2-3)**:** 233-239.

Carranza, F. & Garcia, M. 1990. Kinetic comparison of support materials in the bacterial ferrous iron oxidation in packed-bed columns. *Biorecovery,* 2(1)**:** 15-27.

Cavazza, C., Guigliarelli, B., Bertrand, P. & Bruschi, M. 1995. Biochemical and EPR characterization of a high potential iron sulfur protein in Thiobacillus ferrooxidans. *FEMS microbiology letters,* 130(2 3)**:** 193-199.

Chmielewski, T. & Charewicz, W. A. 1984. The oxidation of Fe(II) in aqueous sulphuric acid under oxygen pressure. *Hydrometallurgy,* 12(1)**:** 21-30.

Clark, D. A. & Norris, P. R. 1996. Oxidation of mineral sulphides by thermophilic microorganisms. *Minerals Engineering,* 9(11)**:** 1119-1125.

Coram, N. J. & Rawlings, D. E. 2002. Molecular Relationship between Two Groups of the Genus Leptospirillum and the Finding that Leptospirillum ferriphilum sp. nov.

Dominates South African Commercial Biooxidation Tanks That Operate at 40°C. *Applied and Environmental Microbiology,* 68(2)**:** 838-845.

Crundwell, F. K. 1997. The kinetics of the chemiosmotic proton circuit of the iron-oxidizing bacterium Thiobacillus ferrooxidans. *Bioelectrochemistry and Bioenergetics,* 43(1)**:** 115-122.

Daoud, J. & Karamanev, D. 2006. Formation of jarosite during Fe^{2+} oxidation by *Acidithiobacillus ferrooxidans*. *Minerals Engineering,* 19(9)**:** 960-967.

De, G. C., Oliver, D. J. & Pesic, B. M. 1997. Effect of heavy metals on the ferrous iron oxidizing ability of Thiobacillus ferrooxidans. *Hydrometallurgy,* 44(1-2)**:** 53-63.

De, G. C., Oliver, D. J. & Pesic, B. M. 1996. Effect of silver on the ferrous iron oxidizing ability of Thiobacillus ferrooxidans. *Hydrometallurgy,* 41(2-3)**:** 211-229.

De, G. C. 1993. *Effect of heavy metals on the ferrous iron oxidizing ability of Thiobacillus ferrooxidans.* Unpublished Ph.D. Thesis, University of Idaho.

Dew, D. W., Lawson, E. N. & Broadhurst, J. L. 1997. The BIOX® process for biooxidation of gold-bearing ores or concentrates. *In:* Rawlings, D. E. (ed.). *Biomining Theory, Microbes and Industrial Processes.* Verlag, Berlin: Springer: 45 - 80.

Dixon, D. G. 2000. Analysis of heat conservation during copper sulphide heap leaching. *Hydrometallurgy,* 58(1)**:** 27-41.

Domic, E. M. 2007. A review of the Development and Current Status of Copper Bioleaching Operation in Chile: 25 Years of Successful Commercial Implementation. *In:* Rawlings, D. E. & Johnson, D. B. (eds.) *Biomining.* Berlin: Springer: 81-95.

Dopson, M., Halinen, A. K., Rahunen, N., Özkaya, B., Sahinkaya, E., Kaksonen, A. H., Lindström, E. B. & Puhakka, J. A. 2007. Mineral and iron oxidation at low temperatures by pure and mixed cultures of acidophilic microorganisms. *Biotechnology and Bioengineering,* 97(5)**:** 1205-1215.

Dopson, M., Baker-Austin, C., Hind, A., Bowman, J. P. & Bond, P. L. 2004. Characterization of Ferroplasma isolates and Ferroplasma acidarmanus sp. nov., extreme acidophiles

from acid mine drainage and industrial bioleaching environments. *Applied and Environmental Microbiology,* 70(4)**:** 2079-2088.

Dopson, M., Baker-Austin, C., Koppineedi, P. R. & Bond, P. L. 2003. Growth in sulfidic mineral environments: metal resistance mechanisms in acidophilic micro-organisms. *Microbiology,* 149(8)**:** 1959-1970.

Doran, P. M. 1995. *Bioprocess engineering principles*, Academic Press, Harcourt Brace and Company.

Du Plessis, C. A., Batty, J. D. & Dew, D. W. 2007. Commercial application of thermophile bioleaching. *In:* Rawlings, D. E. & Johnson, D. B. (eds.) *Biomining.* Berlin: Springer: 57-80.

Dutrizac, J. E. 1984. The behaviour of impurities during jarosite precipitation. *In:* Bautista, R. G. (ed.) *Hydrometallurgical Process Fundamentals.* New York: Plenum Press: 125-169.

Ehrlich, H. L. 2001. Past, present and future of biohydrometallurgy. *Hydrometallurgy,* 59(2-3)**:** 127-134.

Eneroth, E. B. & Koch, C. 2004. Fe-hydroxysulphates from bacterial Fe2+ oxidation. *Hyperfine Interact,* 156/157(1-4)**:** 423-429.

Ferroni, G., Leduc, L. & Todd, M. 1986. Isolation and temperature characterization of psychrotrophic strains of Thiobacillus ferrooxidans from the environment of a uranium mine. *Journal of General and Applied Microbiology,* 32(3)**:** 169-175.

Fogler, H. S. 2006. *Elements of Chemical Reaction Engineering*, Person Education.

Foucher, S., Battaglia-Brunet, F., d'Hugues, P., Clarens, M., Godon, J. J. & Morin, D. 2003. Evolution of the bacterial population during the batch bioleaching of a cobaltiferous pyrite in a suspended-solids bubble column and comparison with a mechanically agitated reactor. *Hydrometallurgy,* 71(1-2)**:** 5-12.

Franzmann, P. D., Haddad, C. M., Hawkes, R. B., Robertson, W. J. & Plumb, J. J. 2005. Effects of temperature on the rates of iron and sulfur oxidation by selected

bioleaching Bacteria and Archaea: Application of the Ratkowsky equation. *Minerals Engineering,* 18(13-14)**:** 1304-1314.

Goebel, B. M. & Stackebrandt, E. 1994. Cultural and phylogenetic analysis of mixed microbial populations found in natural and commercial bioleaching environments. *Applied and Environmental Microbiology,* 60(5)**:** 1614-1621.

Golovacheva, R. & Karavaiko, G. 1978. A new genus of thermophilic spore-forming bacteria, Sulfobacillus. *Microbiology,* 47: 658-664.

Golyshina, O. V., Pivovarova, T. A., Karavaiko, G. I., Kondrat'eva, T. F., Moore, E. R. B., Abraham, W. R., Lunsdorf, H., Timmis, K., Yakimov, M. & Golyshin, P. 2000. Ferroplasma acidiphilum gen. nov., sp. nov., an acidophilic, autotrophic, ferrous-iron-oxidizing, cell-wall-lacking, mesophilic member of the Ferroplasmaceae fam. nov., comprising a distinct lineage of the Archaea. *International journal of systematic and evolutionary microbiology,* 50(3)**:** 997-1006.

Grishin, S. I., Bigham, J. M. & Tuovinen, O. H. 1988. Characterization of jarosite formed upon bacterial oxidation of ferrous sulfate in a packed-bed reactor. *Applied and Environmental Microbiology,* 54(12)**:** 3101-3106.

Grishin, S. I. & Tuovinen, O. H. 1988. Fast kinetics of Fe^{2+} oxidation in packed-bed reactors. *Applied and Environmental Microbiology,* 54(12)**:** 3092-3100.

Guay, R., Silver, M. & Torma, A. E. 1977. Ferrous iron oxidation and uranium extraction by Thiobacillus ferrooxidans. *Biotechnology and bioengineering,* 19(5)**:** 727-740.

Hackl, R. P., Dreisinger, D. B., Peters, E. & King, J. A. 1995. Passivation of chalcopyrite during oxidative leaching in sulfate media. *Hydrometallurgy,* 39(1-3)**:** 25-48.

Halinen, A.-K., Rahunen, N., Kaksonen, A. H. & Puhakka, J. A. 2009. Heap bioleaching of a complex sulfide ore: Part I: Effect of pH on metal extraction and microbial composition in pH controlled columns. *Hydrometallurgy,* 98(1-2)**:** 92-100.

Hallberg, K. B. & Barrie Johnson, D. 2001. Biodiversity of acidophilic prokaryotes. *Advances in Applied Microbiology,* 49: 37-84.

Hallmann, R., Friedrich, A., Koops, H. P., Pommerening-Röser, A., Rohde, K., Zenneck, C. & Sand, W. 1992. Physiological characteristics of Thiobacillus ferrooxidans and Leptospirillum ferrooxidans and physicochemical factors influence microbial metal leaching. *Geomicrobiology Journal,* 10(3)**:** 193-206.

Hansford, G. S. & Vargas, T. 2001. Chemical and electrochemical basis of bioleaching processes. *Hydrometallurgy,* 59(2-3)**:** 135-145.

Hansford, G. S. 1997. Recent development in modelling the kinetics of bioleaching. *In:* Rawlings, D. E. (ed.) *Biomining: Theory, Microbes and Industrial Processes.* Austin, TX: Springer: 24.

Harvey, P. & Crundwell, F. 1997. Growth of Thiobacillus ferrooxidans: a novel experimental design for batch growth and bacterial leaching studies. *Applied and Environmental Microbiology,* 63(7)**:** 2586-2592.

Herbert, D. 1958. Some principles of continuous culture. *In:* Tunevall, G. (ed.) *Recent Progress in Microbiology.* Stockholm: AImkvist and Wiksell: 381-396.

Hippe, H. 2000. *Leptospirillum* gen. nov. (ex Markosyan,m1972), nom. rev., including *Leptospirillum ferrooxidans* sp. nov. (ex Markosyan, 1972), nom. rev. and *Leptospirillum thermoferrooxidans* sp. nov. (Golovacheva et al., 1992). *International Journal of Systematic and Evolutionary Microbiology,* 50: 501-503.

Hiroyoshi, N., Miki, H., Hirajima, T. & Tsunekawa, M. 2001. Enhancement of chalcopyrite leaching by ferrous ions in acidic ferric sulphate solutions. *Hydrometallurgy,* 60(3)**:** 185-197.

Hiroyoshi, N., Hirota, M., Hirajima, T. & Tsunekawa, M. 1997. A case of ferrous sulfate addition enhancing chalcopyrite leaching. *Hydrometallurgy,* 47(1)**:** 37-45.

Hofstee, B. H. J., Ddcon, M. & Webb, E. C. 1959. Non-inverted versus inverted plots in enzyme kinetics. *Nature,* 184:1296-1298.

Huber, G. & Stetter, K. O. 1991. Sulfolobus metallicus, sp. nov., a novel strictly chemolithoautotrophic thermophilic archaeal species of metal-mobilizers. *Systematic and applied microbiology,* 14: 372-378.

Huberts, R. 1994. *Modelling of ferrous sulphate oxidation by iron oxidizing bacteria - a chemiosmotic and electrochemical approach.* Unpublished PhD Thesis, University of Witwatersrand, Johannesburg.

Ingledew, W. J. 1982. Thiobacillus ferrooxidans. The bioenergetics of an acidophilic chemolithotroph. *Biochimica et biophysica acta,* 683(2)**:** 89-117.

Jensen, A. B. & Webb, C. 1995. Ferrous sulphate oxidation using thiobacillus ferrooxidans: a review. *Process Biochemistry,* 30(3)**:** 225-236.

Jensen, A. B. & Webb, C. 1994. A trickle-bed reactor for ferrous sulfate oxidating using *Thiobacillus ferrooxidans*. *Biotechnology Techniques,* 8(2)**:** 87-92.

Johnson, D. B. 1998. Biodiversity and ecology of acidophilic microorganisms. *FEMS Microbiology Ecology,* 27(4)**:** 307-317.

Jones, C. A. & Kelly, D. 1983. Growth of Thiobacillus ferrooxidans on ferrous iron in chemostat culture: influence of product and substrate inhibition. *Journal of Chemical Technology and Biotechnology. Biotechnology,* 33(4)**:** 241-261.

Keller, G. & Warrack, B. 1999. Statistics: for Management and Economics. (5th Edition) Duxbury Thomson Learning, USA.pp. 626-673.

Kelly, D. P. & Wood, A. P. 2000. Reclassification of some species of Thiobacillus to the newly designated genera Acidithiobacillus gen. nov., Halothiobacillus gen. nov. and Thermithiobacillus gen. nov. *International journal of systematic and evolutionary microbiology,* 50(2)**:** 511-516.

Kelly, D. P. & Jones, C. A. 1978. Factors affecting metabolism and ferrous iron oxidation in suspensions and batch cultures of Thiobacillus ferrooxidans: relevance to ferric leach regeneration. *In:* Murr, L. E., Torna, A. E. & Brierley, J. A. (eds.) *Metallurgical Applications of bacterial leaching and related microbiological phenomena.* Academic Press: 19-44.

Kinnunen, P. 2004. *High-rate ferric sulfate generation and chalcopyrite concentrate leaching by Acidophilic microorganisms.* Unpublished PhD Thesis, Tampere University of Technology.

Kinnunen, P. H. M. & Puhakka, J. A. 2005. High-rate iron oxidation at below pH 1 and at elevated iron and copper concentrations by a Leptospirillum ferriphilum dominated biofilm. *Process Biochemistry,* 40(11)**:** 3536-3541.

Kovárová-Kovardagger, K. & Egli, T. 1998. Growth kinetics of suspended microbial cells: From single-substrate-controlled growth to mixed-substrate kinetics. *Microbiology and molecular biology reviews,* 62(3)**:** 646-666.

Kupka, D., Rzhepishevska, O. I., Dopson, M., Lindström, E. B., Karnachuk, O. V. & Tuovinen, O. H. 2007. Bacterial oxidation of ferrous iron at low temperatures. *Biotechnology and bioengineering,* 97(6)**:** 1470-1478.

Lacey, D. & Lawson, F. 1970. Kinetics of the liquid phase oxidation of acid ferrous sulfate by the bacterium Thiobacillus ferrooxidens. *Biotechnology and bioengineering,* 12(1)**:** 29-50.

Lancy, E. D. & Tuovinen, O. H. 1984. Ferrous ion oxidation by Thiobacillus ferrooxidans immobilised in calcium alginate. *Applied Microbiology and Biotechnology,* 20(2)**:** 94-99.

Leduc, L. G., Trevors, J. T. & Ferroni, G. D. 1993. Thermal characterization of different isolates of Thiobacillus ferrooxidans. *FEMS microbiology letters,* 108(2)**:** 189-193.

Lineweaver, H. & Burk, D. 1934. The determination of enzyme dissociation constants. *Journal of the American Chemical Society,* 56(3)**:** 658-666.

Long, Z.-e., Huang, Y., Cai, Z., Cong, W. & Ouyang, F. 2004. Kinetics of continuous ferrous ion oxidation by *Acidithiobacillus ferrooxidans* immobilized in poly(vinyl alcohol) cryogel carriers. *Hydrometallurgy,* 74(3-4)**:** 181-187.

Long, Z.-e., Huang, Y., Cai, Z., Cong, W. & Ouyang, F. 2003. Biooxidation of ferrous iron by immobilised *Acidithiobacillus ferrooxidan*s in poly(vinyl alcohol) cryogel carriers. *Biotechnology Letters,* 25(3)**:** 245-249.

Lugaski, T. 1997. Extracting metal from ore.

Lundgren, D. G. 1975. Microbiological problems in strip mine areas: Relationship to the metabolism of Thiobacillus ferrooxidans. *The Ohio Journal of Science,* 75(6)**:** 280-287.

MacDonald, D. & Clark, R. 1970. The oxidation of aqueous ferrous sulphate by Thiobacillus ferrooxidans. *The Canadian Journal of Chemical Engineering,* 48(6)**:** 669-676.

Maciag, W. J. & Lundgren, D. G. 1964. Carbon dioxide fixation in the chemoautotroph,* 1. *Biochemical and Biophysical Research Communications,* 17(6)**:** 603-607.

Markosyan, G. E. 1972. A new iron-oxidizing bacterium *Leptospirillum ferrooxidans* nov. gen. nov. sp. *Biol. J. Armenia.,* 2526-29 'in Rassian'.

Mazuelos, A., Carranza, F., Romero, R., Iglesias, N. & Villalobo, E. 2010. Operational pH in packed-bed reactors for ferrous ion bio-oxidation. *Hydrometallurgy,* 104(2)**:** 186-192.

Mazuelos, A., Romero, R., Palencia, I., Carranza, F. & Borjas, F. J. 2002. Oxygen transfer in ferric iron biological production in a packed-bed reactor. *Hydrometallurgy,* 65(1)**:** 15-22.

Mazuelos, A., Palencia, I., Romero, R., Rodríguez, G. & Carranza, F. 2001. Ferric iron production in packed bed bioreactors: influence of pH, temperature, particle size, bacterial support material and type of air distributor. *Minerals Engineering,* 14(5)**:** 507-514.

Mazuelos, A., Carranza, F., Palencia, I. & Romero, R. 2000. High efficiency reactor for the biooxidation of ferrous iron. *Hydrometallurgy,* 58(3)**:** 269-275.

Meruane, G., Salhe, C., Wiertz, J. & Vargas, T. 2002. Novel electrochemical–enzymatic model which quantifies the effect of the solution Eh on the kinetics of ferrous iron oxidation with Acidithiobacillus ferrooxidans. *Biotechnology and bioengineering,* 80(3)**:** 280-288.

Monod, J. 1942. Recherches sur la Croissance des Cultures Bacteriennes: Herman & Cie. Paris.

Montealegre, R., Bustos, S., Rojas, J., Neuburg, H., Araya, C., Yanez, H., Tapia, R. & Rauld, J. 1993. Application of the bacterial thin layer leaching process to Quebrada Blanca ores. *Biohydrometallurgical Technologies.,* 11-14.

Murr, L. E. & Brierley, J. A. 1978. The use of large-scale test facilities in studies of the role of microorganisms in commercial leaching operations. *In:* Murr, L. E., Torma, A. E. & Brierley, J. A. (eds.) *Metallurgical Applications of bacterial leaching and related microbiological phenomena.* New York: Academic Press: 526.

Nagpal, S. & Dahlstrom, D. 1994. A mathematical model for the bacterial oxidation of a sulphide ore concentrate. *Biotechnology and Bioengineering,* 43: 357-364.

Nemati, M., Harrison, S. T. L., Hansford, G. S. & Webb, C. 1998. Biological oxidation of ferrous sulphate by Thiobacillus ferrooxidans: a review on the kinetic aspects. *Biochemical Engineering Journal,* 1(3)**:** 171-190.

Nemati, M. & Webb, C. 1997. A kinetic model for biological oxidation of ferrous iron by Thiobacillus ferrooxidans. *Biotechnology and bioengineering,* 53(5)**:** 478-486.

Nikolov, L., Valkova-Valchanova, M. & Mehochev, D. 1988. Oxidation of high ferrous iron concentrations by chemolithotrophic Thiobacillus ferrooxidans in packed bed bioreactors. *Journal of Biotechnology,* 7(2)**:** 87-94.

Norris, P. R., Clark, D. A., Owen, J. P. & Waterhouse, S. 1996. Characteristics of Sulfobacillus acidophilus sp. nov. and other moderately thermophilic mineral-sulphide-oxidizing bacteria. *Microbiology,* 142(4)**:** 775-783.

Ojumu, T. V. & Petersen, J. 2011. The kinetics of ferrous ion oxidation by *Leptospirillum ferriphilum* in continuous culture: The effect of pH. *Hydrometallurgy,* 106(1-2)**:** 5-11.

Ojumu, T. V., Hansford, G. S. & Petersen, J. 2009. The kinetics of ferrous-iron oxidation by *Leptospirillum ferriphilum* in continuous culture: The effect of temperature. *Biochemical Engineering Journal,* 46(2)**:** 161-168.

Ojumu, T. V., Petersen, J. & Hansford, G. S. 2008. The effect of dissolved cations on microbial ferrous-iron oxidation by *Leptospirillum ferriphilum* in continuous culture. *Hydrometallurgy,* 94(1-4)**:** 69-76.

Ojumu, T. V. 2008. *The effects of solution conditions on the kinetics of microbial ferrous-Iron oxidation by Leptospirillum ferriphilum in continuous culture.* Unpublished PhD Thesis, University of Cape Town, South Africa.

Ojumu, T. V., Petersen, J., Searby, G. E. & Hansford, G. S. 2006. A review of rate equations proposed for microbial ferrous-iron oxidation with a view to application to heap bioleaching. *Hydrometallurgy,* 83(1-4)**:** 21-28.

Okibe, N., Gericke, M., Hallberg, K. B. & Johnson, D. B. 2003. Enumeration and characterization of acidophilic microorganisms isolated from a pilot plant stirred-tank bioleaching operation. *Applied and Environmental Microbiology,* 69(4)**:** 1936-1943.

Olson, G. J., Brierley, J. A. & Brierley, C. L. 2003. Progress in bioleaching: applications of microbial processes by the minerals industries. *Applied Microbiology and Biotechnology,* 63(3)**:** 249-257.

Özkaya, B., Sahinkaya, E., Nurmi, P., Kaksonen, A. H. & Puhakka, J. A. 2007. Kinetics of iron oxidation by Leptospirillum ferriphilum dominated culture at pH below one. *Biotechnology and bioengineering,* 97(5)**:** 1121-1127.

Penev, K. & Karamanev, D. 2010. Batch kinetics of ferrous iron oxidation by Leptospirillum ferriphilum at moderate to high total iron concentration. *Biochemical Engineering Journal,* 50(1-2)**:** 54-62.

Peters, E. 1976. Direct Leaching of sulfides: Chemistry and applications. *Metallurgical and Materials Transactions B,* 7(4)**:** 505-517.

Petersen, J., Minaar, S. H. & du Plessis, C. A. 2011. Respirometry studies of the bioleaching of a copper ore in large columns effect of changing temperatures. *In:* Qiu, G., Jiang, T., Qin, W., Liu, X., Yang, Y. & Wang, H. (eds.) *Proceeding of the 19th international Biohydrometallurgy Symposium* China, Changsha: Central South University Press.

Petersen, J. & Ojumu, T. V. 2007. The effect of total iron concentration and iron speciation on the rate of ferrous iron oxidation kinetics of *Leptospirillum ferriphilum* in continuous tank systems. *Advanced Materials Research,* 20: 447-451.

Petersen, J. & Dixon, D. G. 2007. Modelling zinc heap bioleaching. *Hydrometallurgy,* 85(2-4)**:** 127-143.

Petersen, J. & Dixon, D. 2007. Modelling zinc heap bioleaching. *Hydrometallurgy,* 85(2-4)**:** 127-143.

Petersen, J. & Dixon, D. G. 2006. Modeling and Optimization of Heap Bioleach Processes. *Biomining, Springer-Verlag, Berlin,* 153-175.

Petersen, J. & Dixon, D. G. 2004. Bacterial growth and propagation in chalcocite heap bioleach scenarios. *In:* Tsezos, M., Hatzikioseyian, A. & Remoundaki, E. (eds.) *Biohydrometallurgy - a sustainable technology in evolution, IBS 2003.* National Technical University of Athens.

Pirt, S. J. 1965. The maintenance energy of bacteria in growing cultures. *Proceedings of the Royal Society of London.* Biological Sciences.

Plumb, J. J., Muddle, R. & Franzmann, P. D. 2008. Effect of pH on rates of iron and sulfur oxidation by bioleaching organisms. *Minerals Engineering,* 21(1)**:** 76-82.

Plumb, J. J., McSweeney, N. J. & Franzmann, P. D. 2008. Growth and activity of pure and mixed bioleaching strains on low grade chalcopyrite ore. *Minerals Engineering,* 21(1)**:** 93-99.

Pogliani, C. & Donati, E. 2000. Immobilisation of Thiobacillus ferrooxidans: importance of jarosite precipitation. *Process Biochemistry,* 35(9)**:** 997-1004.

Pradhan, N., Nathsarma, K. C., Srinivasa Rao, K., Sukla, L. B. & Mishra, B. K. 2008. Heap bioleaching of chalcopyrite: A review. *Minerals Engineering,* 21(5)**:** 355-365.

Rawlings, D., Tributsch, H. & Hansford, G. 1999. Reasons why 'Leptospirillum'-like species rather than Thiobacillus ferrooxidans are the dominant iron-oxidizing bacteria in many commercial processes for the biooxidation of pyrite and related ores. *Microbiology,* 145(Pt 1)**:** 5-13.

Rawlings, D. E. 2007. Relevance of Cell Physiology and Genetic Adaptability of Biomining Microorganisms to Inductrial Processes. *In:* Rawlings, D. E. & Johnson, D. B. (eds.) *Biomining.* Verlag, Berlin: Springer: 177-198.

Rawlings, D. E. 2005. Characteristics and adaptability of iron- and sulfur-oxidizing microorganisms used for the recovery of metals from minerals and their concentrates. *Microbial Cell Factories,* 4(1)**:** 13.

Rawlings, D. E., Dew, D. & du Plessis, C. 2003. Biomineralization of metal-containing ores and concentrates. *Trends in Biotechnology,* 21(1)**:** 38-44.

Rawlings, D. E. 2002. Heavy Metal Mining Using Microbes 1. *Annual Reviews in Microbiology,* 56(1)**:** 65-91.

Roels, J. A. & Kossen, N. W. F. 1978. On the Modelling of Microbial Metabolism. *In Progress in Industrial Microbiology,* 14: 95-203.

Rohwerder, T. & Sand, W. 2007. Mechansims and biochemical fundamentals of bacterial metal sulphide oxidation *In:* Donati, E. R. & Sand, W. (eds.) *Microbial Processing of Metal Sulphides.* The Netherlands: Springer: 35-58.

Rohwerder, T., Gehrke, T., Kinzler, K. & Sand, W. 2003. Bioleaching review part A. *Bioleaching review part A: Progress in bioleaching: fundamentals and mechanisms of bacterial metal sulphide oxidation,* 63(3)**:** 239-248.

Rossi, G. 1990. *Biohydrometallurgy*, McGraw-Hill.

Rzhepishevska, O. I., Lindström, E. B., Tuovinen, O. H. & Dopson, M. 2005. Bioleaching of sulfidic tailing samples with a novel, vacuum positive pressure driven bioreactor. *Biotechnology and bioengineering,* 92(5)**:** 559-567.

Sand, W., Gehrke, T., Jozsa, P.-G. & Schippers, A. 2001. (Bio)chemistry of bacterial leaching--direct vs. indirect bioleaching. *Hydrometallurgy,* 59(2-3)**:** 159-175.

Sand, W., Gerke, T., Hallmann, R. & Schippers, A. 1995. Sulfur chemistry, biofilm, and the (in) direct attack mechanism—a critical evaluation of bacterial leaching. *Applied Microbiology and Biotechnology,* 43(6)**:** 961-966.

Schippers, A. & Sand, W. 1999. Bacterial leaching of metal sulfides proceeds by two direct mechanisms via thiosulfate or via polysulfides and sulfur. *Applied and Environmental Microbiology,* 65(1)**:** 319 - 321.

Schnell, H. A. 1997. Bioleaching of copper. *In:* Rawlings, D. E. (ed.) *Biomining: Theory, Microbes and Industrial Processes.* Berlin: Springer-Verlag: 21-43.

Segerer, A., Neuner, A., Kristjansson, J. K. & Stetter, K. O. 1986. Acidianus infernus gen. nov., sp. nov., and Acidianus brierleyi comb. nov.: facultatively aerobic, extremely acidophilic thermophilic sulfur-metabolizing archaebacteria. *International journal of systematic and evolutionary microbiology,* 36(4)**:** 559-564.

Silver, M. 1978. Metabolic mechanisms of iron oxidizing *Thiobacilli*. *In:* Murr, L. E., Torma, A. E. & Brierley, J. A. (eds.) *Metallurgical Applications of Bacterial Leaching and Related Microbiological Phenomena.* New York: Academic Press: 3-18.

Silverman, M. P. & Ehrlich, H. L. 1964. Microbial formation and degradation of minerals. *Advances in Applied Microbiology,* 6: 153-206.

Stott, M., Sutton, D., Watling, H. & Franzmann, P. 2003. Comparative leaching of chalcopyrite by selected acidophilic bacteria and archaea. *Geomicrobiology Journal,* 20(3)**:** 215-230.

Stott, M. B., Watling, H. R., Franzmann, P. D. & Sutton, D. 2000. The role of iron-hydroxy precipitates in the passivation of chalcopyrite during bioleaching. *Minerals Engineering,* 13(10-11)**:** 1117-1127.

Sundkvist, J. E., Gahan, C. S. & Sandström, Å. 2007. Modeling of microbial ferrous iron oxidation by *Leptospirillum ferrooxidans* in a continuous bioreactor. *Biotechnology and Bioengineering,* 99(2)**:** 378–389

Third, K. A., Cord-Ruwisch, R. & Watling, H. R. 2000. The role of iron-oxidizing bacteria in stimulation or inhibition of chalcopyrite bioleaching. *Hydrometallurgy,* 57(3)**:** 225-233.

Tributsch, H. 2001. Direct versus indirect bioleaching. *Hydrometallurgy,* 59(2-3)**:** 177-185.

Tuovinen, O. & Kelly, D. 1972. Biology of Thiobacillus ferrooxidans in relation to the microbiological leaching of sulphide ores. *Zeitschrift für allgemeine Mikrobiologie,* 12(4)**:** 311-346.

Valdés, J., Cárdenas, J. P., Quatrini, R., Esparza, M., Osorio, H., Duarte, F., Lefimil, C., Sepulveda, R., Jedlicki, E. & Holmes, D. S. 2010. Comparative genomics begins to unravel the ecophysiology of bioleaching. *Hydrometallurgy,* 104(3-4)**:** 471-476.

Van Aswegen, P. C., van Niekerk, J. & Olivier, W. 2007. The BIOXTM process for the Treatment of Refractory Gold Concentrates. *In:* Rawlings, D. E. & Johnson, D. B. (eds.) *Biomining.* Berlin: Springer: 2-33.

van der Meer, T., Kinnunen, P. H. M., Kaksonen, A. H. & Puhakka, J. A. 2007. Effect of fluidized-bed carrier material on biological ferric sulphate generation. *Minerals Engineering,* 20(8)**:** 782-792.

Verbaan, B. & Crundwell, F. K. 1986. An electrochemical model for the leaching of a sphalerite concentrate. *Hydrometallurgy,* 16(3)**:** 345-359.

Verger, R. & De Haas, G. H. 1976. Interfacial enzyme kinetics of lipolysis. *Annual Review of Biophysics and Bioengineering,* 5(1)**:** 77-117.

Vishniac, W. & Santer, M. 1957. The thiobacilli. *Microbiology and molecular biology reviews,* 21(3)**:** 195-213.

Vogel, A. I. & Svehla, G. 1987. *Vogel's qualitative inorganic analysis*, Longman Scientific & Technical. Wiley.

Watling, H. R. 2006. The bioleaching of sulphide minerals with emphasis on copper sulphides -- A review. *Hydrometallurgy,* 84(1-2)**:** 81-108.

Yarzabal, A., Brasseur, G., Ratouchniak, J., Lund, K., Lemesle-Meunier, D., DeMoss, J. A. & Bonnefoy, V. 2002. The high-molecular-weight cytochrome c Cyc2 of Acidithiobacillus ferrooxidans is an outer membrane protein. *Journal of bacteriology,* 184(1)**:** 313-317.

APPENDICES

Appendix A

A1.1 A theoretical development for the kinetics of microbial ferrous-iron oxidation

In order to determine the kinetic and yield parameters for a Fe^{2+} oxidising culture, the overall cell and substrate mass balances must be established for a packed reactor at different residence times. The following general assumptions are valid:

- As a result of high aeration within the bioreactor, intensive mixing occurs and, therefore, almost to perfect mixing of the liquid in the bioreactor occurs.
- The reaction is carried out at constant temperatures and concentration.
- The total active reactor volume remains constant.
- In a packed bioreactor the micro-organisms grow in the liquid within the bioreactor and are uniformly immobilised on the surface of the inert matrix (ie. packing) in the bioreactor as a monolayer of constant thickness.
- The process is a continuous, steady-state regime.
- The death cell rate is negligible when compared to the growth rate.
- At steady-state condition, the cell concentrations are constant since the rate of cell removal is equal to the cell growth rate. The cell growth rate is normally much lower than the rate of biochemical reaction and, therefore, this assumption is valid for a small period of time in biofilm reactors.
- The culture is substrate-limited with respect to Fe^{2+}.
- The feed solution is sterile and no growth inhibition factors are present.
- There is no diffusion limitation of the substrate. In a thin biofilm, the limiting substrate concentration drop is small and, therefore, has a negligible effect of diffusion.
- There are no kinetic changes of bioprocess after fixation of the micro-organisms.

The overall cell balance for active microbial cells in a packed reactor over time is given by Equation 2.45.

$$V_{AR}\frac{dC_X}{dt} = FC_{X_0} - FC_X + \mu C_X V_{AR} - K_d C_X V_{AR} \qquad 2.45$$

Where V_{AR} is the reactor active volume (L) (V_{AR}= Volume of the reactor – Total volume of the inert packing), F is the inlet and outlet flow rate (L/h); C_X is the bacteria concentration (mmol $C.L^{-1}$); μ and K_d is the specific growth (h^{-1}) and death rate constants (h^{-1}), respectively. K_d implies that cell death and lysis are the primary mechanisms of mass reduction. Assuming that the feed is sterile (C_{X_0} =0), the death rate is negligible (K_d=0) and, if the system is at steady state (dC_X/dt =0), then Equation 2.45 is converted to Equation 2.46:

$$\mu = \frac{F}{V_{AR}} = D = \frac{1}{\tau} \qquad 2.46$$

Where D is the dilution rate (h^{-1}) and τ (h) the residence time.

However, for the overall substrate balance, the amount of Fe^{2+} in the packed reactor at a given time is represented by Equation 2.47.

$$\tau = \frac{V_{AR}}{v_0} = [Fe^{2+}]_{In} \int_0^X \frac{dX}{-r_S} = \int_{[Fe^{2+}]_{Out}}^{[Fe^{2+}]_{In}} \frac{d[Fe^{2+}]}{-r_{Fe^{2+}}} \qquad 2.47$$

Equation 2.30 may be further simplified by substituting for μ to give:

$$[Fe^{2+}]_{In} - [Fe^{2+}]_{Out} = [Fe^{2+}] = \frac{DK_{Fe^{2+}}}{\mu_{\max} - D} \qquad 2.48$$

The Monod equation, indicated by Equation 2.42, may be simplified by substituting for $r^{max}_{Fe^{2+}} = q^{max}_{Fe^{2+}} C_X$:

$$-r_{Fe^{2+}} = \frac{q^{\max}_{Fe^{2+}} C_X [Fe^{2+}]}{K_{Fe^{2+}} + [Fe^{2+}]} \qquad 2.49$$

Equation 2.47 may be further simplified by substituting Equations 2.46 and 2.49:

$$\tau = \frac{1}{D} = \int_{[Fe^{2+}]_{Out}}^{[Fe^{2+}]_{In}} \frac{\left(K_{Fe^{2+}} + [Fe^{2+}]\right) d[Fe^{2+}]}{q^{\max}_{Fe^{2+}} C_X [Fe^{2+}]} \qquad A1.1$$

Assuming the initial ferrous-iron concentration ($[Fe^{2+}]_{In}$) to be equal to the total iron concentration ($[Fe^T]$) and $[Fe^{2+}]_{Out} = [Fe^{2+}]$, Equation A1.1 may be simplified to Equation A1.2:

$$C_X = \frac{D}{q^{\max}_{Fe^{2+}}}\left(K_{Fe^{2+}} \log[Fe^T] + [Fe^T] - K_{Fe^{2+}} \log[Fe^{2+}] - [Fe^{2+}]\right) \quad \text{A1.2}$$

Equation A1.2 may be rewritten by substituting Equation 2.48:

$$C_X = \frac{D}{q^{\max}_{Fe^{2+}}}\left(K_{Fe^{2+}} \log[Fe^T] + [Fe^T] - K_{Fe^{2+}} \log\frac{DK_{Fe^{2+}}}{\mu_{\max} - D} - \frac{DK_{Fe^{2+}}}{\mu_{\max} - D}\right) \quad 2.50$$

The Hansford equation (Equation 2.53) may be rewritten by substitution of $q_{Fe^{2+}} = D$, $q^{\max}_{Fe^{2+}} = D^{\max}$ and $[Fe^{3+}] = [Fe^T]-[Fe^{2+}]$:

$$D = \frac{D^{\max}}{1 + K'_{Fe^{2+}} \dfrac{[Fe^T] - [Fe^{2+}]}{[Fe^{2+}]}} \quad \text{A1.3}$$

Equation A1.3 may be expressed in terms of the ferrous-iron concentration:

$$[F^{2+}] = \frac{DK'_{Fe^{2+}}[Fe^T]}{D^{\max} - D\left(1 - K'_{Fe^{2+}}\right)} \quad 2.45$$

Equation 2.43 may also be rewritten by substituting for $r^{\max}_{Fe^{2+}} = q^{\max}_{Fe^{2+}} C_X$ and $[Fe^{3+}] = [Fe^T] - [Fe^{2+}]$:

$$-r_{Fe^{2+}} = \frac{q^{\max}_{Fe^{2+}} C_X [Fe^{2+}]}{[Fe^{2+}] + K'_{Fe^{2+}}([Fe^T] - [Fe^{2+}])} \quad \text{A1.4}$$

Equation 2.47 may be further simplified by substituting Equations 2.46 and A1.4:

$$\tau = \frac{1}{D} = \int_{[Fe^{2+}]_{Out}}^{[Fe^{2+}]_{In}} \frac{\{[Fe^{2+}] + K'_{Fe^{2+}}([Fe^T] - [Fe^{2+}])\}\, d[Fe^{2+}]}{q^{\max}_{Fe^{2+}} C_X [Fe^{2+}]} \quad \text{A1.5}$$

Assuming $[Fe^{2+}]_{In} = [Fe^T]$ and $[Fe^{2+}]_{Out} = [Fe^{2+}]$, Equation A1.5 may be simplified to Equation A1.6:

$$C_X = \frac{D}{q^{\max}_{Fe^{2+}}}\left[K'_{Fe^{2+}}[Fe^T]\log[Fe^T] - K'_{Fe^{2+}}[Fe^T] + [Fe^T] - K'_{Fe^{2+}}[Fe^{2+}]\log[Fe^{2+}] + K'_{Fe^{2+}}[Fe^{2+}] - [Fe^T]\right] \quad \text{A1.6}$$

Equation A1.6 may be rewritten by substituting Equation 2.51:

$$C_X = \frac{D}{q^{\max}_{Fe^{2+}}}\left[[Fe^T]\left\{K'_{Fe^{2+}}\left(\log[Fe^T]-\log\frac{DK'_{Fe^{2+}}[Fe^T]}{D^{\max}-D(1-K'_{Fe^{2+}})}-1\right)+1\right\}+\log\frac{DK'_{Fe^{2+}}[Fe^T]}{D^{\max}-D(1-K'_{Fe^{2+}})}(1-K'_{Fe^{2+}})\right] \quad 2.54$$

Appendix B

B1.1 Calculation of dilution rate by weight decrease of feed vessels

The dilution rate ((residence time)$^{-1}$) was calculated by the weight decrease of the feed vessel using Equation B1.1:

$$D = \frac{1}{\tau} = \frac{m_{initial} - m_{final}}{V_{bioreactor}\rho_{feed}\left(t_{final} - t_{initial}\right)} \qquad \text{B1.1}$$

where D is the dilution rate (h^{-1})

τ is the residence time (h)

$m_{initial} - m_{final}$ is the weight decrease of the feed vessel (g)

$t_{final} - t_{initial}$ is the time interval for the weight decrease (h)

$V_{bioreactor}$ is the working volume of the bioreactor (L)

ρ_{feed} is the density of the feed solution ($g.L^{-1}$)

B1.2 The theoretical aspect of the calibration using the Nernst equation

The relationship between the redox potential E_h, the standard redox potential, E_h^0 , and the ratio of ferric to ferrous-iron concentrations, $[Fe^{3+}]/[Fe^{2+}]$ in solution is governed by the Nernst equation:

$$E_h = E_h^0 + \frac{RT}{nF}\ln\frac{a_{Fe^{3+}}}{a_{Fe^{2+}}} \qquad \text{B1.2}$$

For a redox couple of the half cell reaction $Fe^{2+} \rightarrow Fe^{3+} + e$, the standard redox potential, E_h^0, is 770 mV. This is obtained from thermodynamic data and refers to a situation in which the activities of both ferric, $a_{Fe^{3+}}$, and ferrous-iron, $a_{Fe^{2+}}$, are equal, measured with a standard Hydrogen electrode. The activity of a compound *i*, a_i is equal to its concentration only when the ionic strength is zero. For ionic strength greater than zero, $a_i = \gamma_i C_i$, where γ_i

is the activity coefficient. Therefore, the actual value of E_h at equal ferric and ferrous iron concentrations would change at increasing ionic strength as a result of the influence of other cations and anions. The presence of complexing agents (e.g. $SO_4^{2-}OH^-$) causes a decrease of free ferrous and ferric ions (Nagpal and Dahlstrom, 1994)[1]. It has also been shown by simulation using Visual Minteq and HSC® Chemistry softwares that stronger complexes are formed with ferric rather than with ferrous ions. Equation B1.2 may be rewritten as:

$$E_h = E'_h + \frac{RT}{nF}\ln\frac{[Fe^{3+}]}{[Fe^{2+}]} \qquad 3.3$$

where $E'_h = E^0_h + \frac{RT}{nF}\ln\frac{\gamma_{Fe^{3+}}}{\gamma_{Fe^{2+}}}$

Thus, the term E'_h is defined as the solution potential measured at equal total ferric and ferrous-iron concentrations and it accounts for activity coefficients $Fe^{3+}$and Fe^{2+}, the formation of complexes with $Fe^{3+}$and Fe^{2+} and the type of electrode. The adapted Nernst equation relates the measured redox (solution) potential, E_h, the standard redox potential and the ratio between the total concentrations of ferric and ferrous ions. Therefore, for a specific electrode E'_h, values may be determined from the intercept of the plot of E_h versus $ln([Fe^{3+}]/[Fe^{2+}])$, while the slope gives RT/nF.

Table B1.1: Parameters determined from the standard calibration curve for redox probes used in this study

Temperature (°C)	E'_h **(mV)**	RT/nF **(C J.mol^{-2})**	R^2
25	452.51	24.38	0.9982
30	456.97	25.45	0.9997
35	461.10	26.80	0.9999

1. Nagpal, S. & Dahlstrom, D. 1994. A mathematical model for the bacterial oxidation of a sulphide ore concentrate. *Biotechnology and Bioengineering,* 43: 357 - 364.

Appendix C

Statistical analysis: Relationship between sum of squares and correlation coefficient

C1.1 Sum of squares

Consider two quantities: y_n, the measured data, and $\hat{y}_n$, the predicted data, which may be represented by the regression line $\hat{y} = a + bx$, where a and b are the intercept and the slope of the regression line respectively.

The sum of squares error (SSE) is the difference between the observed quantity and the predicted quantity, as shown in Equation C1.1.

$$SSE = \sum \left(y_n - \hat{y}_n\right)^2 = \sum \left(y_n - a - bx_n\right)^2 \qquad \text{C1.1}$$

This quantity will be small if the observed values $\hat{y}_n$ fall close to the regression line, $\hat{y} = a + bx$, and will be large if they do not fall close to the regression line.

The term $y_n - \hat{y}_n$ is known as the error or residual for the nth observation. By substituting $a = \bar{y} - b\bar{x}$ into Equation C1.1, *SSE* may be expressed as follows:

$$\begin{aligned} SSE &= \sum \left(y_n - \bar{y} + b\bar{x} - \bar{x}_n\right)^2 = \sum \left(\left(y_n - \bar{y}\right) - b\left(\bar{x}_n - \bar{x}\right)\right)^2 \\ &= \sum \left(y_n - \bar{y}\right)^2 - 2b\sum \left(y_n - \bar{y}\right)\left(x_n - \bar{x}\right) + b^2 \sum \left(x_n - \bar{x}\right)^2 \\ &= SS_y + 2bSS_{xy} + b^2 SS_x \end{aligned} \qquad \text{C1.2}$$

However, $b = SS_{xy} / SS_x$, and, therefore, SSE may written as Equation C1.3:

$$SSE = SS_y - bSS_{xy} \qquad \text{C1.3}$$

The first term on the right-hand side of Equation C1.3 is known as the total sums of squares and is denoted by SST, so that $SST = SS_y$

The second term measures by how much the total variability is reduced by the regression line $\hat{y} = a + bx$. Thus the term $\mathrm{bSS_{xy}}$, denoted by SSR, is known as the sum of squares due to regression. Therefore Equation C1.3 may be written as:

$$SSE = SST - SSR \qquad \text{C1.4}$$

Equation C1.4 is important because it shows that SST may be decomposed into SSR and the error sum of squares, SSE, the decomposition is explained by regression. Equation C1.4 may be written as:

$$\frac{SSE}{SST} = 1 - \frac{SSR}{SST} \qquad \text{C1.5}$$

Where,

$$\frac{SSR}{SST} = \frac{bSS_{xy}}{SS_y} = \frac{SS_{xy}^2}{SS_{xy}SS_y} = R^2$$

$$SS_x = \sum x^2 - \left(\sum x\right)^2 \Big/ n$$

$$SS_y = \sum y^2 - \left(\sum y\right)^2 \Big/ n$$

$$SS_{xy} = \sum xy - \left(\sum x\right)\left(\sum y\right) \Big/ n$$

Therefore, using Equation C1.5, the error sum of squares (SSE) and the coefficient of regression (R^2) may be related, as is shown in Equation C1.6 (Keller and Warrack, 1999)[2].

$$R^2 = 1 - \frac{SSE}{SST} \qquad \text{C1.6}$$

This relationship will be used for an error analysis between the modelled and measured data which was obtained in this experiment − See section C1.2.

C1.2 Error analysis between modelled and measured data

The resultant regression coefficients (shown in Table C1.1) which were obtained using Equation C1.1 suggests that the model obtained in chapters 4 and 5 accurately predicts the measured data.

Table C1.1: Error analysis of experimental data

	Microbial ferrous-iron oxidation rate $r_{Fe^{2+}}$											
	25 °C			**30 °C**						**35 °C**		
							Jarosite accumulated data					
	Measured data	a	b	Measured data	a	b	Measured data	a	b	Measured data	a	b
	2.76	2.23	2.28	2.96	2.13	2.10	2.86	1.93	1.92	2.84	2.78	2.73
	3.19	3.17	3.15	3.31	3.42	3.45	3.18	3.63	3.67	3.31	4.1	4.12
	4.10	4.42	4.40	4.57	4.93	4.87	3.80	3.69	3.65	4.10	3.53	3.51
	5.80	6.22	6.22	5.45	6.23	6.15	6.02	6.57	6.59	5.56	5.35	5.41
	7.42	7.00	7.01	7.72	6.97	7.09	8.52	8.15	8.13	7.70	7.70	7.68
SSR		0.72	0.65		2.00	1.74		1.50	1.61		1.00	1.04

a represents the predicted data using the Monod equation, while b is for Hansford equation.

2. Keller, G. & Warrack, B. 1999. Statistics: for Management and Economics. (5th Edition) Duxbury Thomson Learning, USA.pp. 626 - 673.

Appendix D

Determination of concentration of iron species

D1.1 Reagent preparation

D1.1.1 Spekker acid

The spekker acid solution was prepared by mixing equal volumes of concentrated sulphuric acid (98% H_2SO_4) and phosphoric acid (85%) with water in a ratio of 3:4 (acid solution:distilled water).

- Measure 600 mL distilled water using a 2 L beaker.
- Carefully add 225 mL of concentrated sulphuric acid (98%) and 225 mL of phosphoric acid (85%) by slowly pouring the acid mixture against the wall of the beaker (Caution: rapid addition of the acid mixture to the distilled water will result in heat of mixing which will cause localised boiling, especially when using concentrated H_2SO_4).
- Allow the mixture to cool to room temperature before transferring into a storage bottle.

D1.1.2 Ferric acid

The ferric acid solution was prepared from the spekker acid:

- Measure 600 mL distilled water using a 2 L beaker.
- Slowly and carefully add 150 mL of spekker acid and then 300 mL of concentrated hydrochloric acid (32% HCl) to the distilled water.
- Agitate the mixture using a magnetic stirrer and allow to cool to room temperature before transferring into a storage bottle.

D1.1.3 Stannous chloride solution ($SnCl_2$)

- Weigh out 30 g stannous chloride in a 200 mL beaker.
- Add 100 mL concentrated hydrochloric acid (32%) and agitate at 50°C until it dissolves completely.
- Allow to cool to room temperature and dilute with 200 mL distilled water.

- Add a small amount of granular tin to the solution to retard precipitation.

D1.1.4 Mercuric Chloride solution ($HgCl_2$)

- Weigh out 50 g mercuric chloride in a 2 L beaker.
- Add 1 L of distilled water and agitate until the solute has dissolved completely (about 2 hours).
- Add a spatula tip of $HgCl_2$ and stir for 2 hours before storage.

D1.1.5 Potassium Dichromate solution (0.0149 M $K_2Cr_2O_7$)

- Dry approximately 10 g of $K_2Cr_2O_7$ (Molar mass 294.20 $g.mol^{-1}$) in an oven at 105 – 110°C for 1 – 2 hours. Cool in a desiccator.
- Accurately weigh out 8.78 g of the dried $K_2Cr_2O_7$ into a 100 mL beaker.
- Transfer quantitatively into a 2 L beaker.
- Add 1.5 L of distilled water and agitate until dissolved completely.
- Transfer quantitatively into a 2 L standard volumetric flask and fill to the 2 L mark with distilled water.

D1.1.5 Barium Diphenyllamine Sulphonate (BDS) solution ($C_{24}H_{20}BaN_2O_6S_2$)

- Weigh out 1.0 g of barium diphenylamine suphonate in a 250 mL beaker and add 100 mL of concentrated sulphuric acid (98%). Agitate until the solute has dissolved completely.

D1.2 Determination of ferrous-iron concentration by titration with potassium dichromate solution[3]

- Pipette 5 mL of the required aliquot solution into a 125 mL conical flask.
- Add 10 mL of spekker acid solution.
- Add 2 – 3 drops of BDS indicator.
- Titrate the potassium dichromate (0.0149 M $K_2Cr_2O_7$) solution until the first permanent colour change from yellow to intense purple is obtained.

Ferrous-iron concentration may be calculated using Equation D1.1:

$$\left[Fe^{2+}\right] = \frac{\left[K_2Cr_2O_7\right] \times V_T \times \left(55.84 \times 6\right)}{V_{Solution}} \qquad \text{D1.1}$$

Where,

$[Fe^{2+}]$ = Ferrous-iron concentration ($g.L^{-1}$)

$K_2Cr_2O_7$ = $K_2Cr_2O_7$ concentration (i.e. 0.0149 M $K_2Cr_2O_7$)

V_T = Titration volume (mL) (amount of 0.0149 M $K_2Cr_2O_7$ added)

$V_{Solution}$ = Solution aliquot volume (mL)

3. It is not possible to determine a ferrous-iron concentration of less than 0.5 $g.L^{-1}$ accurately using this method, and a combination of solution potential and total iron concentration will allow for an accurate estimation.

D1.3 Determination of total iron concentration by titration with potassium dichromate solution[4]

1. Filter 5 mL aliquot of sample solution.
2. Pipette the required amount of aliquot (i.e. 5 mL) into a 125 mL conical flask.
3. Add 10 mL of spekker acid solution and heat until the mixture boils.
4. Add stannous ($SnCl_2$) solution dropwise until the yellow colour disappears completely. Add one extra drop and record the amount of stannous chloride added (Note: It is important to record this amount, especially when doing duplicate titrations since it gives some an idea of the amount of $SnCl_2$ required for the next duplicate titrations).
5. Allow the solution to cool to room temperature and add 10 mL of mercuric chloride ($HgCl_2$) solution. A silky-white precipitate should appear. If no precipitate forms, too little stannous chloride was added in step 4. If the precipitate is heavy and grey/black, too much stannous chloride was added. In either case, abort the experiment and start over.
6. Add 3 – 4 drops of barium diphenylamine indicator solution (BDS) and titrate with the potassium dichromate solution until the first permanent colour change from yellow to intense purple is obtained.

Total iron concentration may be calculated using Equation D1.2:

$$\left[Fe^{T}\right] = \frac{\left[K_2Cr_2O_7\right] \times V_T \times \left(55.84 \times 6\right)}{V_{Solution}} \qquad \text{D1.2}$$

Where,

$[Fe^T]$ = Total iron concentration ($g.L^{-1}$)

$K_2Cr_2O_7$ = $K_2Cr_2O_7$ concentration (i.e. 0.0149 M $K_2Cr_2O_7$)

V_T = Titration volume (mL) (amount of 0.0149 M $K_2Cr_2O_7$ added)

$V_{Solution}$ = Solution aliquot volume (mL)

4. Potassium chromate and mercuric chloride are toxic and care should be taken when analysing samples that may contain arsenic, as this may be converted to toxic volatile arsine gas (AsH_3) during the stannous chloride reduction in step 4.

D1.4 Vishniac Trace Metal Solution

Vishniac Trace Metal Solution was prepared according to the method suggested by Vishniac and Santer (1957).

Weigh the reagents accurately and dilute to 1 L volume with distilled water (dH_2O).

1. Prepare 6% potassium hydroxide (KOH) by weighing 15 g KOH and dilute to 250 mL with dH_2O.
2. Dissolve 50 g EDTA (Ethylenediaminetetraaacetic acid disodium salt dihydrate) in 200 mL of 6% KOH using a magnetic stirrer.
3. In a separate 500 mL beaker weigh the salts listed below and dissolve in 400 mL dH_2O for 30 minutes using a magnetic stirrer.

$ZnSO_4.7H_2O$	22 g
$CaCl_2.2H_2O$	9.24 g
$MnCl_2.4H_2O$	5.06 g
$FeSO_4.7H_2O$	5 g
$(NH_4)_6Mo_7O_{24}.4H_2O$	1.1 g
$CuSO_4.5H_2O$	1.58 g
$CoCl_2.6H_2O$	1.62

1. Transfer the solution prepared in step 2 quantitatively into the solution prepared in step 3 and make up to 1 L with dH_2O by rinsing the 500 mL beaker with 400 mL dH_2O. A deep greenish brown solution should result.

Appendix E

Experimental data at different temperatures

Table E1.1: Experimental data

Temperature	Dilution rate (h^{-1})	$[Fe^{T}]_{in}$	$[Fe^{T}]_{out}$	Precipitation of Fe^{3+}	% of jarosite formation	$[Fe^{2+}]_{in}$	$[Fe^{2+}]_{out}$
	0.03	89.53	87.74	1.79	2.00	84.15	0.32
	0.04	89.53	87.74	1.79	2.00	82.36	0.49
25 °C	0.05	89.53	87.74	1.79	2.00	84.15	0.80
	0.07	89.53	87.74	1.79	2.00	84.15	1.53
	0.09	89.53	87.74	1.79	2.00	82.36	2.03
	0.04	89.53	88.33	1.19	1.33	82.96	0.45
	0.04	89.53	88.33	1.19	1.33	84.15	0.85
30 °C	0.06	88.33	85.94	2.39	2.70	82.36	1.40
	0.07	88.33	87.14	1.19	1.35	84.15	2.09
	0.09	89.53	87.74	1.79	2.00	82.36	2.79
	0.03	89.53	81.17	8.36	9.33	89.02	0.86
	0.04	89.53	83.56	5.97	6.67	88.87	1.47
35 °C	0.05	89.53	82.96	6.57	7.33	88.82	1.19
	0.07	88.93	84.15	4.77	5.37	88.37	2.18
	0.10	88.33	80.54	7.79	8.82	87.94	4.05
	0.03	87.14	87.14	0.00	0.00	4.80	0.01
	0.04	85.94	85.94	0.00	0.00	4.72	0.02
30 °C*	0.04	88.93	85.35	3.58	4.03	4.88	0.02
	0.07	86.54	84.75	1.79	2.07	4.77	0.04
	0.10	88.63	86.84	1.79	2.02	4.93	0.06

Units: $[Fe^{T}]_{in}$ (mmol.L^{-1}), $[Fe^{T}]_{out}$ (mmol.L^{-1}), $[Fe^{2+}]_{in}$ (mmol Fe^{2+}.L^{-1}) and $[Fe^{2+}]_{out}$ (mmol Fe^{2+}.L^{-1}).

*Jarosite accumulation data.